VIBRATIONAL STUDIES OF TETRAHALOGENOCUPRATES(II)

A thesis

submitted to the

University of Waikato

for the degree of

Doctor of Philosophy

by

TENG KWONG YEOH M.Sc.(Hons.)

University of Waikato, Hamilton

October, 1979

To

my parents

ABSTRACT

The compounds $(R_4N)_2CuBr_nCl_{4-n}$ ($R = CH_3$, C_2H_5; $n = 1 - 3$) were studied by far infra-red spectroscopy. The results, in conjunction with the evidence of X-ray powder diffraction measurements we reported earlier, show that, within each series, the mixed bromochlorocuprates(II) are isomorphous with each other and with the corresponding compounds where $n = 0, 4$. There is also evidence of discrete $CuBr_nCl_{4-n}^{2-}$ anions with flattened tetrahedral configurations.

The assignment problems associated with the vibrational spectrum of caesium tetrachlorocuprate(II) were critically discussed. A unit cell analysis of the compound was performed with two primary objectives:

(A) to interpret the vibrational spectrum; and

(B) to develop a competent model force field for such study.

The analysis produces a physically sensible set of force constants which supports one particular set of assignments.

The potential force field developed in the unit cell analysis of Cs_2CuCl_4 was extended to the study of the vibrations of Cs_2ZnCl_4 crystal with encouraging results.

ACKNOWLEDGEMENTS

I wish to express my sincere gratitude to Dr. D.W. Smith who conceived this research project as well as supervised me with great efficiency. The amicable and satisfying working relationship between us has been a feature of my stay in New Zealand.

I am indebted to Professor K.M. Mackay for his continuous concern and for providing me with the best possible working conditions during the course of this work. Thanks are also due to Mr. F.E. Bailey, the university draughtsman, and his colleague, Mr. K. Stewart, for drawing the many impressive diagrams, and Mr. C. Rickard of the university workshop for building the unit cell model of caesium tetrachlorocuprate(II). I am especially grateful to Mr. P.N. Schaare for his generous assistance with computer programming and Mrs. K. Fransham for her patient and efficient preparation of the typescript.

Finally, I would like to thank the University of Waikato for a Post-graduate Study Award, during the tenure of which this work was completed.

ABBREVIATIONS

The common abbreviations used in this work are as follows:

Me	methyl group - CH_3
Et	ethyl group - C_2H_5
Pr	propyl group - C_3H_7
Ph	phenyl group - C_6H_5
X	halogen
MO	molecular orbital
ν	stretch
δ	deformation
vs	very strong
s	strong
m	medium
w	weak
vw	very weak
br	broad
sh	shoulder

CONTENTS

LIST OF TABLES

LIST OF FIGURES

CHAPTER 1 INTRODUCTORY SURVEY OF CHLOROCUPRATES(II)

1.1 *GENERAL INTRODUCTION*

Chlorocuprate(II) compounds of the general formula $A_x Cu_y Cl_z$ have received wide-spread and sustained attention over the last twenty years. Such d^9 copper(II) complexes exhibit intriguing properties which have no doubt contributed to making them an interesting subject for magnetic and structural studies as well as a readily accessible 'testing ground' for various theoretical models of bonding and structure.

Several reviews [1-4] have been written on chlorocuprates(II), among which the most recent and most comprehensive is that by Smith[1] who has covered the subject up to and including part of 1975. Scarsely five years have passed, and numerous valuable additions to the literature are now noticeable. For this reason, as well as the particular relevance to the topic of this thesis, we present an up-to-date survey of chlorocuprates(II) in this chapter, beginning where Smith left off. Emphasis is placed on the experimental results only, since theoretical discussion, especially in the areas of spectroscopic and magnetic properties, has already been amply covered by Smith[1].

1.2 *ANION STRUCTURES*

Smith[1] classified chlorocuprates(II) according to structural types irrespective of stoichiometry (table 1.2.1). This has the obvious advantage of avoiding any possible confusion arising from chlorocuprates(II) of a certain stoichiometry having different types of structure. For this reason and also for the sake of consistency, similar classifications are adopted here.

Several new chlorocuprates(II) have been identified over the last five years, but only three[9-11] have been subject to full X-ray analysis.

1.2.1 *Chlorocuprates(II) Containing Discrete $CuCl_4^{2-}$ Ions*

These are the most thoroughly studied of all chlorocuprates(II). Until recently, the anion in this category has usually been found to be a flattened tetrahedron. Smith[1] has already presented an excellent discussion regarding the configuration of the $CuCl_4^{2-}$ ion from the theoretical as well as the experimental viewpoints. It is clear that while the intrinsic property of a d^9 $CuCl_4^{2-}$ ion may, on theoretical grounds, favour a distorted tetrahedral structure, such distortion could be further enhanced by the physical properties associated with a crystalline environment. Thus the effect of crystal forces on the anion geometry was explicitly considered by McGinnety[5-7], while the structures of the high- and low-temperature forms of $(PhCH_2CH_2NMeH_2)_2CuCl_4$[8] demonstrate graphically the effect of hydrogen-bonding in stabilising square coplanar $CuCl_4^{2-}$ ions.

TABLE 1.2.1

Structural types of chlorocuprates(II)[1]

Structural Type	Example
discrete $CuCl_4^{2-}$ ions:	
(a) flattened tetrahedral	Cs_2CuCl_4
(b) square coplanar	$(PhCH_2CH_2NMeH_2)_2CuCl_4$ (Low temperature form)
tetragonally-elongated $CuCl_6$ octahedra	$(NH_4)_2CuCl_4$
discrete $CuCl_5^{3-}$ ions	$[Cr(NH_3)_6]CuCl_5$
dimeric $Cu_2Cl_6^{2-}$ ions:	
(a) 4-coordinate copper	$(Ph_4P)CuCl_3$
(b) 5-coordinate copper	$(Me_2NH_2)CuCl_3$
(c) 6-coordinate copper	$KCuCl_3$
others:	
(a) infinite chains with face-sharing distorted $CuCl_6$ octahedra	$CsCuCl_3$
(b) $Cu_2Cl_8^{4-}$ dimers	$[Co(en)_3]CuCl_5.H_2O$ en = 1,2-diaminoethane

The recently characterised tetrachlorocuprates(II) are given in table 1.2.2, of which the X-ray crystal structures of N-phenylpiperaziniumtetrachlorocuprate(II) and cretininium tetrachlorocuprate(II) have been reported. In all the other compounds, the anion geometries were derived from the indirect evidence of infra-red and electronic absorption spectra (tables 1.2.4, 1.2.5), magnetic studies and other characterisation techniques.

The crystal structure[9] of $(NPhipzH_2)CuCl_4$ consists of N-phenylpiperazinium dications and discrete $CuCl_4^{2-}$ anions which show a flattened tetrahedral geometry. The mean of the two larger Cl-Cu-Cl angles is *ca.* 140^o while that of the four smaller angles is *ca.* 96^o; the average bond distance is *ca.* 2.25 Å. These represent a considerable distortion from the regular tetrahedral structure. While the massive size of the cation most probably ensures the observed anion coordination of four, other reasons must be sought for the degree of flattening of the $CuCl_4^{2-}$ anion geometry. Battaglia et al.[9] suggested that this could be attributed to the effect of crystal packing forces in the form of Cl ... N interactions. As seen from figure 1.2.1, all four chlorine atoms in each $CuCl_4^{2-}$ unit are involved in NH ... Cl hydrogen bonds. Other evidence, spectroscopic as well as magnetic, also confirms such a deduction.

In contrast, the crystal structure[10] of creatininium tetrachlorocuprate(II) reveals another example of discrete square coplanar $CuCl_4^{2-}$ ion. Prior to this, only one other example of this kind has been reported , that is the low-temperature form of $(PhCH_2CH_2NMeH_2)_2CuCl_4$; in all the other chlorocuprates(II) with arguable square coplanar $CuCl_4^{2-}$ anions[17-24], neighbouring Cl

TABLE 1.2.2

Chlorocuprates(II) containing discrete $CuCl_4^{2-}$ ions

Compound	Anion Geometry	Reference
$(PipdH)_2CuCl_4$ [a]	distorted tetrahedral	12
$(MorphH)_2CuCl_4$ [b]	approx. square coplanar	12
$(NEtmorphH)_2CuCl_4$ [c]	distorted tetrahedral	13
$(Pipz.HCl)_2CuCl_4$ [d]	approx. square coplanar	14
$(PipzH_2)CuCl_4$ [e]	distorted tetrahedral	14
$(NPhpipzH_2)CuCl_4$ [f]	distorted tetrahedral	9
$(Cret)_2CuCl_4$ [g]	square coplanar	10
$(Dadtl)_2CuCl_4$ [h]	distorted tetrahedral	15
$(4\text{-chloro-Dmadtl})_2CuCl_4$ [i]	distorted tetrahedral	15
$(TTF)_2CuCl_4$ [j]	approx. square coplanar	16
$(TTF)CuCl_4$ [j]	distorted tetrahedral	16

a $PipdH^+$ = piperidinium cation, 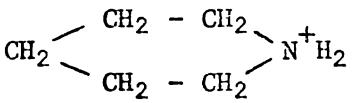

b $MorphH^+$ = morpholinium cation, 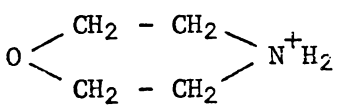

c $NEtmorphH^+$ = N-ethylmorpholinium cation, 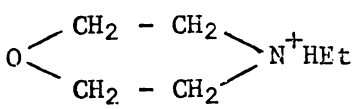

d $PipzH^+$ = piperazinium mono-cation, 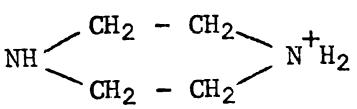

e $(PipzH_2)^{2+}$ = piperazinium di-cation, 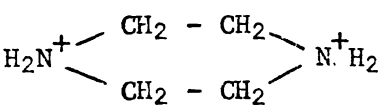

f $(NPhpipzH_2)^{2+}$ = N-phenylpiperazinium di-cation,

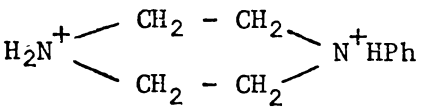

g $Cret^{+}$ = cretininium cation,

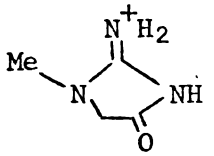

h $Dadtl^{+}$ = 3,5-diamino-1,2-dithiolylium cation,

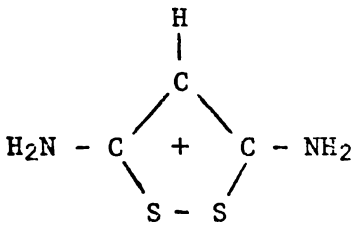

i $(4\text{-chloro-Dmadtl})^{+}$ = 4-chloro-3,5-di(Methylamino)-1,2-dithiolylium cation,

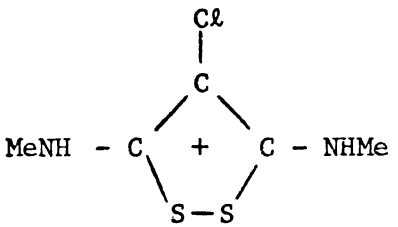

j Copper derivatives of tetrathiafulvalene,

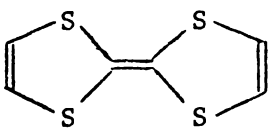

Figure 1.2.1

Projection of the structure of

$(NPhpipzH_2)CuCl_4$ along [010][9]

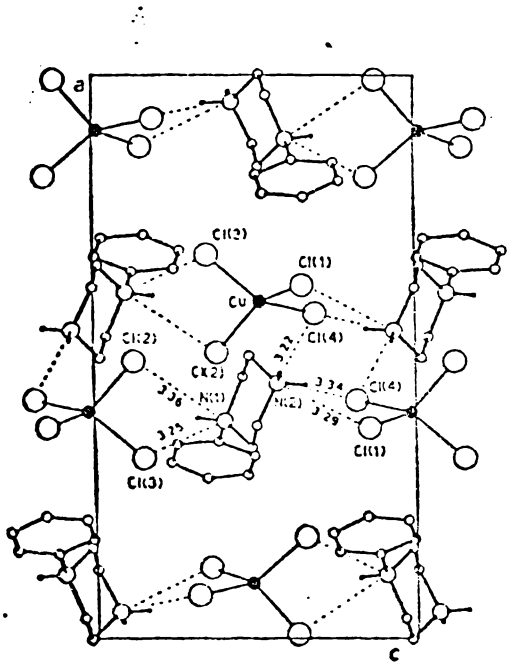

atoms have been found to occupy octahedral sites at distances varying between 2.79 - 3.10 Å. Smith[1] has argued strongly that Cl atoms as far away as 3 Å are definitely bonded to the copper, both from orbital overlap consideration[25] and the evidence of electronic spectra which are significantly different for tetragonal octahedral $CuCl_6$ chromophores and square coplanar $CuCl_4^{2-}$ ions.

The $CuCl_4^{2-}$ anion of creatininium tetrachlorocuprate(II) is centrosymmetric, and the copper atom is surrounded by four Cl atoms in a square planar arrangement; the average Cu-Cl bond distance is 2.251 Å [10]. The creatininium cation is also approximately planar, and each cation is linked to $CuCl_4^{2-}$ units through

hydrogen bonding involving the amino and imino nitrogen atoms (figure 1.2.2). There is no evidence of axial perturbations of the Cu atoms; the closest neighbours in axial positions are carbonyl oxygen atoms at distances of *ca.* 3.64 Å which do not constitute a bonding situation.

Figure 1.2.2

Projection of the unit cell of creatininium tetrachlorocuprate(II)[10]

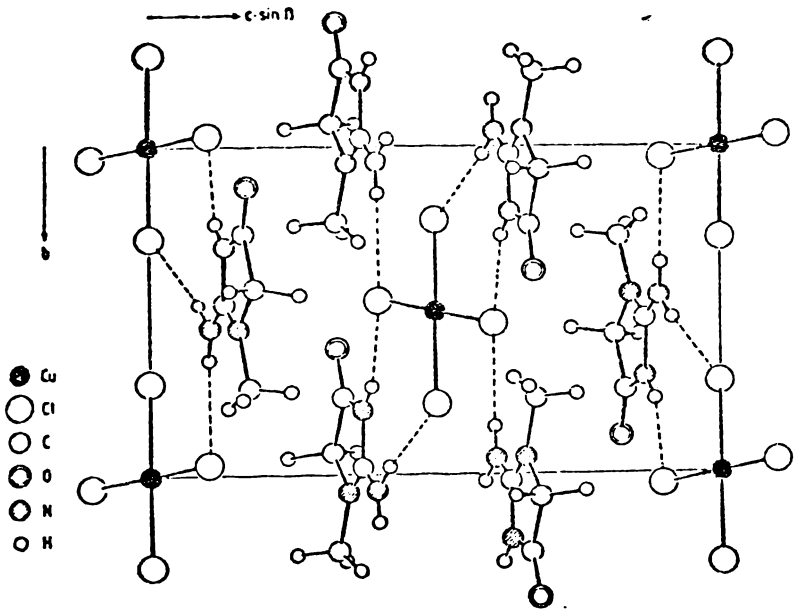

The spectral properties of the thermochromic salt, $(Et_2NH_2)_2CuCl_4$, have intrigued many workers[26-28] in the past. Recently, Harlow and Simonsen[29] presented a preliminary report of the crystal structure of this compound, and it was shown that three different types of discrete four-coordinate $CuCl_4^{2-}$ anions apparently exist in the crystal; the averages of the two larger Cl-Cu-Cl angles associated with each type of anions are 178, 159 and 145°. The publication of the full report on this crystal structure is eagerly awaited.

1.2.2 *Chlorocuprates(II) Containing Dimeric $Cu_2Cl_6^{2-}$ Ions*

The recent additions to this category are given in table 1.2.3. However, no X-ray crystal structure has been reported for any of these compounds; thus, the structural diagnoses must be received with a certain degree of caution.

TABLE 1.2.3

Chlorocuprates containing discrete $Cu_2Cl_6^{2-}$ ions

Compound	Anion Geometry	Reference
$(PipdH)CuCl_3$	near planar dimer	12
$(MorphH)CuCl_3$	near planar dimer	12
$(PipzH_2)Cu_2Cl_6$	near planar dimer	14
$(NPhpipzH)CuCl_3$	near planar dimer	9
$(Ph_4Sb)CuCl_3$	non-planar dimer	30
$(n\text{-}PrPh_3P)CuCl_3$*	non-planar dimer	30

*$n\text{-}PrPh_3P^+ = n\text{-}(C_3H_7)(C_6H_5)_3P^+$ cation

It was suggested[9], from the similarity between its solid electronic spectrum (refer table 1.2.4) and the spectra of the analogous dimers[1], that the structure of (NPhpipzH)$CuCl_3$ consists of $Cu_2Cl_6^{2-}$ dimers with an approximately square-planar configuration. In particular, a band at 19,050 cm^{-1} was taken to be indicative[1] of such a structure. An infra-red band at 258 cm^{-1} (refer table 1.2.5) was identified as the Cu-Cl stretching frequency involving bridging chlorines.

Based on similar grounds, Marcotrigiano et al.[12] suggested that the structures of (PipdH)$CuCl_3$, (MorphH)$CuCl_3$ and ($PipzH_2$)Cu_2Cl_6 also consist of near square-planar $Cu_2Cl_6^{2-}$ dimers.

Although the compounds (Ph_4Sb)$CuCl_3$ and (n-$PrPh_3P$)$CuCl_3$ have yet to be subject to a full X-ray analysis, it seems most likely that they contain discrete $Cu_2Cl_6^{2-}$ ions with strictly four-coordinate copper, similar to those found in (Ph_4P)$CuCl_3$[31] and (Ph_4As)$CuCl_3$[32]. These previous studies[31,32] have shown that the massive size of the quaternary phosphonium and arsonium cations are largely responsible for stabilising the discrete dimers each of which consists of two distorted tetrahedra sharing an edge. As expected, the electronic spectra of (Ph_4Sb)$CuCl_3$ and (n-$PrPh_3P$)$CuCl_3$ are remarkably similar to those of the tetraphenylphosphonium and tetraphenylarsonium analogues. However, Estes et al.[30] suggested that the two groups of compounds are probably not isomorphous on the evidence of the EPR spectra, in particular the observation in the former compounds of the unusually well-resolved rhombic g-tensor anisotropy; this could not be explained solely on the grounds of the slight differences in the size of the cations.

TABLE 1.2.4

Room-temperature (unless otherwise stated) solid electronic spectra (in cm^{-1}) of chlorocuprate(II) anions

Compound	d-d bands	C.T. bands	Ref
$(PipdH)_2CuCl_4$	6620, 9710	25000	12
$(NPhpipzH_2)CuCl_4$	8930, 10750	23810 sh, 27030	9
$(Dadtl)_2CuCl_4$*	7143, 10000	24691	15
$(4\text{-chloro-Dmadtl})_2CuCl_4$*	8969, 11494	25000	15
$(PipzH_2)CuCl_4$	6850, 9620	25320	14
$(PipzH.HCl)_2CuCl_4$	11490	23810 sh, 27400	14
$(PipzH.HCl)_2CuCl_4$ at 373° K	6760 sh, 10640		14
$(Ph_4P)CuCl_3$*	8000, 11111 sh	21739, 24390, 32258	30
$(Ph_4Sb)CuCl_3$*	9523, 10638 sh	21739 24390 sh	30
$(n\text{-}PrPh_3P)CuCl_3$*	10000 br	22222, 25000 sh	30

Table 1.2.4 continued

(NPhpipzH)$CuCl_3$	9710 sh, 11110	19050 sh, 24390, 27780 sh	9
(PipdH)$CuCl_3$	10870	19050 sh, 24100 sh	12
(MorphH)$CuCl_3$	12500	19230, 24700 sh	12
$(MorphH)_2CuCl_4$	12200	22730 sh, 26320	12
$(PipzH_2)Cu_2Cl_6$	11690	18870, 24390 sh	14

* The spectra of these compounds are given in nm in the original papers.

TABLE 1.2.5

Room-temperature far infra-red powder spectra (in cm^{-1}) of chlorocuprate(II) anions

Compound	ν(Cu-Cℓ)	δ(Cℓ-Cu-Cℓ)	Ref
$(NPhpipzH_2)CuCl_4$	300 vs,	172 s,	9
	278 w	128 m,	
		87 w*	
$(NPhpipzH)CuCl_3$	292 vs, terminal	166 m,	9
	276 s, terminal	138 s,	
	258 s bridging	68 w*	
$(PipzH.HCl)_2CuCl_4$	298 sh,	182 vs, br	14
	282 vs		
$(PipzH_2)CuCl_4$	303 vs,	187 sh,	14
	264 vs,	172 vs, br	
	233 m		
$(PipzH_2)Cu_2Cl_6$	292 vs,	183 ms	14
	273 vs		
$(PipdH)CuCl_3$	287 vs,	174 m,	12
	265 sh,	148 ms	
	237 m		
$(PipdH)_2CuCl_4$	302 vs,	160 s,	12
	280 vs	140 sh	
$(MorphH)CuCl_3$	313 sh,	182 sh	12
	298 vs,		
	236 vw		

Table 1.2.5 continued

$(MorphH)_2CuCl_4$	295 vs	181 m	12
$(Dadtl)_2CuCl_4$	287 vs,	150 m, br	15
	270 sh	114 m	
$(4\text{-chloro-Dmadtl})_2CuCl_4$	286 vs,	157 m,	15
	273 sh	123 sh	

* These are probably lattice modes

1.2.3 *Other Chlorocuprates(II) With Cu-Cl-Cu Bridges*

Only one new addition to this category has been reported[11]: the tetramethylammonium trichlorocuprate(II), $(Me_4N)CuCl_3$. This has the $CsCuCl_3$-type structure [33-35] which contains infinite chains formed by highly distorted $CuCl_6$ octahedra sharing faces (figure 1.2.3).

FIGURE 1.2.3

Chain structure of the anion in $CsCuCl_3$-type crystal

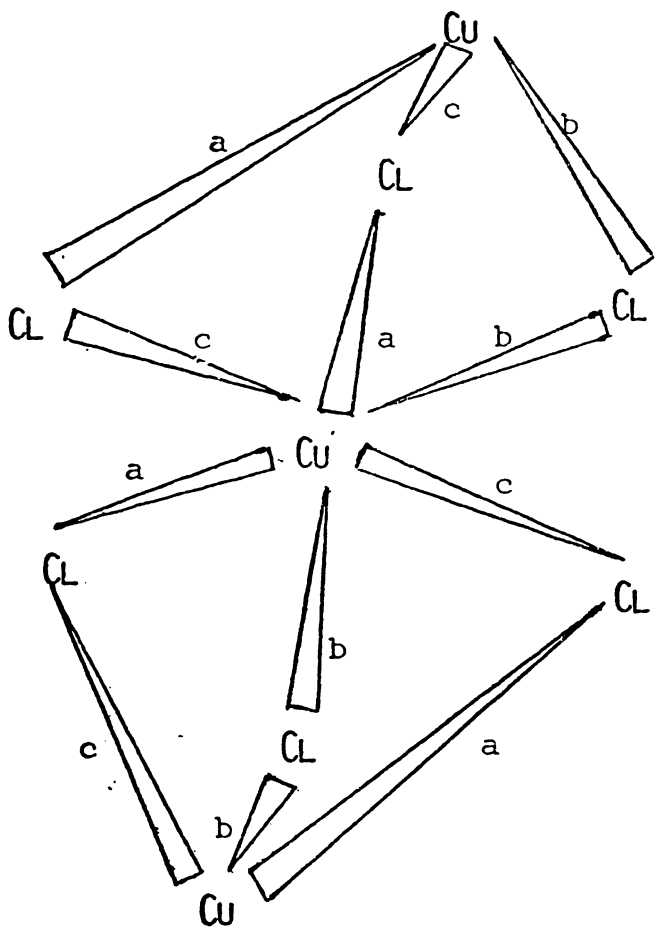

Footnote: Cu-Cl bond distances of similar magnitude are indicated by a, b and c.

1.3 *SOLUTION STUDIES*

Two recent papers on the solution studies of chlorocuprates(II) are relevant to this review. One deals solely with the chloro-copper(II) complexes in aqueous solutions[36], while the other with halo-copper(II) complexes in acetic acid anhydride[37].

Schwing-Weill[38] reported earlier the overall stability constants β_j ($\beta_j = [CuCl_j^{(j-2)-}]/[Cu^{2+}][Cl^-]^j$) of chloro-copper(II) complexes in aqueous solutions as 4.0, 4.7, 1.6 and 0.17 for j = 1, 2, 3 and 4, respectively. These represent rather low values, and the formation of $CuCl_4^{2-}$ species is achieved only in solutions containing a large excess of chloride. An extension of this study was recently reported by Khan and Schwing-Weill[36], in which the refined values of β_j are given as 4.0, 4.7, 1.96 and 0.23, indicating consistency. Attempts were made to deduce structural information, from the calculated electronic spectra, concerning the $CuCl_4^{2-}$ species in solution. However, as in previous attempts by other workers[1], the results were rather inconclusive. The authors summed up by agreeing with Eswein et al.[39] and stated that there could be an equilibrium in solution between $CuCl_4^{2-}$ species of D_{2d} and D_{4h} configurations; at the same time, they did not rule out the possibility of a tetragonally distorted octahedral geometry with two water molecules coordinated to each $CuCl_4^{2-}$ ion.

Previous studies of chloro-copper(II) complexes in non-aqueous solutions have shown that genuine chlorocuprate(II) species may indeed exist; Furlani and Morpurgo[40] identified the flattened tetrahedral $CuCl_4^{2-}$ ions in acetonitrile and nitromethane solutions containing excess chloride, while Ludwig and Textor[41] reported

the presence of monomeric $CuCl_3^-$ species in dichloromethane solution of trichlorocuprates(II) with large cations. However, Smith[1] rejected the latter claim on the grounds that the electronic spectra of such $CuCl_3^-$ species are similar to those of the discrete non-planar $Cu_2Cl_6^{2-}$ dimers as found in crystalline $(Ph_4As)CuCl_3$ and $(Ph_4P)CuCl_3$, indicating retention of the dimeric anion configuration in solution.

Recently, Biela and Gazo[37] reported a spectrophotometric study of the system $Cu(ClO_4)_2.6H_2O$-LiCl-AA (AA = acetic acid anhydride) which shows convincingly the presence of $CuCl_4^{2-}$ species at high concentrations of chloride. The absorption spectra in the visible region of the solution system at Cl/Cu ratios from 3 to 10 shows only a single band at 21,000 cm^{-1} with another band at 11,400 cm^{-1} in the near infra-red region and also a low-intensity band at *ca.* 8,800 cm^{-1}. On increasing the concentration of chloride, a new absorption band appears at 25,000 cm^{-1} and the intensity of the band at 8,800 cm^{-1} increases while the original bands simultaneously diminish. It was deduced that at Cl/Cu ratios less than 10, only one chloro-copper(II) complex is present while two complexes exist at higher Cl/Cu ratios. The absorption bands at 25,000 cm^{-1} and 8,800 cm^{-1} could be taken to indicate the presence of flattened tetrahedral $CuCl_4^{2-}$ ions on comparison with the electronic spectra of Cs_2CuCl_4 and $(Me_4N)_2CuCl_4$ [42], while the band at 21,000 cm^{-1} could be attributed to $CuCl_3AA^-$ species, which is a solvolysis product of $CuCl_4^{2-}$ and apparently has a strongly distorted tetrahedral structure.

Other recent papers related to the studies of chloro-copper(II) complexes in non-aqueous solutions include those of Sykora et al.[43,44] (in acetonitrile), Braun[45] (in N,N-dimethylformamide), Sasaki et al.[46] (in propylene carbonate, N,N-dimethylformamide and dimethylsulphoxide), Machtinger et al.[47] (in molten dimethyl sufone) and Klein and Miller[48] (in the micellar system, cetyldimethylbenzylammonium chloride/benzene).

1.4 *MAGNETIC AND E.S.R. STUDIES*

The study of the magnetic properties of chlorocuprates(II) constantly attracts wide attention. Not surprisingly, numerous papers on this topic have appeared over the last few years with some rather interesting results.

Moreno[49,50] suggested a general formalism for calculating the third-order contribution, $[G]$, to the g-tensor, using the MO approach, and applied to a D_{4h} $CuCl_4^{2-}$ complex. His results showed that neither $[G]$ nor the second-order contribution $[\delta g]$ from the bonding states, B_{2g} and E_g, is negligible; however, the two tensors cancel each other out to a considerable extent. Thus the g-tensors of the D_{4h} complexes can often be explained without a full understanding of the second- and third-order contributions owing to this fortuitous cancellation.

Lahiry et al.[51,52] measured the magnetic susceptibilities and the temperature dependencies of the magnetic anisotropy constants of $(Me_3BzN)_2CuCl_4$ and $(Et_3BzN)_2CuCl_4$ (Bz = benzyl) which have flattened tetrahedral anions; their results show that the ions in these two compounds are not magnetically equivalent. Bloembergen[53] examined the magnetic contribution to the specific heat of some layered chlorocuprates(II). Iwashita and Uryu[54] estimated the anisotropic exchange constants in $[(NH_3CH_2CH_2)_2NH_2][CuCl_4]Cl$ using the spin wave analyses of the magnetic susceptibility.

Magnetic measurements have often been employed as a complementary characterisation technique; in particular, previous workers have at times obtained valuable structural information from these measurements. Thus, the similarity between the magnetic parameters

of K_2CuCl_4 and its dihydrate, $K_2CuCl_4.2H_2O$, was taken to indicate that both consist of octahedral anions[55,56]. Siedle et al.[16] obtained for $(TTF)_2CuCl_4$ (refer table 1.2.2) the values of $g_{\|} = 2.232$, $g_{\perp} = 2.053$, $\Delta H_{\|} = 43G$ and $\Delta H_{\perp} = 41G$. From the relatively narrow lines and the spread of the g values, they suggested a parallel arrangement of square-planar $CuCl_4^{2-}$ units, in the crystal, which participate in intramolecular exchange. For $(TTF)CuCl_4$, they obtained $g_{\|} = 2.476$, $g_{\perp} = 2.123$, $\Delta H_{\|} = 69G$ and $\Delta H_{\perp} = 175G$ and suggested, from the line-widths, that there is still appreciable exchange but the g values are consistent with a flattened tetrahedral coordination geometry about copper.

An area of great importance in the magnetic work has been the study of ferromagnetic intracluster exchange such as that of the ferromagnetically coupled $Cu_2Cl_6^{2-}$ dimers in $(Ph_4As)CuCl_3$[32]. The magnetic properties of the analogous $(Ph_4P)CuCl_3$, $(Ph_4Sb)CuCl_3$ and $(n\text{-}PrPh_3P)CuCl_3$ (refer table 1.2.3) have now been thoroughly studied by Estes et al.[30], and some interesting results have emerged. It was found that the ferromagnetic exchange coupling constants ($2J$) in these compounds are consistently larger than that in $(Ph_4As)CuCl_3$; moreover, the EPR data of the two $Cu_2Cl_6^{2-}$ ions with slightly different cations, (Ph_4Sb^+) and ($n\text{-}PrPh_3P^+$), exhibit the best resolved fully anisotropic triplet-state spectra of any polycrystalline complexes yet known. Estes et al. further suggested that the deviations from the simple pair model observed at very low temperatures are the results of intracluster rather than intercluster exchange.

One other important paper which appeared earlier (1974) but was not included in Smith's review[1] is that by Witteveen[57] on the magnetic study of the layer-type compounds, including Rb_2CuCl_4, which have the NH_4CuCl_4-type structure[17]. The magnetic properties of this group of compounds are described by a ferromagnetic intralayer interaction and a much weaker interlayer interaction. Witteveen obtained for Rb_2CuCl_4 $g_{\parallel} = 2.26$, $g_{\perp} = 2.06$ ($g_{powder} = 2.14$), the antiferromagnetic transition temperature $T_N = 13.7^{\circ}K$ and also the values for the intralayer and interlayer exchange parameters J/k and J'/k, and the anisotropy fields.

1.5 *OTHER STUDIES*

1.5.1 *Phase transitions*

There have been several examples[1] of the thermochromic tetrachlorocuprates(II) showing first-order phase transition. The latest addition to this category is $(PipzH.HC\ell)_2CuC\ell_4$ reported by Marcotrigiano et al.[14]. Referring to table 1.2.4, the room-temperature electronic spectrum of this yellow complex shows a d-d band at 11,490 cm^{-1}, which the authors consider to be indicative of an approximately square-planar anion configuration; upon heating to 80 - 95°C, the complex converts to a more intensely coloured form and the d-d band shifts to a lower energy at 10,640 cm^{-1} with a shoulder at 6,760 cm^{-1}, suggesting a change to a distorted tetrahedral configuration[1]. Such a phase transition can be attributed to a weakening of the hydrogen-bonding network, which tends to stabilise square-planar $CuC\ell_4^{2-}$ ions at low temperature, as a result of the increasing disorder due to the thermal motion. It is worth pointing out, however, that all previously reported chlorocuprates(II) with genuine square coplanar $CuC\ell_4^{2-}$ anions are invariably green in colour, and the corresponding electronic spectra include a band at *ca.* 16,000 cm^{-1}. These characteristic features are missing in the room-temperature-phase of $(PipzH.HC\ell)_2CuC\ell_4$ which is yellow; thus, the anions are probably not strictly square-planar, and the phase transition described here may be of quite a different nature to those previously reported.

A recent trend in the study of the thermochromic behaviour of chlorocuprates(II) has been that of pressure effects. Ferraro[58] suggests that pressure-induced phase transition is facilitated by a starting solid phase having a distorted structure. Since the pressure-stable phase is the square-planar configuration, an attempt was made to show that an increase in density occurs as the square-planar structure is approached. Unfortunately, the result was less than spectacular mainly because of insufficient structural parameters to demonstrate a trend, and also because the density is largely determined by the bulk of the cation and only in part by the geometry of the $CuCl_4^{2-}$ anion.

Sherren and Ferraro[59] described the effect exerted by hydrogen-bonding on the anion geometry as the 'internal pressure'. They presented a systematic study of such internal and also the external pressure on the symmetry of the ions MCl_4^{2-}, where M = Mn(II), Fe(II), Co(II), Ni(II) and Cu(II). It was found that considerably less external pressure is required to convert the anions to the pressure-stable phase if there is some degree of distortion of the anion geometry due to the internal pressure. In $(Me_4N)_2CuCl_4$, in which there is no hydrogen-bonding, phase transition was not achieved altogether. This is rather surprising as the distorted tetrahedral anions in Cs_2CuCl_4 have been successfully converted to the square-planar phase at high pressure[60].

Other recent papers dealing with phase transitions in chlorocuprates(II) include those by Soboleva and Vasil'eva[61] on the differential thermal analysis of $CsCuCl_3$, and Sawada et al.[62] who discuss birefringence and optical activity measurements as a way to investigating phase transition that takes place in crystals.

1.5.2 *Nuclear Magnetic Resonance*

The NMR of $^{63}Cu^{2+}$ in $(MeNH_3)_2CuCl_4$, $(EtNH_3)_2CuCl_4$ and $CsCuCl_3$ were observed by pulse methods at 1.75 K[63]; the experimental values were compared with the calculated ones using an ionic model. Also, the Cu^{2+} hyperfine field directions were determined by measuring the $^{63}Cu^{2+}$ magnetic resonance on a single crystal of $CsCuCl_3$ in a d.c. magnetic field[64].

1.5.3 *Dispersion-Induced Circular Dichroism (DICD)*

Schipper[65] suggested the use of dispersion-induced circular dichroism in the assignment of the d-d transitions in Cu(II) complexes. Both the theoretical and the experimental aspects were discussed, and the DICD selection rules derived were deemed useful for spectroscopic assignment.

1.5.4 *Theoretical Studies*

The electronic spectra of the chlorocuprates(II) have been interpreted using various theoretical models[1]. The recent papers in this area are briefly described here.

To explain the apparent anomaly of the electronic spectrum of square coplanar $CuCl_4^{2-}$ ion, Smith[66] proposes an extension to the angular overlap model to include the effects of d-s and d-p mixing; a satisfactory account of the effects of distant ligands in tetragonal $CuCl_6$ chromophores was obtained. Cruse and Gerloch[67] determined from the single-crystal polarised electronic spectrum of Cs_2CuCl_4 the unambiguous values for the angular-overlap ligand

field parameters, e_σ and e_π; these were found to be 6,800 and 1,800 cm^{-1}, respectively. Unfortunately, the crystallographic data[70,71] used in this work were rather out-of-date. McGinnety[5] has considerably refined the crystal structure of Cs_2CuCl_4 whose anions are shown to be more distorted than previously found. It is clear that if Cruse and Gerloch had used these latest structural data, their results would have been siginficantly different.

Smit et al.[68] performed *ab initio* calculation of the charge distribution and the ligand field splitting in $CuCl_4^{2-}$ by means of the restricted Hartree-Fock method. SCF MO calculations were reported for $CuCl_4^{2-}$ ion at the SCF-X_α level and also at the *ab initio* gaussian level using a large basis set[69].

CHAPTER 2 FAR INFRA-RED STUDIES OF TETRAALKYLAMMONIUM BROMOCHLOROCUPRATES(II)

2.1 *INTRODUCTION*

2.1.1 *General*

A range of mixed-halide compounds $(NEt_4)_2ZnX_nY_{4-n}$ (n = 1 - 3) have been characterised and shown to contain discrete tetrahedral $ZnX_nY_{4-n}^{2-}$ anions[72,73]. We have earlier carried out some preliminary investigation of the analogous copper(II) compounds as well as $(NMe_4)_2CuBr_nCl_{4-n}$, and partially characterised them by means of X-ray powder diffraction measurements[74]. In this chapter, we present the continued studies of these compounds and their complete characterisation using far infra-red spectroscopy; part of our results has already been published[75].

2.1.2 *Review of Mixed Halogenocuprates(II)*

Whereas chlorocuprates(II) have been extensively studied[1](see also chapter 1) , much less is known about bromocuprates(II) and very little work has been done on mixed halogenocuprates(II). This is rather surprising as the electronic properties of discrete halocuprate(II) anions with a heterogeneous coordination sphere consisting of more than one type of halogen could be of considerable theoretical interest. Boca[76] successfully applied his extended maximum overlap approximation (EMOA) method to construct the hybrid

atomic orbitals in arbitrary molecules of transition metal compounds; among the molecules or ions he studied were $CuCl_4^{2-}$, $CuCl_3F^{2-}$, cis-$CuCl_2F_2^{2-}$, trans-$CuCl_2F_2^{2-}$, $CuClF_3^{2-}$ and CuF_4^{2-}.

In table 2.1.1, we give the list of mixed halogenocuprates(II) reported in the literature to date. While the list is by no means exhaustive, it is safe to assume that the number of compounds we have cited here is sufficient to highlight all the special features associated with mixed halogenocuprates(II). These are now surveyed under the following categories.

(i) Types of Ligands

Referring to table 2.1.1, except for $K_2CuF_2Cl_2$, all the other compounds are mixed bromochlorocuprates(II). Incorporation of I^- into the coordination sphere of Cu^{2+} has been rarely achieved because of the problems associated with the reduction of Cu^{2+}. Differences in their ionic radii (1.33 Å for F^-, 1.81 Å for Cl^{2-} and 1.96 Å for Br^-) render the F^- ion incompatible with either Cl^- or Br^- ions for heterogeneous coordination to Cu^{2+}. In their preparation of $K_2CuF_2Cl_2$, Witteveen et al.[81] also noted the presence of small amounts of $KCuF_3$ and KCl in the sample; hence the composition of the compound is rather uncertain.

(ii) Types of Cations

Since the existence of mixed halogenocuprates(II) invariably implies that of the corresponding homogeneous halocuprates(II), the cations are similar to those found in the chlorocuprates(II)[1].

TABLE 2.1.1

List of reported mixed halogenocuprates(II)

Compound		Reference
$(Me_3NH)CuBr_nCl_{4-n}$	n = 1, 2, 3	77
$[Li(DA)_2]_2CuBr_nCl_{4-n}$	n = 1, 2, 3	78
$[Cr(NH_3)_6]CuBr_3Cl_2$		79,80
$(Me_2CHNH_3)_2CuBrCl_3$		26
$Rb_2CuBr_nCl_{4-n}$	n = 1, 2	57,81
$K_2CuF_2Cl_2$		81
$(MeNH_3)_2CuBr_nCl_{4-n}$	n = 1, 2, 3	82
$CuBr_nCl_{3-n}^-$	n = 1, 2	83,41
$CuBr_nCl_{3-n}AA^-$	n = 1, 2	84
$(Ph_4P)_2Cu_2Br_nCl_{6-n}$	n = 2, 4	30
$(PipdH)_2CuBr_nCl_{4-n}$	n = 1, 2	12
$(MorphH)_2CuBr_nCl_{4-n}$	n = 1, 2	12
$(NEtmorphH)_2CuBr_nCl_{4-n}$	n = 1, 2, 3	13
$(PipzH.HCl)_2CuBrCl_3$		14
$(PipzH_2)CuBr_nCl_{4-n}$	n = 1, 2	14
$(NPhpipzH)_2CuBr_4Cl_2$		9
$(NPhpipzH_2)CuBrCl_3$		9

Footnote: The abbreviations adopted for the cations in this table have been defined in chapter 1.

In the compounds of table 2.1.1, the range of counter ions include the simple inorganic cations (K^+, Rb^+), the complex inorganic cations ($[Li(diacetamide)_2]^+$, $[Cr(NH_3)_6]^{3+}$), the substituted ammonium cations ($(Me_3NH)^+$, $(Me_2CHNH_3)^+$, $(MeNH_3)^+$), the quaternary phosphonium cations ($(Ph_4P)^+$) and a range of biologically-active complex organic cations (piperidinium, morpholinium, N-ethylmorpholinium, piperazinium mono- and di-, N-phenylpiperazinium mono- and di-cations).

(iii) Methods of Preparation

Most of the mixed halogenocuprates were prepared by crystallisation from the alcoholic solutions containing stoichiometric amounts of starting reagents, (cation)X and CuX_2 where X = Br or Cℓ. However, in their preparation of $(Me_3NH)_2CuBr_nCℓ_{4-n}$ (n = 1 - 3) by reacting $CuBr_2$ and $Me_3NHCℓ$ in ethanol, Il'yukevich and Shagisultanova [77] probably derived at the correct proportions by painstaking trial-and-error approach. Gentile et al.[78] prepared $[Li(DA)_2]_2CuBr_nCℓ_{4-n}$ (DA = diacetamide) using solid-solid interactions. For each synthesis, exact stoichiometric quantities of the starting materials (LiCℓ.2DA, LiBr.2DA, $CuCℓ_2$, $CuBr_2$) were ground to form a paste with water and dried *in vacuo* to yield the anhydrous product. The preparation[57,81] of $Rb_2CuBr_nCℓ_{4-n}$ (n = 1, 2) using solid-solid interactions requires a more drastic experimental condition. This involved melting stoichiometric qunatities of starting materials for two days at 600°C in an evacuated, sealed silica tube and annealed afterwards at temperatures of 50 - 100°C below the melting point of the desired product for two weeks.

Biela et al.[82] employed various methods to prepare $(MeNH_3)_2CuBr_nCl_{4-n}$ (n = 1 - 3). They reported that for n = 1 the product could be obtained by the oxidation of $(MeNH_3)_2CuCl_3$ with bromine vapour at room temperature for 48 hours. It was also found that solid-solid interactions of $CuCl_2$, $CuBr_2$, $MeNH_2.HCl$ and/or $MeNH_2.HBr$ would not proceed in the absence of air moisture; in such a case, only a mechanical mixture of the starting materials was obtained. However, if $CuCl_2.2H_2O$ is used, or when the compounds are ground in air, bromochlorocuprates(II) are obtained.

(iv) Characterisation and Structural Studies

The reported mixed halogenocuprates(II) were mostly characterised by X-ray powder diffraction and electronic absorption spectroscopy. Some workers[9] also employed the differential scanning calorimetric analysis; only a sharp endothermic peak corresponding to their melting point should be indicated if the products are true compounds and not mixtures. In some cases, structural information could be obtained from the nature of the products obtained. Thus, within the series $[Li(DA)_2]_2[CuBr_nCl_{4-n}]$, two different species were obtained for n = 2 depending on the choice of starting materials; the brown isomer, designated $[Li(DA)_2]_2[CuCl_2Br_2]$, was formed from $CuCl_2$ and 2LiBr.2DA whereas the green isomer, $[Li(DA)_2]_2[CuBr_2Cl_2]$, was formed from $CuBr_2$ and 2LiCl.2DA. Based on this evidence as well as the studies of absorption spectra, Gentile et al.[78] concluded that these mixed bromochlorocuprates(II) (n = 1 - 3) are of square-planar or octahedral rather than tetrahedral configurations.

The compounds $(MeNH_3)_2CuBr_nCl_{4-n}$ (n = 1 - 3) were shown[82] to be isomorphous to each other by X-ray powder diffraction; for n = 1, 2, the evidence of electronic absorption spectra indicates that their structures are similar to that of $(MeNH_3)_2CuCl_4$ whose anion is approximately planar with weak axial perturbations[17]. However, unlike the $[Li(DA)_2]_2[CuX_2Y_2]$, no evidence of the formation of cis- and trans- isomers was found for $(MeNH_3)_2CuBr_2Cl_2$.

It is worth noting that the mixed halogenocuprates(II) are not all of ordered structures. Raymond et al.[79,80] reported a dark-red compound of composition $[Cr(NH_3)_6]CuBr_3Cl_2$; their preliminary investigation led to a conclusion of ordered structure[79], however, subsequent structure determination revealed that there was random disorder, in the crystal, of bromine and chlorine atoms between axial and equitorial positions. It was also reported that salts containing anions of the stoichiometry $CuBr_nCl_{5-n}^{3-}$ were generally obtainable; however, in these cases, n was non-integral and continuously variable, and disorder of the halides was evident.

Witteveen et al.[57,81] carried out a detailed structural investigation of the compounds $Rb_2CuBr_nCl_{4-n}$ (n = 0 - 2) and showed that these have the $(NH_4)_2CuCl_4$ structure[17], a deformation of the K_2NiF_4 structure (figure 2.1.1). A significant result of their studies is that the expected ordering between Br and Cl atoms in $Rb_2CuBrCl_3$ and $Rb_2CuBr_2Cl_2$ was confirmed.

Structure of K_2NiF_4[57,81]

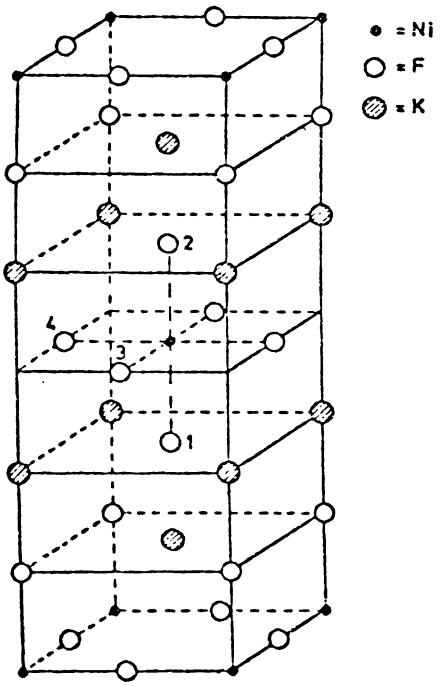

Referring to figure 2.1.1, two different crystallographic sites exist for the halogen atom. It was argued that the Br atom, being larger than Cℓ and hence more polarizable, would prefer positions 1 and 2 where it is coordinated by five Rb atoms and one Cu atom, and the linear configuration is Rb-Br-Cu. A less favourable situation arises if Br substitution takes place at positions 3 and 4 where it would be coordinated by four Rb and two Cu atoms, and the linear configuration is Cu-Br-Cu. Thus, it is expected that in $Rb_2CuBr_2Cl_2$, where one-half of Cℓ atoms are replaced by Br atoms, the anion structure should be in the

form of ($CuCl_4Br_2$) octahedra with Cl atoms occupying the equitorial positions (sites 3 and 4) and the Br atoms occupying the axial positions (sites 1 and 2). In the case of $Rb_2CuBrCl_3$, two possible structures could be expected:

(A) equal number of ($CuCl_6$) and ($CuCl_4Br_2$) octahedra;

(B) only ($CuCl_5Br$) octahedra in which Br atoms always occupy the axial positions.

Witteveen et al.[81] were able to show that $Rb_2CuBr_2Cl_2$ has the expected structure with ordered ($CuCl_4Br_2$) octahedra, and that in $Rb_2CuBrCl_3$, both ($CuCl_6$) and ($CuCl_4Br_2$) octahedra are present in 1:1 ratio and probably randomly distributed through the lattice. There was no evidence of ordered structure in the form of ($CuCl_5Br$) octahedra. The same group of workers [81] also reported a successful synthesis of $K_2CuF_2Cl_2$ but no structural analysis.

Mixed halogenocuprates(II) in solutions have also been reported. Kompisova and Gazo [83] showed by electrochemical methods the presence of complex ions $CuBr_nCl_{3-n}^{-}$ (n = 0 - 3) and $CuBr_nCl_{4-n}^{2-}$ (n = 0 - 4) in the system Cu^{2+}-Cl^{-}-Br^{-}-acetone. Earlier, Biela et al.[84] reported a spectrophotometric study of the system $Cu(ClO_4)_2.6H_2O$-LiCl-LiBr-AA (AA = acetic acid anhydride) in which the complex ions $CuCl_3AA^{-}$, $CuBrCl_2AA^{-}$, $CuBr_2ClAA^{-}$ and $CuBr_3AA^{-}$ were present in equilibrium at X/Cu ratio of 3 (X = Cl + Br). The absorption spectra in the near infra-red region of the solutions containing varying Br:Cl ratios were quite similar to those of $CuCl_3AA^{-}$ and $CuBr_3AA^{-}$, all showing

an absorption band at 11,500 cm^{-1}; this was taken to indicate that the symmetry of the complex anion $CuX_nY_{3-n}^-$ was not substantially affected by changes in the coordination sphere. Ludwig and Textor[41] also detected the presence of $CuBr_nCl_{3-n}^-$ species in the system Cu^{2+}-Br^--Cl^--CH_2Cl_2; their studies showed that the stability of these complexes decreases in the order $CuBr_3^-$ > $CuBr_2Cl^-$ > $CuBrCl_2^-$ > $CuCl_3^-$. This is in the opposite order to that reported[77] for the $CuBr_nCl_{4-n}^{2-}$ complex ions in acetone.

Nevertheless, the existence of monomeric CuX_3^- species, even in solution, deserves more careful investigation. When isolated from the solution as their complex salts of the type (cation)CuX_3, the anions were invariably shown[30,31] to exist as dimers $Cu_2X_6^{2-}$. Estes et al.[30], in the course of their studies of such dimeric species containing halogen bridges between copper(II) ions, prepared and characterised the Ph_4P^+ complexes of mixed halides, $(Ph_4P)_2Cu_2Br_nCl_{6-n}$ (n = 0, 2, 4, 6). The studies of their electronic spectra in the near infra-red and the visible regions led to the suggestion that the Cu^{2+} ions are in a distorted tetrahedral environment in the mixed-halide species. From the magnetic data as well as the far infra-red spectra of the mixed-halide compounds in the region of Cu-Cl stretching frequencies, it was further deduced that the bridging units involve chloride ions only.

Very recently, Marcotrigiano et al.[9,12-14] prepared a wide range of mixed bromochlorocuprates(II) using a variety of biologically-active organic cations which differ in their sizes or hydrogen-

bonding abilities. Characterisation was carried out by means of far infra-red, infra-red and near infra-red spectroscopy, magnetic moments and conductivity measurements. Various geometries of the anions were obtained; these could generally be explained in terms of the effects of size or hydrogen-bonding due to the cations. The piperidinium cation and the morpholinium cation have nearly identical dimensions, but the latter is recognised to have greater hydrogen-bonding ability. Thus, the anions in $(MorphH)_2CuCl_4$ and $(MorphH)_2CuBrCl_3$ are found to be nearly square-planar while the $CuBr_2Cl_2^{2-}$ anion in $(MorphH)_2CuBr_2Cl_2$ has a distorted tetrahedral structure since the decrease in the number of Cl atoms causes an increase in the disorder of the hydrogen-bonding. In $(PipdH)_2CuBr_nCl_{4-n}$ (n = 1, 2), all the anions have distorted tetrahedral structure. The studies of the hydrogen-bonding effect on the anion geometry was extended to the bromochlorocuprates(II) of piperazinium mono- and di- cations, and consistent results were obtained [14]. The interesting compound in this series is the thermochromic salt, $(PipzH.HCl)_2CuBrCl_3$ which changes from a red-orange colour at room temperature to a more intense colour upon heating to 80 - 95°C, and the accompanying electronic spectrum shifts to longer wavelengths of the d-d transitions. This indicates a phase transition involving a change in the coordination geometry, from the near square-planar to the distorted tetrahedral, induced by a weakening of the hydrogen-bonding network as a result of the increasing disorder due to the thermal motion. The study of the size effect was carried out with compounds of

N-phenylpiperazinium mono- and di- cations[9] as well as N-ethylmorpholinium cation[13]. The prediction of distorted tetrahedral anions as a result of having such bulky cations was largely realized experimentally, and a dimeric species $CuBr_4Cl_2^{2-}$ was found with the N-phenylpiperazinium mono-cation.

(v) Summary

Various methods have been employed in the preparation of mixed halogenocuprates(II). Characterisation of the products was largely carried out by means of X-ray powder diffraction and electronic absorption spectroscopy. To date, structural studies and the effects of the cations on the anion geometries have been the focus of interest.

It is seen from table 2.1.1 that where the compounds are prepared as a series of the same cation, there are sometimes noticeable gaps with compounds missing, especially when $n > 2$. Presumably, increasing Br content causes structural disorder in these cases. Where ordered structures do exist in a bromochlorocuprate(II), increasing substitution of the Cl atoms by Br has been found to be disruptive to the NH ... Cl hydrogen-bonding network, giving rise to distorted tetrahedral anions[12].

In conclusion, it is clear from this survey that the studies of mixed halogenocuprates(II) have only begun to receive attention since the turn of the decade. In the light of the ever-increasing interest in homogeneous halocuprates(II), the studies of the mixed-halide compounds provide a refreshingly

new but closely related area of research which could prove both interesting and fruitful as is evident from the works of Witteveen et al.[57,81] and Marcotrigiano et al.[9,12-14]. Areas which remain to be further explored include the vast field of theoretical and experimental magnetic studies which have recently attracted workers such as Zaspel and Drumheller [85].

2.2 *EXPERIMENTAL*

The compounds were prepared by dissolving anhydrous cupric bromide, cupric chloride, tetraalkylammonium bromide and tetraalkylammonium chloride in ethanol*, in the appropriate stoichiometric proportions; the products were recovered by removal of the solvent in a rotary evaporator. In all cases, the products were recrystallised at least once from alcohol. The bromotrichlorocuprates(II) appeared red, the dibromodichlorocuprates(II) deep purple, and the tribromochlorocuprates(II) black.

As described before [74], the compounds could be analysed for copper using the atomic absorption method, for carbon, hydrogen and nitrogen using micro-analytical techniques and for halogens using gravimetric analyses. In the present work, only the last analyses were carried out since there was no apparent irregularity in the method of preparation, and the products were obtained in a straightforward manner as before. The results are shown in table 2.2.1.

It is noted that although satisfactory element analyses were obtained for all the products, they do not materially assist in their characterisation. In order to obtain samples which were free from ethanol, it was necessary to remove the solvent completely by evaporation; since no other volatile products were present, the analytical results reflect the purity of the starting materials and the errors inherent in the analytical methods, rather than the purity of the product.

* In the case of tetramethylammonium bromide, addition of methanol was necessary to enhance solubility.

TABLE 2.2.1

Gravimetric analyses for halogen in $(NR_4)_2CuBr_nCl_{4-n}$; R = Me, Et, n = 0 - 4

	% Halogen	
	Calc	Expt
$(Me_4N)_2CuCl_4$	40.10	39.39
$(Me_4N)_2CuBrCl_3$	46.79	44.75
$(Me_4N)_2CuBr_2Cl_2$	52.13	51.03
$(Me_4N)_2CuBr_3Cl$	56.50	55.21
$(Me_4N)_2CuBr_4$	60.14	59.61
$(Et_4N)_2CuCl_4$	30.44	29.13
$(Et_4N)_2CuBrCl_3$	36.50	34.99
$(Et_4N)_2CuBr_2Cl_2$	41.59	40.11
$(Et_4N)_2CuBr_3Cl$	45.92	43.93
$(Et_4N)_2CuBr_4$	49.66	48.97

X-ray powder diffraction measurements were made on a Phillips PW 1130 X-ray spectrometer, copper K_α radiation being used. These appeared identical to those reported earlier[74] and hence confirmed that similar products had been obtained.

The infra-red spectra were measured at room temperature as Nujol mulls, on a Perkin-Elmer 180 spectrophotometer which was thoroughly purged with dry nitrogen. Polythene cell windows were used as these are transparent in the far infra-red region (below 300 cm^{-1}). Only low-resolution spectra were measured, and the band positions were accurate to ± 2 cm^{-1}. In all cases the Cu-halogen stretching frequencies were readily distinguishable (between 150-300 cm^{-1}). The same cannot be said of the bending frequencies. These were much less clearly observed since they were partly obscured by broad, poorly resolved lattice mode absorption below 100 cm^{-1}.

2.3 *RESULTS AND DISCUSSION*

The compounds of compositions $(NR_4)_2CuBr_nCl_{4-n}$ (n = 1 - 3) were isolated with little experimental difficulty. However, these do not necessarily contain discrete $CuBr_nCl_{4-n}^{2-}$ ions. Such a product could be a mixture of the tetrabromo-and tetrachlorocuprate(II), or might be a compound containing discrete $CuBr_4^{2-}$ and $CuCl_4^{2-}$ ions in the ratio n : (4 - n). There is also the possibility of a disordered structure, with a more or less random distribution of bromide and chloride ligands about the metal ions. It appeals to reason that X-ray powder diffraction patterns should reveal the presence of mixtures, while far infra-red spectra in the metal-halogen stretching and bending region (100-300 cm^{-1}) may indicate the nature of the anionic species present.

In our earlier work[74], the X-ray powder diffraction results showed quite clearly that the products were not mixtures of $(NR_4)_2CuBr_4$ and $(NR_4)_2CuCl_4$; the powder patterns of such mixtures showed, as expected, lines due to both components. In contrast, the lines observed in the mixed halide products were distinctively unique. In the tetramethylammonium series (n = 0 - 4), there is an almost perfect line-for-line correspondence. Since $(NMe_4)_2CuCl_4$ is known[86] to crystallise in the orthorhombic space group $Pnma(D_{2h}^{16})$, the tetramethylammonium compounds constitute an isomorphous series in this space group. Similarly, the tetraethyl-ammonium compounds are isomorphous with $(NEt_4)_2CuCl_4$ which belongs to the tetragonal space group $P4/nmm(D_{4h}^{7})$[87].

We also measured the diffuse reflectance spectra of the compounds in the near infra-red[75]; these appeared closely similar to one another, with a broad band at about 9000 cm^{-1}. This shows that all the compounds contain discrete $CuBr_nCl_{4-n}^{2-}$ anions, with the flattened tetrahedral configuration. However, since bromide appears to be very much like chloride in its crystal field splitting effects in copper(II) compounds[88], the *d-d* spectra give little other information about the anions.

The room-temperature low-resolution far infra-red spectra of $(NR_4)_2CuBr_nCl_{4-n}$ (R = Et, Me; n = 0 - 4) have now been measured during the course of this work. Their frequencies as given in table 2.3.1 are classified into Cu-Cl stretches, Cu-Br stretches and X-Cu-Y deformations where X,Y = Br or Cl.

Referring to table 2.3.1, the spectra of the tetraethylammonium compounds can be satisfactorily interpreted within the isolated-ion approximation in terms of flattened tetrahedral $CuBr_nCl_{4-n}^{2-}$ ions, particularly in the copper-halogen stretching region; such a configuration is indicated by the diffuse reflectance spectra as discussed earlier. The $CuCl_4^{2-}$ and $CuBr_4^{2-}$ anions may be taken to have D_{2d} symmetry; $CuBrCl_3^{2-}$ and $CuBr_3Cl^{2-}$ are likely to have C_s symmetry while $CuBr_2Cl_2^{2-}$ is expected to be approximately C_{2v}. Thus, within the isolated-ion approximation, the infra-red selection rules predict the following copper-halogen stretching modes:

$CuCl_4^{2-}$: two Cu-Cl stretches (b_2 and e);

$CuBrCl_3^{2-}$: three Cu-Cl stretches ($2a'$ and a'') and one Cu-Br stretch (a');

o

TABLE 2.3.1

Far infra-red spectra (80-300 cm^{-1}) of $(NR_4)_2CuBr_nCl_{4-n}$; R = Et and Me, n = 0 - 4

compound	ν(Cu-Cl)	ν(Cu-Br)	δ(X-Cu-Y)
$(NEt_4)_2CuCl_4$	265 s, 243 m	-	113 w, 116 m
$(NEt_4)_2CuBrCl_3$	271 s, 255 sh	186 m	109 m
$(NEt_4)_2CuBr_2Cl_2$	269 s, 255 sh	185 s (*br*)	100 m (*br*)
$(NEt_4)_2CuBr_3Cl$	272 m	208 s, 171 m	88 m (*br*)
$(NEt_4)_2CuBr_4$	-	210 s, 172 m	85 m
$(NMe_4)_2CuCl_4$	276 s, 264 s, 234 m	-	143 s, 126 s
$(NMe_4)_2CuBrCl_3$	279 sh, 271 s	199 w, 186 m, 179 m	118 m
$(NMe_4)_2CuBr_2Cl_2$	275 s, 264 sh	207 sh, 197 s, 165 m	116 m
$(NMe_4)_2CuBr_3Cl$	273 m, 269 sh	213 s, 204 sh, 166 m	100 m
$(NMe_4)_2CuBr_4$	-	212 s, 164 m	87 s

$CuBr_2Cl_2^{2-}$: two Cu-Cl stretches (a_1 and b_1) and
two Cu-Br stretches (a_1 and b_1);

$CuBr_3Cl^{2-}$: one Cu-Cl stretch (a') and
three Cu-Br stretches ($2a'$ and a'');

$CuBr_4^{2-}$: two Cu-Br stretches (b_2 and e).

There appeared little doubt that these predictions are largely fulfilled in the tetraethylammonium compounds. The frequencies we measured for $(Et_4N)_2CuCl_4$ and $(Et_4N)_2CuBr_4$ agree satisfactorily with those previously reported[89] for the same compounds; these correpsond nicely to an interpretation in D_{2d} symmetry of the anions. In $(NEt_4)_2CuBr_2Cl_2$, rather poor resolution was obtained in the Cu-Br stretching region and only the centre of gravity of this band was reported. However, this band is so broad that it is conceivable that two bands are enveloped in it. Thus, the spectrum could be interpreted in terms of a C_{2v} symmetry for the $CuBr_2Cl_2^{2-}$ anion. It is noted that no possible isomers should exist if $CuBr_2Cl_2^{2-}$ is a discrete entity with flattened tetrahedral structure; and indeed, all the evidences point to there being only one form of such an anion. The spectra of the tetraethylammonium salts containing $CuBrCl_3^{2-}$ and $CuBr_3Cl^{2-}$ anions showed one less band in the Cu-halogen stretching region than could be interpreted in terms of C_s symmetry. However, poor resolution or accidental degeneracy of two bands could be the reasons why the splitting of the D_{2d} e modes is not observed in such anions. In figure 2.3.1, the spectra for the series of compounds, $(NEt_4)_2CuBr_nCl_{4-n}$ (n = 0 - 4), are given. As these were measured under different conditions for optimal quality, valid comparison can only be made on their relative band positions and not on the relative intensities across the spectra.

Figure 2.3.1

Far infra-red spectra of $(NEt_4)_2 CuBr_n Cl_{4-n}$; n = 0-4

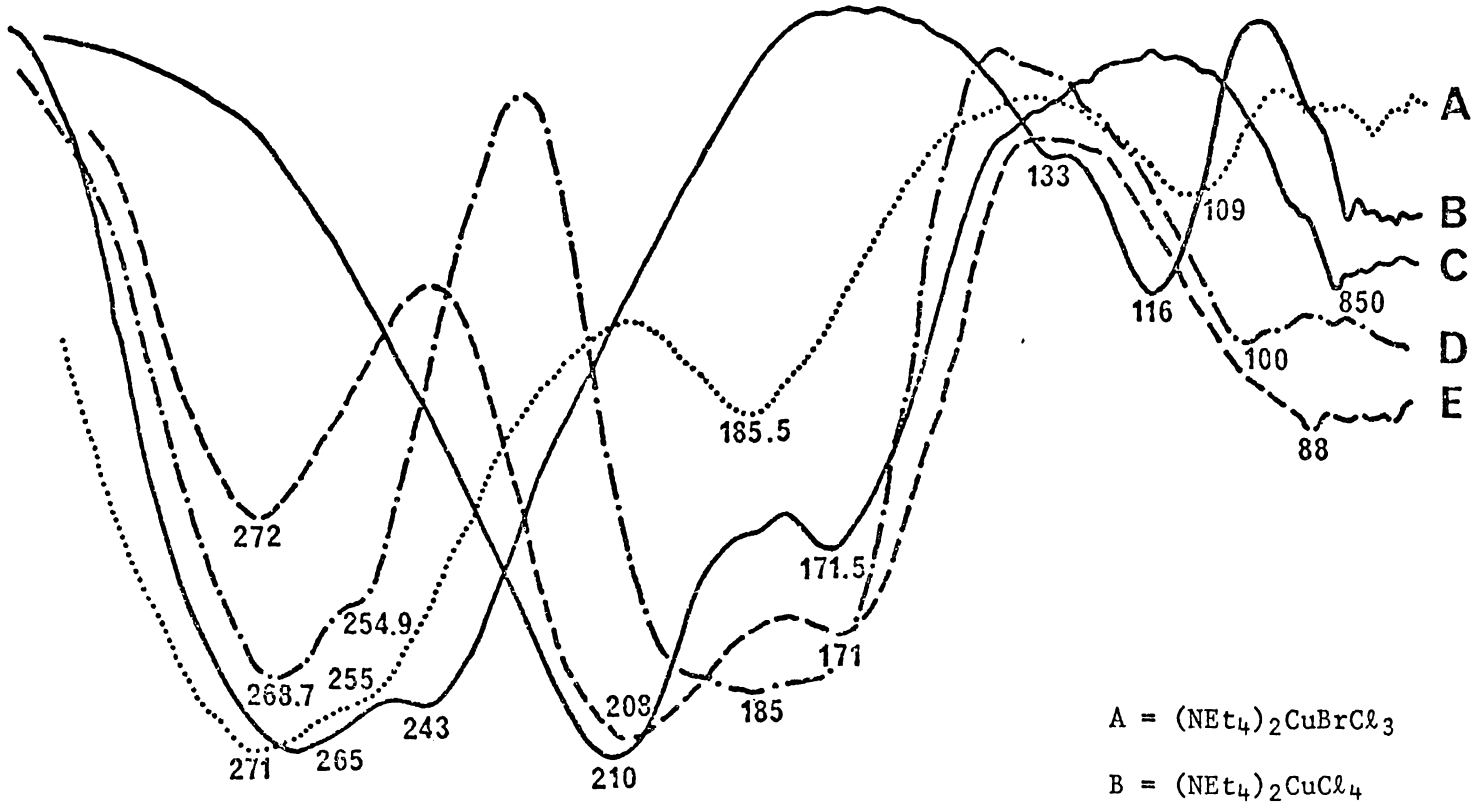

A = $(NEt_4)_2CuBrCl_3$

B = $(NEt_4)_2CuCl_4$

C = $(NEt_4)_2CuBr_4$

D = $(NEt_4)_2CuBr_2Cl_2$

E = $(NEt_4)_2CuBr_3Cl$

The spectra of the tetramethylammonium compounds cannot be simply interpreted in terms of the isolated-ion approximation. Referring to table 2.3.1 again, more bands are observed than would be predicted. This might be taken to indicate that these are not pure homogeneous compounds and that there is disorder of the halides around the metal ions. However, there are other possible explanations for the apparently excessive number of bands. Factor group splitting is expected to be more marked in the tetramethylammonium compounds; the smaller cation, relative to Et_4N^+ cation, should lead to stronger cation-anion and anion-anion interactions. In the low-temperature, polarised single-crystal reflectance spectrum of $(NMe_4)_2CuCl_4$ [90], the higher isolated-ion stretching mode $\nu(e)$ is seen to be split by *ca.* 10 cm^{-1}. Even after allowing for factor group splitting, there are too many bands in some of the compounds. In $(NMe_4)_2CuBrCl_3$, three bands are observed in the Cu-Br stretching region; factor group analysis predicts only two. Such 'extra' bands have also been observed in the high-resolution spectrum of $(NMe_4)_2CuCl_4$, and were attributed to small rotational displacements of the anions, removing some of the mirror planes in the unit cell [90]. It should also be noted that X-ray analysis reveals a tripling of the unit cell along the *a*-axis in this compound [86]. This may not be very significant from the crystallographic point of view, but could have important implications for the interpretation of spectra.

Thus, the infra-red spectra of the tetramethylammonium compounds fail to provide any firm evidence for the presence of only one type of anion in each mixed-halide product. However, it is not possible to interpret the infra-red spectra on the basis that each mixed-halide

system contains more than one type of anion, assuming that each bromochlorocuprate(II) anion has a unique spectrum whose features should be evident in any compound which contains it to any great extent. A mull sample as prepared by grinding an approximately 1:1 mixture of $(Et_4N)_2CuCl_4$ and $(Et_4N)_2CuBr_4$ produced an infra-spectrum closely similar to one by superimposing the spectra due to both compounds; in contrast, the spectrum of $(Et_4N)_2CuBr_2Cl_2$ exhibits distinctive features which could be interpreted in terms of approximately C_{2v} symmetry of the $CuBr_2Cl_2^{2-}$ anion.

2.4 *CONCLUSION*

We report two new series of bromochlorocuprates(II) in $(NMe_4)_2CuBr_nCl_{4-n}$ and $(NEt_4)_2CuBr_nCl_{4-n}$ (n = 1, 2, 3). These were characterised by X-ray powder diffraction[74] and far infra-red spectroscopy. Within each series, the compounds are isomorphous with each other and with the corresponding compounds where n = 0, 4. All the compounds contain $CuBr_nCl_{4-n}^{2-}$ anions, with flattened tetrahedral configurations. In particular, the tetraethylammonium compounds appear to contain discrete $CuBr_nCl_{4-n}^{2-}$ anions with ordered structures, no doubt due to the bulky and hence highly stabilising NEt_4^+ cations[91]. In the tetramethylammonium compounds less is known about the nature of the anions; however, it appears plausible that lattice interactions are more pronounced here, rendering an interpretation within the isolated-ion approximation relatively inappropriate.

During the course of this work, our attention was drawn to the assignment problems of the vibrational spectra of tetrachlorocuprates(II). We would have liked to interpret the infra-red spectra of our compounds in more detail; however, such attempts were restricted by insufficient experimental basis as well as the rather obscure literature in this area. Insofar as the spectra on polycrystalline samples are concerned, splitting of the tetrahedral t_2 modes is evident in the $CuCl_4^{2-}$ anion; however, no attempt has been made to identify the (b_2 + e) modes which are the corresponding vibrations under D_{2d} symmetry. In principle, experimental evidence such as that provided by the single-crystal

vibrational spectra should lead to unequivocal assignment of the crystal modes which could then be correlated with the isolated-ion modes. Our research into the literature revealed that rather confusing and sometimes contradictory assignments of the single-crystal vibrational spectra of tetrachlorocuprates(II) have been reported; these problems are discussed in chapter 3. We propose that, in the absence of conclusive experimental evidence, normal coordinate analysis could be useful as a tool to derive the correct assignment. Investigations into this area are detailed in the ensuing chapters.

CHAPTER 3 NORMAL COORDINATE ANALYSIS OF ISOLATED $CuCl_4^{2-}$ ION

3.1 *INTRODUCTION*

Of all the reported chlorocuprates(II),[1] caesium tetrachlorocuprate(II), Cs_2CuCl_4, in particular, has been most thoroughly studied. Its crystal structure has been determined and refined three times in the past[70,71,5]; its magnetic properties (including e.s.r. spectra) have been minutely examined[67,92-98]; its electronic spectrum, both in the ligand field and charge transfer regions, has been the subject of much experimental[99-101] and theoretical[66,102-107] work; its infra-red and Raman spectra have been measured[109-113]; and it has been the subject of thermochemical[114-116], ^{133}Cs n.m.r.[117], ^{35}Cl n.q.r.[118] and high pressure optical absorption[60] studies. In view of the great interest in this compound, it is noteworthy that the interpretation of its vibrational spectrum remains a controversial issue. In this section, we shall discuss in detail the assignment problems associated with the vibrational spectrum of Cs_2CuCl_4.

3.1.1 *$CuCl_4^{2-}$ Anion in Cs_2CuCl_4*

In his comprehensive review on the subject, Smith[1] saw fit to classify chlorocuprates(II) into various structural types irrespective of stoichiometry. Thus, Cs_2CuCl_4 belongs to the category of chlorocuprates(II) containing discrete $CuCl_4^{2-}$ ions.

Within this category, the geometry of an anion about the central copper atom approximates a flattened tetrahedron (figure 3.1.1) in which two Cℓ-Cu-Cℓ angles, θ, are larger than the tetrahedral angle of 109.5° while four Cℓ-Cu-Cℓ angles, ϕ, are smaller than 109.5°. By convention, θ provides a measure of the extent of distortion of $CuCl_4^{2-}$ anions from the regular tetrahedral symmetry.

Figure 3.1.1

Flattened tetrahedral structure of a $CuCl_4^{2-}$ ion

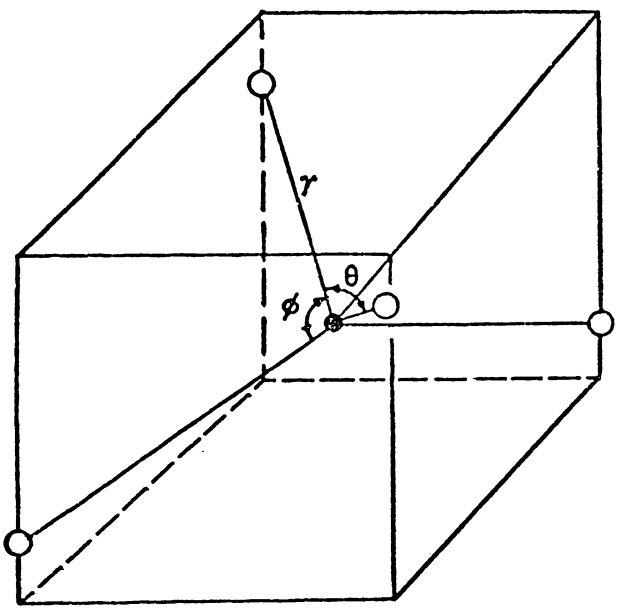

● Copper atom

○ Chlorine atom

In practice, the geometrical parameters in a discrete $CuCl_4^{2-}$ ion very seldom correspond exactly to a regular flattened tetrahedron. However, to a good approximation, the bond lengths and bond angles (θ, ϕ) can be averaged so that an idealised D_{2d} symmetry is achieved.

Cs_2CuCl_4 crystallises in the orthorhombic space group *Pnma*-$D_{2h}^{16}(Z=4)$[5]. The $CuCl_4^{2-}$ ions are discrete, and they are of approximately D_{2d} symmetry although the site symmetry at the Cu atoms is strictly C_s. The mean of the two larger Cl-Cu-Cl angles, θ, is 129.2°, while the four smaller angles, ϕ, have a mean value of 100.6° (refer figure 3.1.1). The mean Cu-Cl bond length is 2.23 Å.

Smaller alkali metal counter ions like Rb^+ and K^+ can only stabilise tetragonally-elongated $CuCl_6$ octahedra, each of which has four short Cu-Cl bonds and two long bonds. In the absence of hydrogen bonding here, the size of the counter ions is the dominant factor governing the coordination geometry of the $CuCl_4^{2-}$ ions. Thus, Cs^+ cation possibly represents, by virtue of its size, the lower limit of all simple inorganic cations that stabilise discrete D_{2d} $CuCl_4^{2-}$ anions.

3.1.2 *Isolated-Ion Modes*

For an isolated $CuCl_4^{2-}$ ion with idealised D_{2d} symmetry, group theoretical methods show that the irreducible representations of the fundamental modes are $(2a_1 + b_1 + 2b_2 + 2e)$. Hence, in accordance with the vibrational selection rules, we expect in the infra-red two stretching modes, $\nu(e)$ and $\nu(b_2)$, with bending modes $\delta(e)$ and $\delta(b_2)$ at lower energy. In addition, there is the Raman-active stretching mode, $\nu(a_1)$, and the Raman-active bending modes $\delta(a_1)$ and $\delta(b_1)$. The correlation between the fundamental modes of idealised T_d, D_{2d} and D_{4h} symmetries for a MX_4 species is as shown in figure 3.1.2.

Figure 3.1.2

CORRELATION TABLE FOR MX_4 SPECIES OF SYMMETRIES T_d, D_{2d} & D_{4h}

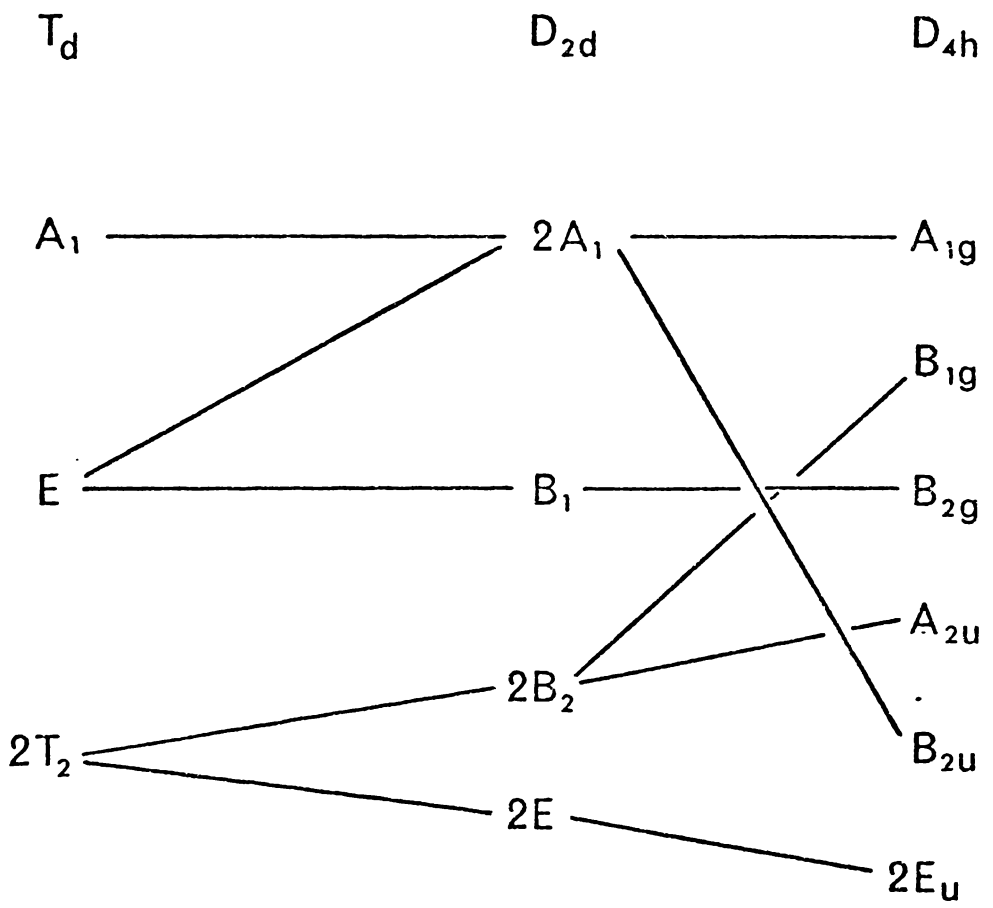

When the t_2 modes of tetrahedral symmetry split under D_{2d} symmetry, it is not immediately apparent which of the b_2 and e modes should be higher in energy. However, if the experimental evidence, such as from the vibrational spectum, is unambiguous, the order can usually be unravelled without much difficulty. Sherren and Ferraro[59] argued qualitatively that under D_{2d} symmetry the $\nu(e)$ mode should always be higher in energy than $\nu(b_2)$ because, with further symmetry degradation to the D_{4h} symmetry, the latter mode becomes an out-of-plane bending mode, $\delta(a_{2u})$, of lower energy while the former becomes a $\nu(e_u)$ mode of almost equal energy. A serious flaw of this argument is, of course, that $\nu(b_2)$ mode of D_{2d} symmetry does not correlate with $\delta(a_{2u})$ mode of D_{4h} but indeed with $\nu(b_{1g})$ mode.

Nevertheless, similar qualitative arguments can be extended in support of the ordering $\nu(e)$ higher than $\nu(b_2)$. In the infra-red spectra of tetrachlorocuprates(II) containing discrete D_{2d} anions, the higher-energy band in the Cu-Cℓ stretching region is always the more intense[1]. This would suggest its assignment to $\nu(e)$ rather than $\nu(b_2)$, particularly when it is noted that the latter correlates with the Raman-active $\nu(b_{1g})$ mode in the limit of square coplanarity (D_{4h}). If we imagine that the isolated-ion $\nu(t_2)$ stretching mode in a tetrahedral anion consists of three degenerate bands of equal intensity, then a slight distortion towards D_{2d} symmetry by flattening the tetrahedron just to the point where $\nu(e)$ and $\nu(b_2)$ can be resolved should lead to the observation in the infra-red two bands whose relative intensities are in the ratio 2:1. As the tetrahedron is further distorted towards D_{2d} symmetry, this intensity ratio should increase to infinity in the limit of square coplanarity. However,

it is not necessarily obvious that this intensity ratio between $\nu(e)$ and $\nu(b_2)$ should increase monotonically although a reversal of their relative intensities at some point between T_d and D_{4h} would be surprising. It appears[119,120] that in square coplanar molecules and ions, $\nu(e_u)$, which correlates with $\nu(e)$ in D_{2d}, is always found at higher energy than $\nu(b_{1g})$. It is therefore reasonable to suppose that $\nu(e) > \nu(b_2)$ in D_{2d} if the splitting of the tetrahedral $\nu(t_2)$ increases monotonically as the tetrahedron is flattened towards D_{4h}. The vibrational spectrum of the discrete, square coplanar $CuCl_4^{2-}$ ion has yet to be analysed in detail, but in $(MeNH_3)_2CuCl_4$, which contains planar $CuCl_4^{2-}$ ions linked by long axial Cu-Cl bonds, bands around 190 cm^{-1} in the Raman spectrum have been associated with the isolated ion $\nu(b_{1g})$[112], and in studies of pressure effects on the structures of chlorocuprates(II), the appearance of a band around 180 cm^{-1} has been taken to indicate a transition to a phase containing square coplanar anions[121]. It would appear that in square coplanar $CuCl_4^{2-}$ ion, $\nu(e_u)$ lies some 60-80 cm^{-1} higher in energy than $\nu(b_{1g})$, so that in Cs_2CuCl_4, where θ is 129.2° compared with 109.5° for T_d symmetry and 180° for D_{4h}, we might reasonably expect $\nu(e)$ to be some 20-30 cm^{-1} higher in energy than $\nu(b_2)$.

Such qualitative arguments cannot be justifiably extended to the bending region of the vibrational spectra. The bending modes of chlorocuprates(II) usually lie below 150 cm^{-1} [1], and interactions with the lattice modes are a distinct possibility. Only experimental evidence can shed some light as to their proper assignments.

Isolated-ion modes are usually obtained experimentally from low-resolution spectra on polycrystalline material. In high-resolution measurements on single crystals, factor group perturbations may lead to a large number of bands. Figure 3.1.3 shows the correlation of D_{2d} ion modes with the site group C_s and the factor group D_{2h}, as is relevant to Cs_2CuCl_4 crystal[5].

3.1.3 *Observed Vibrational Frequencies*

Chlorocuprate(II) anion vibrations occur in the far infra-red region[1], usually below 300 cm^{-1}. Work in this low-energy region was technically difficult until about 1960. Early infra-red studies on Cs_2CuCl_4 were carried out on polycrystalline samples using absorption techniques[108-111]; as a result, only very broad bands were observed and the spectra showed no factor group splitting. The only single-crystal infra-red spectrum reported by far is that of Dunsmuir and Lane[113] who employed polarised reflectance techniques.

Cs_2CuCl_4 exists as bright yellow solid at room temperature. Such highly coloured species were beyond the means of conventional Raman spectroscopy until the development of laser techniques about fifteen years ago. The first report on the Raman spectrum of Cs_2CuCl_4 was by Avery et al.[110] who used powdered samples. Since then, the single-crystal Raman spectrum of the compound has been measured by Beattie et al.[112].

Table 3.1.1 is a summary of the vibrational frequencies of Cs_2CuCl_4 reported in the literature. Where measurements were made on single crystals, only the internal modes are included in the table. All the spectra were measured at 298°K.

Figure 3.1.3

CORRELATION TABLE FOR Cs_2CuCl_4

SPACE GROUP D_{2h}^{16}

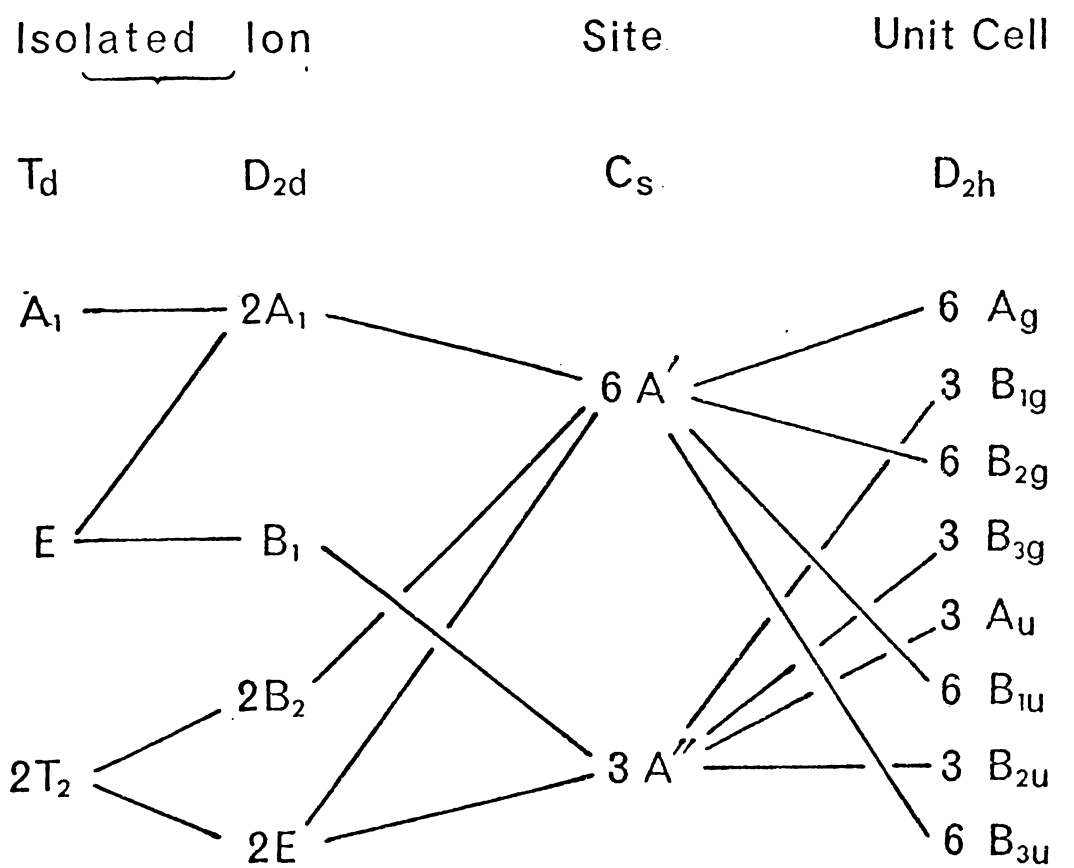

TABLE 3.1.1

Vibrational frequencies of Cs_2CuCl_4 from the literature

$\nu(cm^{-1})$	$\delta(cm^{-1})$	Technique*	Reference
288, 256	-	IR	[109](1963)
292, 257	-	IR	[108](1967)
288, 255	-	IR	[110](1968)
295, 265	-	IR	[111](1969)
292, 260	149, 126	IR	[113](1971)
295, 250	134, 116	R	[110](1968)
299, 253	140, 121, 106	R	[112](1969)
297, 280, 256, 253, 251	149, 141, 136, 126, 120, 105, 103	RC	[112](1969)

* IR = Infra-red, powder

IRC = Infra-red, single-crystal

R = Raman, powder

RC = Raman, single-crystal

We consider, for the meanwhile, only the powder spectra. As seen from table 3.1.1, the frequencies correspond closely to the prediction of vibrational selection rules. Two stretching and two bending modes are observed in the infra-red; in the Raman, the additional a_1 modes are also observed. Bands at 295 and 299 cm^{-1} are very intense, and are undoubtedly the totally

symmetric a_1 modes. In these cases, the higher of the e or b_2 stretching modes could conceivably be obscured hence unobserved. The means of the $\nu(e)$ and $\nu(b_2)$ modes, without specifying their exact ordering, then, are 291.0 and 256.6 cm^{-1}, amounting to a splitting of 34.4 cm^{-1} of the parent tetrahedral $\nu(t_2)$ mode. The means of the corresponding bending modes are 141 and 121 cm^{-1}; however, these modes can only be regarded as approximate for reasons mentioned earlier.

We now discuss the single-crystal Raman spectrum of Cs_2CuCl_4 in more detail. Beattie et al.[112] observed 12 of the 18 Raman-active internal modes as well as 10 lattice modes. Tentative assignments of the internal modes were made, and the bands were correlated with their isolated-ion parentage (refer figure 3.1.3) These are now reproduced in table 3.1.2.

Referring to table 3.1.2, the band at 280 cm^{-1} was assigned to a crystal component of $\nu(b_2)$, while bands at 256, 253 and 251 cm^{-1} were assigned to components of $\nu(e)$. Referring to the correlation diagram (figure 3.1.3), only two bands, namely a_g and b_{2g}, at most should appear in the Raman as components of $\nu(b_2)$ while four, namely a_g, b_{1g}, b_{2g} and b_{3g}, are expected from $\nu(e)$. However, the band at 253 cm^{-1} is very weak[112] and could be a combination band. If this were the case, then an alternative assignment would be possible by placing the components of $\nu(e)$ (only one observed band in this case) at higher energy than those of $\nu(b_2)$. In the bending region, crystal modes at 149, 141 and 136 cm^{-1} were correlated with $\delta(e)$ while bands at 126 and 120 cm^{-1} with $\delta(b_2)$. Here, again, the alternative assignment is possible if bands at 141 and 136 cm^{-1} are grouped with those at 126 and 120 cm^{-1} and collectively assigned as components

TABLE 3.1.2

Single-crystal Raman measurements for Cs_2CuCl_4 and tentative assignments[112]

Frequency (cm^{-1})	Crystal Mode (D_{2h})	Internal Mode (D_{2d})
297	$a_g + (b_{2g}?)$	a_1
280	a_g or b_{2g}	b_2 or a_1 *
256	b_{2g}	
253	$b_{1g} + b_{3g}$	e
251	a_g	
149	a_g	
141	b_{3g}	e
136	$b_{1g} + (a_g?)$	
126	b_{2g}	b_2
120	a_g	
105	b_{1g}	b_1
103	$a_g + b_{2g}$	a_1
	External Modes	
86	b_{2g}	
76	a_g	
71	b_{3g}	
62	$a_g + b_{2g} + (b_{1g}?)$	
58	a_g	
51	a_g	
47	b_{1g}	
38	$b_{2g} + b_{3g} + (b_{1g}?)$	

* Verified by Dunsmuir and Lane[113] as a component of $\nu_3(T_d)$ having a_g symmetry

of $\delta(e)$ so that these, a_g, b_{1g}, b_{2g} and b_{3g}, are now lower in energy than the $\delta(b_2)$ component at 149 cm^{-1}.

In the single-crystal polarised infra-red reflectance spectrum of Cs_2CuCl_4, rather incomplete data were obtained[113] and no positive correlations with the isolated-ion modes were possible. The observed bands were correlated with the T_d symmetry; these are reproduced in table 3.1.3.

TABLE 3.1.3

Polarised infra-red reflectance data for Cs_2CuCl_4 [113]

Frequencies (cm^{-1})	Crystal Mode (D_{2h})	Internal Mode (T_d)
296	b_{2u}	
288	b_{1u} or b_{3u}	$\nu_3(t_2)$
258	b_{1u} or b_{3u}	
151	b_{1u} or b_{3u}	
136	b_{2u}	$\nu_4(t_2)$
123	b_{1u} or b_{3u}	
	External Modes	
83	b_{1u} or b_{3u}	
79	b_{2u}	
61	b_{2u}	

Referring to the table of infra-red data for Cs_2CuCl_4 in the original paper[113], Dunsmuir and Lane labelled the crystal modes in terms of b_{1u} and a mixture of b_{2u} or b_{3u} symmetries. This would most certainly be a printing error and the subscripts $1u$ and $2u$

should rightly be interchanged. By the authors' own admission, the spectra of the crystal were recorded from the natural (101) faces. We quote: "this gave the b_{2u} modes when the incident radiation was polarised along the crystallographic b-axis and a mixture of b_{1u} and b_{3u} modes when polarisation was perpendicular to the b-axis". Earlier, the authors had stated that the b_{1u}, b_{2u} and b_{3u} modes were recorded by aligning the electric vector of the incident radiation with the c, b and a axes of the crystal respectively. The evidence of infra-red would therefore contradict the assignments of Beattie et al.[112] as the band at 296 cm^{-1} (b_{2u}) could only arise from the $\nu(e)$ isolated-ion mode (refer correlation diagram, figure 3.1.3). In the bending region of the infra-red data, the presence of a band at 136 cm^{-1} (b_{2u}) would indicate that this belongs to $\delta(e)$, but no positive correlations with the isolated-ion modes of the bands at 151 and 123 cm^{-1} (b_{1u} or b_{3u}) could be made. It is conceivable though that the band at 151 cm^{-1} arises from $\delta(b_2)$ while the band at 123 cm^{-1} from $\delta(e)$, since the latter mode is closer to the 136 cm^{-1} band.

In making comparison between the infra-red and Raman spectra of Cs_2CuCl_4 (and Cs_2ZnCl_4), Dunsmuir and Lane noted that the infra-red-active and Raman-active components derived from a particular tetrahedral mode are close in frequency. On this basis, they concluded that the band at 280 cm^{-1} in the Raman spectrum of Cs_2CuCl_4 (table 3.1.2) should be a component of ν_3 having a_g symmetry since one of the infra-red bands assigned to ν_3 occurs at 288 cm^{-1} (table 3.1.3). A slight contradiction to this argument is that the infra-red band at 296 cm^{-1}, which has also been correlated to

ν_3, is 16 cm^{-1} higher than the corresponding Raman band and 8 cm^{-1} higher than the other ν_3 component in the infra-red, constituting rather large correlation or factor group splittings. The evidence of Raman and infra-red, then, is rather confusing to say the least. If, however, the infra-red band at 296 cm^{-1} is indeed the component of ν_3 origin, then there could be no doubt that $\nu(e)$ isolated-ion mode should be higher in energy than $\nu(b_2)$; hence the observed Raman spectrum would have to be reassigned.

With tetramethylammonium tetrachlorocuprate(II), $(NMe_4)_2CuCl_4$, however, Dunsmuir and Lane[90] obtained a much more complete infra-red spectrum and made unambiguous assignment of the bands which when correlated with the isolated-ion modes places $\nu(e)$ higher than $\nu(b_2)$ and $\delta(b_2)$ higher than $\delta(e)$. The assignment given here would seem to be incompatible with that of Beattie et al.[112]; while the spectra of $(NMe_4)_2CuCl_4$ and Cs_2CuCl_4 are not exactly comparable - the larger cation causes the bands to be at a slightly lower energy in the former - it seems most unlikely that the ordering of $\nu(e)$ and $\nu(b_2)$ should be reversed by changing the cation. In the bending region, the issue is not so clearcut as the crystal modes could possibly mix with each other or with the lattice modes. However, insofar as these two compounds are concerned, the authors have made positive assignments of the $\delta(e)$ and $\delta(b_2)$ modes in each case; their ordering is again in the opposite sense. The two compounds are isomorphous, and their anions have almost identical geometries (table 3.1.4).

TABLE 3.1.4

Internal parameters of $CuCl_4^{2-}$ anion in Cs_2CuCl_4[5] and $(NMe_4)_2CuCl_4$[86]

	Cs^+	$(NMe_4)^+$
Bond Lengths (Å)		
Cu-Cl$_1$	2.244(4)	2.25(1)
Cu-Cl$_2$	2.235(4)	2.23(1)
Cu-Cl$_3$	2.220(3)	2.21(1)
Bond Angles (°)		
Cl(1)-Cu-Cl(2)	131.2(1)	132.1(2)
Cl(1)-Cu-Cl(3)	101.6(1)	101.1(3)
Cl(2)-Cu-Cl(3)	99.7(1)	100.8(2)
Cl(3)-Cu-Cl(3)	127.1(2)	126.4(3)

As a side issue here, Dunsmuir and Lane[90] were slightly astray in their attempt to relate the variation in the splitting of the symmetric stretching mode ν_3 of T_d symmetry with the degree of distortion of the MCl_4^{2-} tetrahedra in various complexes. They attributed the larger splitting of ν_3 (*ca.* 55 cm^{-1}) in $(NMe_4)_2CuCl_4$ than that of Cs_2CuCl_4 (*ca.* 35 cm^{-1}) to the greater extent of distortion of the $CuCl_4^{2-}$ ion in the former compound. We know now that the two anions are remarkably similar indeed in their geometries. Other reasons must be sought for their difference in ν_3 splitting; crystal effects, for instance, must be duely considered.

The assignment problem mentioned above has also been discussed in some detail by McGinnety[5] who performed a normal coordinate analysis on the anion in Cs_2CuCl_4 within the isolated-ion

approximation, using a general valence force field. He defined five force constants to fit six experimentally observed bands using solid state spectra on the ground that the structure of the anion in the crystal is known. An excellent fit of the five force constants with the observed frequencies was obtained for an assignment similar to that of Beattie et al.[112], with $\nu(b_2)$ higher than $\nu(e)$ and $\delta(b_2)$ lower than $\delta(e)$; these are shown in table 3.1.5. When adopting the alternative ordering, a much poorer fit was obtained.

TABLE 3.1.5

Force constants (in millidyne Å^{-1}) for $CuCl_4^{2-}$ isolated-ion according to McGinnety[5]

f_r	1.08	
f_{rr}	0.17	
$f_{rr'}$	0.43	
f_θ	0.074	$\theta = 129.2$
f_ϕ	0.119	$\phi = 100.6$

However, to reduce the number of force constants in the valence force field to five in this case involved many approximations (see section 3.2.4); as such, it is not at all unusual that the results do not fit the spectrum exactly. The primary aim of the analysis should be to produce a physically reasonable set of force constants within acceptable agreement with the experimental data. In this respect, the force constants obtained by McGinnety

are unsatisfactory. He found that f_{rr}' (table 3.1.5), the stretch-stretch interaction constant between bonds at an angle of 129.2°, was 0.43 millidyne Å^{-1}, compared with 1.08 millidyne Å^{-1} for f_r, the primary Cu-Cℓ stretching force constant, and 0.17 millidyne Å^{-1} for f_{rr}, the interaction constant between bonds at an angle of 100.6°. In tetrahedral halides and complex halides[122], the ratio f_{rr}/f_r is never greater than 0.2; in square coplanar tetrahalogeno-anions[119], f_{rr}'/f_{rr} is usually between 2 and 3, but, again, f_{rr}'/f_r never exceeds 0.2. Thus, McGinnety's value for f_{rr}' is much too high for the flattened tetrahedral anion in Cs_2CuCl_4 - a fact he noted with some concern; both f_{rr}'/f_{rr} and f_{rr}'/f_r are excessive. Ferraro et al.[123] also reported a force constant analysis on $CuCl_4^{2-}$ ion using the Raman data of Beattie et al.[112] and assuming a T_d symmetry for the ion. Four force constants were defined in the valence force field: f_r, f_{rr}, f_α, $f_{\alpha\alpha}$ and their calculated values were 0.92, 0.31, 0.13 and 0.03 millidyne Å^{-1} respectively. These are quite similar to McGinnety's values; the ratio of f_{rr}/f_r is in excess of 0.3.

However, in their force constant analysis, Ferraro et al. adopted a force field which is much too simple to represent the real situation; the known symmetry of $CuCl_4^{2-}$ ion is closer to D_{2d} than T_d. In choosing the frequency of 252 cm^{-1}, which is the average of Raman bands 250, 251 and 253 cm^{-1} (refer table 3.1.2) as the ν_3 mode, the authors have neglected completely the band at 280 cm^{-1} which is no doubt of the same origin. This contradicts experimental evidence, and is obviously unacceptable.

3.1.4 *Aim of this Work*

The aim of the present work is to investigate the normal coordinate analysis of Cs_2CuCl_4 in more detail in order to find an assignment which leads to the most sensible set of force constants, while being compatible with the experimental data. The isolated-ion approximation is used for the meanwhile so that the vibrations of $CuCl_4^{2-}$ can be studied from the most simplistic yet fundamental viewpoint; also, the force constants derived would serve as a direct comparison with those of McGinnety's. On the evidence of the infra-red polarised reflectance spectrum[113], $\nu(e)$ should be higher than $\nu(b_2)$; hence, our analysis shall seek to confirm that assignment. As McGinnety has reported that with this ordering of e and b_2 modes, rather poor fit with the observed frequencies was obtained, we shall examine closely the approximations involved in the general valence force field so as to improve on the method, within the isolated-ion approximation.

3.2 *FUNDAMENTAL ASPECTS OF MOLECULAR VIBRATIONS*[120,124-129]

Insofar as the $CuCl_4^{2-}$ ion is considered an isolated species, the study of its vibrations is not differentiated from the general study of molecular vibrations. In this section, we present a discussion of normal vibrations and normal coordinates as well as a brief survey of various models of molecular force field.

The common notations adopted here are:

n = number of atoms in a molecule

k = degree of internal freedom

r_i = internal coordinates

x_i = Cartesian coordinates

q_i = normal coordinates

m_i = atomic masses

p_i^x = conjugate momenta associated with Cartesian coordinates

p_i^r = conjugate momenta associated with internal coordinates

V = potential energy

T = kinetic energy.

For a matrix $\underset{\sim}{A}$ of dimension $m \times n$:

a_{ij} = elements of $\underset{\sim}{A}$

$\underset{\sim}{A}^t$ = transpose of $\underset{\sim}{A}$

$\underset{\sim}{A}^{-1}$ = inverse of $\underset{\sim}{A}$

$|\underset{\sim}{A}|$ = determinant of $\underset{\sim}{A}$.

3.2.1 *Potential Energy Function*

A vibrating molecule departs from its equilibrium configuration through bond stretching or bond angle deformation. The first necessary assumption is that such atomic displacements are small. Hence, Taylor's expansion of the vibrational potential energy function can be employed, in which the cubic and higher terms can be ignored.

For a molecule consisting of n atoms, its vibrational potential energy V is expressed as a function of its internal parameters r_i:

$$V = f(r_1, r_2, \ldots, r_k) \qquad (1),$$

where k is the degree of internal freedom.

In equation (1), which is the general definition of a molecular force field, the internal parameters can be the bond lengths and bond angles within the molecule. However, it is often more convenient to use the internal displacement coordinates which are the changes in bond lengths and bond angles from their respective equilibrium values. Since the potential energy is sensitive only to the relative positions of the atoms and is invariant to the rotatory and translatory motions of the molecule, k is $(3n - 6)$ for a non-linear molecule and $(3n - 5)$ for a linear molecule.

Assuming that the internal coordinates are linearly independent of each other, then Taylor's expansion of the vibrational potential energy in atomic displacements from equilibrium is:

$$V = V_0 + \sum_{i=1}^{k} \left(\frac{\partial V}{\partial r_i}\right)_0 r_i + \frac{1}{2!} \sum_{i,j=1}^{k} \left(\frac{\partial^2 V}{\partial r_i \partial r_j}\right)_0 r_i r_j + \ldots (2)$$

In equation (2) , V_0, the potential energy of the molecule in equilibrium configuration, is arbitrarily set to zero; also, $\left(\frac{\partial V}{\partial r_i}\right)_0$ is zero as the potential energy must be at a minimum when r_i are zero, $i = 1, 2, \ldots, k$. Hence, neglecting cubic and higher terms,

$$V = \frac{1}{2} \sum_{i,j}^{k} \left(\frac{\partial^2 V}{\partial r_i \partial r_j}\right)_0 r_i r_j \qquad (3).$$

Equation (3) is the common description of a harmonic oscillation. The force constants, f_{ij}, in the harmonic approximation are defined as:

$$f_{ij} = \left(\frac{\partial^2 V}{\partial r_i \partial r_j}\right)_0$$

so that equation (3) is now written as:

$$V = \frac{1}{2} \sum_{i,j}^{k} f_{ij} r_i r_j \qquad (4).$$

In general, the number of force constants f_{ij} is equal to $k(k + 1)/2$[130]. This can be reduced if the molecule possesses symmetry, a consequence of which is that some force constants are identical.

Equation (4) can be expressed as a sum of two terms[125]:

$$V = \frac{1}{2} \sum_{i}^{k} f_{ii} r_i^2 + \frac{1}{2} \sum_{\substack{i,j \\ i \neq j}}^{k} f_{ij} r_i r_j \qquad (5),$$

in which f_{ii} are called primary force constants while f_{ij} are interaction constants.

A primary force constant f_{ii} is a measure of the restoring force to the equilibrium configuration of the molecule after a small displacement to the ith internal coordinate.

Jones [125] derived a mathematical expression for the interaction constant f_{ij}:

$$f_{ij} \approx - f_{jj}(r_j)_i \qquad (6),$$

which, when put into words, defines f_{ij} as equal to the negative of the product of the primary force constant of one coordinate, j, times the displacement of that coordinate caused by unit small displacement of the other coordinate, i.

In equation (4), the force constants, f_{ij}, are more conveniently expressed as a symmetric matrix, $\underset{\sim}{F}$. Hence, in matrix form, the potential energy function in the harmonic approximation is

$$2V = \underset{\sim}{R}^t \underset{\sim}{\underset{\sim}{F}} \underset{\sim}{R} \qquad (7),$$

where $\underset{\sim}{R}$ is a column matrix of internal coordinates, r_i, and $\underset{\sim}{R}^t$ its transpose.

3.2.2 *Kinetic Energy Function*

The vibrational kinetic energy of a polyatomic molecule is best described in terms of its $3n$ Cartesian coordinates which are then transformed into the internal coordinates.

Again, in the harmonic approximation, the kinetic energy, T, can be expressed as:

$$T = \frac{1}{2} \sum_{i}^{3n} m_i \dot{x}_i^2 \qquad (8),$$

which corresponds closely to the potential energy expression of equation (4).

In matrix form,

$$2T = \underset{\sim}{\dot{X}}\, {}^{t}\underset{\sim\sim}{M}\underset{\sim}{\dot{X}}$$

where $\underset{\sim}{M}$ is a diagonal matrix of atomic masses, m_i, of rank $3n$, $\underset{\sim}{X}$ is a column matrix of Cartesian displacement coordinates, x_i, and $\underset{\sim}{\dot{X}}$ its time derivative.

In terms of the Cartesian coordinate conjugate momenta $\underset{\sim}{P}^x$ to the $\underset{\sim}{\dot{X}}$,

$$2T = (\underset{\sim}{P}^x)\, {}^{t}\underset{\sim}{M}^{-1}\underset{\sim}{P}^x \qquad (9),$$

in which the diagonal elements of $\underset{\sim}{M}^{-1}$ are the reciprocals of the atomic masses.

To transform Cartesian coordinates into the internal coordinates, it is necessary to introduce a new matrix $\underset{\sim}{B}$ such that:

$$\underset{\sim}{R} = \underset{\sim\sim}{B}\underset{\sim}{X} \qquad (10).$$

In $\underset{\sim}{B}$, the element b_{ij} is equal to the displacement of the ith internal coordinate caused by a small unit displacement of the jth Cartesian coordinate.

From equation (10),

$$\dot{\underset{\sim}{R}} = \underset{\sim\sim}{B}\dot{X} \ ,$$

and $$\frac{\partial \dot{r}_i}{\partial \dot{x}_j} = b_{ij} \ ,$$

since $$p^x_j = \frac{\partial T}{\partial \dot{x}_j} = \sum_i \frac{\partial \dot{r}_i}{\partial \dot{x}_j} \cdot \frac{\partial T}{\partial \dot{r}_i} \ ,$$

and $$p^r_i = \frac{\partial T}{\partial \dot{r}_i} \ ,$$

where p^r_i are the conjugate momenta associated with the time derivatives of the internal coordinates r_i.

Hence,

$$p^x_j = \sum_i b_{ij} p^r_i \ .$$

In matrix form,

$$\underset{\sim}{P}^x = \underset{\sim}{B}^t \underset{\sim}{P}^r \ .$$

Equation (9) can now be expressed as

$$2T = (\underset{\sim}{P}^r)^t \underset{\sim\sim}{BM}^{-1} \underset{\sim}{B}^t \underset{\sim}{P}^r \ ,$$

from which

$$2T = (\underset{\sim}{P}^r)^t \underset{\sim\sim}{G} \underset{\sim}{P}^r \qquad (11).$$

In equation (11) $\underset{\sim}{G}$ is symmetric and is defined as

$$\underset{\sim}{G} = \underset{\sim\sim}{BM^{-1}}\underset{\sim}{B}^{t} \qquad (12).$$

It is now possible to express the kinetic energy function in terms of internal coordinates, r_i.

Since

$$\frac{\partial T}{\partial p_i^r} = r_i$$

and, from equation (11),

$$\frac{\partial T}{\partial p_i^r} = g_i p_i^r \ ;$$

hence

$$\dot{r}_i = g_i p_i^r \ ,$$

or

$$\underset{\sim}{\dot{R}} = \underset{\sim\sim}{G}\underset{\sim}{P}^r \ .$$

If $\underset{\sim}{G}^{-1}$ exists, then

$$\underset{\sim}{P}^r = \underset{\sim}{G}^{-1}\underset{\sim}{\dot{R}} \ ,$$

and

$$(\underset{\sim}{P}^r)^t = \underset{\sim}{\dot{R}}^t\underset{\sim}{G}^{-1} \quad ((\underset{\sim}{G}^{-1})^t = \underset{\sim}{G}^{-1} \text{ since } \underset{\sim}{G}^{-1} \text{ is symmetric.})$$

Equation (11) can now be written as

$$2T = \dot{\underset{\sim}{R}}^{t}\underset{\sim}{G}^{-1}\underset{\sim\sim}{G}\underset{\sim\sim}{G}^{-1}\dot{\underset{\sim}{R}}$$

$$= \dot{\underset{\sim}{R}}^{T}\underset{\sim}{G}^{-1}\dot{\underset{\sim}{R}} \qquad (13),$$

which is an expression of the vibrational kinetic energy in terms of internal coordinates, r_i.

3.2.3 *Normal Vibrations and the GF-Matrix*

In a polyatomic molecule, the vibrations of the atoms represent a very complex situation in which all the atoms perform their own individual oscillations. This confused picture is more readily understood if the molecular vibrations are expressed in terms of k normal modes of vibrations (k as defined before). In a given normal mode, all atoms perform simple harmonic oscillations about their equilibrium positions with the same frequency and in phase with each other. The frequency of a normal mode is then called a normal frequency or a fundamental frequency of the molecule.

The normal modes are associated with a set of normal coordinates q_i which can be related to the internal coordinates by

$$\underset{\sim}{R} = \underset{\sim\sim}{L}\underset{\sim}{Q} \qquad (14),$$

where $\underset{\sim}{L}$ is a transformation matrix between the internal coordinates and the normal coordinates.

The potential energy and the kinetic energy expressions derived earlier (equations (7) and (13)) can now be expressed in terms of normal coordinates:

$$2V = \underset{\sim}{Q}^{t}\underset{\sim}{L}^{t}\underset{\sim}{F}\underset{\sim}{L}\underset{\sim}{Q} \qquad (15),$$

$$2T = \dot{\underset{\sim}{Q}}^{t}\underset{\sim}{L}^{t}\underset{\sim}{G}^{-1}\underset{\sim}{L}\dot{\underset{\sim}{Q}} \qquad (16).$$

The expressions of potential energy and kinetic energy can now be employed to solve the Newton's equation of motion:

$$\frac{d}{dt}\left(\frac{\partial T}{\partial \dot{q}_i}\right) + \frac{\partial V}{\partial q_i} = 0 \qquad (17).$$

The approximate conditions for solving equation (17) require that the potential energy and the kinetic energy be expressed only in terms of diagonal elements of normal coordinate matrix $\underset{\sim}{Q}$ [120,124]. In other words,

$$V = \frac{1}{2}\sum_i \lambda_i q_i^2 \ ;$$

$$T = \frac{1}{2}\sum_i \dot{q}_i^2 \ .$$

In matrix form,

$$2V = \underset{\sim}{Q}^{t}\underset{\sim}{\Lambda}\underset{\sim}{Q} \qquad (18),$$

$$2T = \dot{\underset{\sim}{Q}}^{t}\underset{\sim}{E}\dot{\underset{\sim}{Q}} \qquad (19).$$

In equation (18) $\underset{\sim}{\Lambda}$ is a diagonal matrix with elements λ_i such that

$$\lambda_i = 4\pi^2 c^2 v_i^2 \ ,$$

where v_i is in cm^{-1} and c is the velocity of light. Converting the constants into numerical values,

$$\lambda_i = \left(\frac{\nu_i}{1302.9}\right)^2 \qquad (20).$$

In equation (19), $\underset{\sim}{E}$ is a unit matrix.

By correlating with equations (15) and (16), we obtain

$$\underset{\sim}{L}^t \underset{\sim\sim}{F} \underset{\sim}{L} = \underset{\sim}{\Lambda} ;$$

$$\underset{\sim}{L}^t \underset{\sim}{G}^{-1} \underset{\sim}{L} = \underset{\sim}{E} .$$

Hence,

$$\underset{\sim}{L}^t = \underset{\sim}{L}^{-1} \underset{\sim}{G} ,$$

and

$$\underset{\sim}{L}^{-1} \underset{\sim\sim}{GF} \underset{\sim}{L} = \underset{\sim}{\Lambda} ,$$

or

$$\underset{\sim\sim}{GF} \underset{\sim}{L} = \underset{\sim}{L} \underset{\sim}{\Lambda} \qquad (21).$$

Equation (21) is the familiar eigenvector-eigenvalue equation; the eigenvalues of $\underset{\sim\sim}{GF}$ are the roots of the secular equation:

$$\left| \underset{\sim\sim}{GF} - \underset{\sim}{E}\lambda_i \right| = 0 \qquad (22),$$

while the eigenvectors in columns of $\underset{\sim}{L}$ are related to the normal modes as defined in equation (14). $\underset{\sim}{E}$ is the unit matrix with the same order as that of $\underset{\sim}{G}$ and $\underset{\sim}{F}$ matrices.

3.2.4 *Model Force Fields*

The molecular force field of a polyatomic molecule (equation (1)) as expressed in terms of $\underset{\sim}{F}$ matrix (equation (7)) is a general one, and no prior assumptions as to its nature are made. Assumptions are usually necessary when the problem of immediate concern is to determine the force constants given a known set of vibrational frequencies. Such assumptions set out to control the off-diagonal elements of the $\underset{\sim}{F}$ matrix within the confines of a model force field. For a general force field (GFF) the basic coordinates should be linearly independent and equal in number to the degrees of internal freedom, k. For a model force field, the number of coordinates used is arbitrary, usually larger than k; they are not linearly independent and redundancy conditions often exist.

Various types of force fields have been presented in the past; however, only a few of them are of importance in practice. These are briefly described as follows:

(A) Central Force Field (CFF)

This is one of the simplest force fields in which all off-diagonal elements of $\underset{\sim}{F}$ matrix are taken as zero. Only forces acting between pairs of atoms (bonded or non-bonded) are considered; contributions of the bending modes are completely ignored.

The potential energy function is:

$$V = \frac{1}{2}\sum k_{ij}\ (\Delta r_{ij})^2 + \frac{1}{2}\sum f_{ij}(\Delta q_{ij})^2 \qquad (23),$$

where r is the bond length and q is the distance between a non-bonded pair. k_{ij} are the stretching force constants and f_{ij} are the repulsive force constants.

(B) Valence Force Field (VFF)

This represents a slight modification of the central force field in that the forces considered include those which oppose the bending or torsion of bonds. Interactions between non-bonded pairs are not considered. The potential function is:

$$V = \frac{1}{2} \sum k_{ij}(\Delta r_{ij})^2 + \frac{1}{2} \sum h_{ijk}(\Delta \phi_{ijk})^2 + \frac{1}{2} \sum y_{ijkl}(\Delta t_{ijkl})^2 \quad (24),$$

where r is the bond length, ϕ is the bond angle and t is the internal angle of rotation.

Again, the $\underset{\sim}{F}$ matrix is diagonal. In cases where the interaction terms are insignificant, this model provides an acceptable description of the potential energy function of the molecule although any treatment of vibrational problem based on this model is at best only semiquantitative.

(C) General Valence Force Field (GVFF)

This model takes into account all the interaction terms which are left out in the valence force field, and is therefore an improvement on VFF in that sense. For simple molecules where there are no redundancy problems associated with the internal coordinates, the force field is the same as the general force field (equation (5)).

Compared to CFF and VFF where there is usually a surplus of observed frequencies over the number of force constants to be determined, the GVFF invariably involves more force constants than there are observed frequencies. To reduce the number of force constants required in the calculation, some approximations have to be made by ignoring certain minor interaction terms or postulating relationship between certain force constants.

This force field is nevertheless very useful in practice as it gives meaningful correlation with electronic structure and bonding properties; as well, the force constants derived have the added attraction that they can be directly transferred to other molecules. For these reasons, the GVFF is the model force field we have chosen for the normal coordinate analysis of $CuCl_4^{2-}$ ion which will be described in section 3.3.

(D) Urey-Bradley Force Field (UBFF)

In view of the limitations of GVFF in which the number of force constants is usually larger than desired, a new model force field was presented to incorporate the basic features of GVFF but include fewer parameters. This is the Urey-Bradley Force Field[131,132](UBFF) in which the interaction constants as appeared in GVFF are replaced by repulsive terms between non-bonded atoms. The potential energy function is then

$$V = \frac{1}{2}\sum k_{ij}(\Delta r_{ij})^2 + \frac{1}{2}\sum h_{ijk}(\Delta\phi_{ijk})^2 + \frac{1}{2}\sum y_{ijkl}(\Delta t_{ijkl})^2$$

$$+ \frac{1}{2}\sum f_{ij}(\Delta q_{ij})^2 \qquad (25),$$

where q is the distance between non-bonded atoms.

The limitation of this field is that Δq is not independent of Δr's and $\Delta\phi$'s; hence, redundancy conditions always exist. More importantly, the force field does not represent the true situation for most coordination compounds and so its applicability is rather restrictive.

Other force fields worth mentioning are the local symmetry force field (LSFF) which employs the transferability of GVFF and modifies it to suit the study of organic molecules having CH_3 and CH_2 groups; the flexible bond model in which bond angle deformation is assumed to be due to bond "bending" and not change in bond angle; the orbital valence force field (OVFF) which ascribes molecular deformation to changes in the overlapping orbitals forming chemical bonds.

3.2.5 *Anharmonicity*

An exact solution of the Schrödinger equation for the vibrational energy function of a harmonic oscillator (equation (3)) expresses the energy levels as

$$E_{k,v_k} = h\nu_k(v_k + \tfrac{1}{2}) \qquad (26),$$

where ν_k is the harmonic frequency for a given kth normal mode, and v_k is the vibrational quantum number which can be 0, 1, 2, ...

If the general potential energy function (equation (2)) is used, in which the cubic and higher terms are non-zero, then an approximate solution is

$$E_{k,v_k} = h\nu_k(v_k + \tfrac{1}{2}) - h\nu_k x_k(v_k + \tfrac{1}{2})^2 \qquad (27),$$

where χ_k is an 'anharmonicity constant'.

For polyatomic molecules, the approximate solution involves more anharmonicity constant terms to correct for the greater number of observed frequencies.

In the harmonic approximation, the vibrational selection rule $\Delta v_k = \pm 1$ is applicable. For a given k, if the transitions are from $v_k = 0$ to $v_k = 1$, then the absorption bands are called the 'fundamentals'. Applying equation (26), the frequency of a given fundamental absorption is $(E_{k,1} - E_{k,0})$, i.e. $h\nu_k$, corresponding to the frequency of the kth normal mode.

There are two important effects of anharmonicity on molecular vibrations. Firstly, while the regular spacing of the energy levels is $h\nu_k$ in the harmonic approximation, this is now modified by the inlcusion of anharmonicity constants, e.g. equation (27) Secondly, the selection rule $\Delta v_k = \pm 1$ does not now strictly apply. Thus, transitions with, say, $\Delta v_k = \pm 2$ become allowed.

In measuring the vibrational spectra, observation of overtones, which have frequencies of approximately $2\nu_k$, $3\nu_k$, etc., and combination bands, which have frequencies at approximately $l\nu_k \pm l'\nu_k$, $(l, l' = 1, 2, ..)$, indicates a breakdown of the harmonic approximation. Such approximation adopted in the study of molecular vibrations represents an idealised situation in which vibrational displacements from equilibrium are small. Deviation from ideality as a consequence of anharmonicity could induce as much as 5% error in the calculation of force constants from observed frequencies[127].

3.3 *ISOLATED-ION ANALYSIS*

3.3.1 *Method*

The $CuCl_4^{2-}$ anion of Cs_2CuCl_4 was considered to assume an idealised D_{2d} symmetry (figure 3.1.1). The mean structural parameters were obtained from reference[5] (see also section 3.1.1).

We used a general quadratic valence force field (refer section 3.2.4) in which the experimentally observed energies (in cm^{-1}) of the fundamental modes are related to the roots λ_i of the determinantal equation (equation (22)) by the relation expressed in equation (20).

The elements of F_S, the F matrix associated with the symmetry coordinates, are given in table 3.3.1 (see appendix I for its derivation). These are expressed in terms of the force constants f_{ij} by the usual expression for the potential energy of the system (equation (4)), neglecting cubic and higher terms and with all redundancies removed. Each primary force constant f_{ii} is associated with one internal displacement coordinate Δr_i while each interaction constant f_{ij} is associated with two internal displacement coordinates Δr_i and Δr_j (see appendix I). (The force constants in table 3.3.1 are defined in table 3.3.2 in terms of their associated internal displacement coordinates.)

The elements of G_S, the G matrix associated with the symmetry coordinates, are of the same form as those of F_S matrix; these are given in table 3.3.3. The elements of G_R, the G matrix associated with the internal displacement coordinates and from which the G_S matrix elements were calculated, were obtained from

TABLE 3.3.1

$\underset{\sim}{F}_S$ matrix elements for D_{2d} $CuCl_4^{2-}$, in terms of valence force constants (defined in table 3.3.2)

Symmetry	F_{ij}
a_1	$F_{11} = f_r + f_{rr}' + 2f_{rr}$
	$F_{12} = 2r[a(f_{r\theta} + f_{r\theta}') + 2b(f_{r\phi} + f_{r\phi}')]$
	$F_{22} = 2r^2[a^2(f_\theta + f_{\theta\theta}) + 2b^2(f_\phi + f_{\phi\phi}' + 2f_{\phi\phi}) + 8abf_{\theta\phi}]$
b_1	$F_{33} = r^2(f_\phi + f_{\phi\phi}' - 2f_{\phi\phi})$
b_2	$F_{44} = f_r + f_{rr}' - 2f_{rr}$
	$F_{45} = 2^{\frac{1}{2}}r(f_{r\theta} - f_{r\theta}')$
	$F_{55} = r^2(f_\theta - f_{\theta\theta})$
e	$F_{66} = f_r - f_{rr}'$
	$F_{67} = 2^{\frac{1}{2}}r(f_{r\phi} - f_{r\phi}')$
	$F_{77} = r^2(f_\phi - f_{\phi\phi}')$

Footnote: $a = [2(1 + 2\cos^2\psi)]^{-\frac{1}{2}}$

$b = (\cos\psi)[2(1 + 2\cos^2\psi)]^{-\frac{1}{2}}$

$\cos\psi = -\sin\theta/2\sin\phi$

TABLE 3.3.2

Force constants for D_{2d} $CuCl_4^{2-}$ and their associated internal displacement coordinates Δr_i and Δr_j. Δr indicates a bond length displacement; $\Delta\phi$ and $\Delta\theta$ indicate bond angle deformations

Force constant		Internal coordinate(s)
f_r	$\Delta r(Cu\text{-}Cl_a)$	
f_{rr}	$\Delta r(Cu\text{-}Cl_a)\,\Delta r(Cu\text{-}Cl_b)$	$(Cl_a\text{-}Cu\text{-}Cl_b = 100.6^\circ)$
f_{rr}'	$\Delta r(Cu\text{-}Cl_a)\,\Delta r(Cu\text{-}Cl_b)$	$(Cl_a\text{-}Cu\text{-}Cl_b = 129.2^\circ)$
f_ϕ	$\Delta\phi(Cl_a\text{-}Cu\text{-}Cl_b)$	$(\phi = 100.6^\circ)$
f_θ	$\Delta\theta(Cl_a\text{-}Cu\text{-}Cl_b)$	$(\theta = 129.2^\circ)$
$f_{\phi\phi}$	$\Delta\phi(Cl_a\text{-}Cu\text{-}Cl_b)\Delta\phi(Cl_a\text{-}Cu\text{-}Cl_c)$	$(\phi = 100.6^\circ)$
$f_{\phi\phi}'$	$\Delta\phi(Cl_a\text{-}Cu\text{-}Cl_b)\Delta\phi(Cl_c\text{-}Cu\text{-}Cl_d)$	$(\phi = 100.6^\circ)$
$f_{\theta\theta}$	$\Delta\theta(Cl_a\text{-}Cu\text{-}Cl_b)\Delta\theta(Cl_c\text{-}Cu\text{-}Cl_d)$	$(\theta = 129.2^\circ)$
$f_{\theta\phi}$	$\Delta\theta(Cl_a\text{-}Cu\text{-}Cl_b)\Delta\phi(Cl_a\text{-}Cu\text{-}Cl_c)$	$(\phi = 100.6^\circ)$ $(\theta = 129.2^\circ)$
$f_{r\phi}$	$\Delta r(Cu\text{-}Cl_a)\Delta\phi(Cl_a\text{-}Cu\text{-}Cl_b)$	$(\phi = 100.6^\circ)$
$f_{r\phi}'$	$\Delta r(Cu\text{-}Cl_a)\Delta\phi(Cl_b\text{-}Cu\text{-}Cl_c)$	$(\phi = 100.6^\circ)$
$f_{r\theta}$	$\Delta r(Cu\text{-}Cl_a)\Delta\theta(Cl_a\text{-}Cu\text{-}Cl_b)$	$(\theta = 129.2^\circ)$
$f_{r\theta}'$	$\Delta r(Cu\text{-}Cl_a)\Delta\theta(Cl_b\text{-}Cu\text{-}Cl_c)$	$(\theta = 129.2^\circ)$

TABLE 3.3.3

$\underset{\sim}{G}_s$ matrix elements for D_{2d} $CuCl_4^{2-}$ ion

Symmetry	g_{ij}
a_1	$g_{11} = \mu_{Cl}$
	$g_{12} = 0$
	$g_{22} = 4r^{-2}\mu_{Cl}\{a^2 + 2b^2(1 + (\cos\theta - \cos^2\phi)/\sin^2\phi) + 4ab\cos\psi\}$
b_1	$g_{33} = 2r^{-2}\mu_{Cl}\{1 - (\cos\theta - \cos^2\phi)/\sin^2\phi\}$
b_2	$g_{44} = \mu_{Cl} + 2\mu_{Cu}\ (1 + \cos\theta)$
	$g_{45} = -2(2)^{\frac{1}{2}}r^{-1}\mu_{Cu}\sin\theta$
	$g_{55} = 2r^{-2}\{\mu_{Cl} + 2\mu_{Cu}\ (1 - \cos\theta)\}$
e	$g_{66} = \mu_{Cl} + \mu_{Cu}\ (1 - \cos\theta)$
	$g_{67} = -2(2)^{\frac{1}{2}}r^{-2}\mu_{Cu}\sin\phi$
	$g_{77} = 2r^{-2}\{\mu_{Cl} + 2\mu_{Cu}\ (1 - \cos\phi)\}$

Footnote: μ_x = reciprocal mass of an atom x;

$\cos\psi = -\sin\theta/2\sin\phi$;

$a = [2(1 + 2\cos^2\psi)]^{-\frac{1}{2}}$

$b = (\cos\psi)[2(1 + 2\cos^2\psi)]^{-\frac{1}{2}}$

For a flattened tetrahedron of D_{2d} symmetry (as in figure 3.1.1) there exists a trigonometric relationship between the angular parameters θ and ϕ such that $\cos\phi = -\sin^2\theta/2(1 - \cos\theta)$.

TABLE 3.3.4

G_R matrix elements of D_{2d} $CuCl_4^{2-}$ ion

Similar notations as the force constants of table 3.3.2 are adopted in this table.

$$g_r = \mu_{Cl} + \mu_{Cu}$$

$$g_{rr} = \mu_{Cu}\cos\phi$$

$$g_{rr}' = \mu_{Cu}\cos\theta$$

$$g_\phi = 2r^{-2}\{\mu_{Cl} + \mu_{Cu}(1 - \cos\phi)\}$$

$$g_\theta = 2r^{-2}\{\mu_{Cl} + \mu_{Cu}(1 - \cos\theta)\}$$

$$g_{\phi\phi} = r^{-2}\mu_{Cl}\{(\cos\theta - \cos^2\phi)/\sin^2\phi\}$$

$$g_{\phi\phi}' = 2r^{-2}\mu_{Cu}\{(1 - \cos\phi)^2(\cos\theta + \cos\phi)/\sin^2\phi\}$$

$$g_{\theta\theta} = 4r^{-2}\mu_{Cu}\{(\cos\phi)(1 - \cos\theta)^2/\sin^2\theta\}$$

$$g_{\theta\phi} = r^{-2}\mu_{Cl}\{(\cos\phi)(1 - \cos\theta)/\sin\theta\sin\phi\}$$

$$g_{r\phi} = -r^{-1}\mu_{Cu}\sin\phi$$

$$g_{r\phi}' = -r^{-1}\mu_{Cu}\{(\cos\theta + \cos\phi)(1 - \cos\phi)/\sin\phi\}$$

$$g_{r\theta} = -r^{-1}\mu_{Cu}\sin\theta$$

$$g_{r\theta}' = -2r^{-1}\mu_{Cu}\{(\cos\phi)(1 - \cos\theta)/\sin\theta\}$$

the tabulations of Wilson et al.[124]. These are shown in table 3.3.4 in terms of parameters relevant to this study (also refer to appendix I).

We see from tables 3.3.1 and 3.3.2 that 13 force constants are required to form a kinematically complete set which describes the vibrations of the anion. In practice, only seven experimental quantities can be obtained if all the isolated-ion modes are observed. Obviously, some approximations have to be made as is often required in GVFF.

The force field can be simplified if F_{12} is ignored. In the limit of tetrahedral symmetry ($\theta = \phi = 109.5^{o}$), this element vanishes since $(f_{r\theta} + f_{r\theta}') = (f_{r\phi} + f_{r\phi}')$, and $a = -2b$. In the limit of square coplanarity (D_{4h}), F_{12} also vanishes since $(f_{r\theta} + f_{r\theta}')$ becomes zero, as does b. For all intermediate situations, F_{12} is the sum of two terms of opposite sign. It is not immediately apparent that they should be equal in magnitude, but this would be the case if we make the following approximation:

$$(f_{r\theta} + f_{r\theta}')/(f_{r\phi} + f_{r\phi}') = \sin\theta/\sin\phi \qquad (28).$$

If F_{12} is set equal to zero, the number of independent force constants is reduced by two, since $(f_{r\theta} - f_{r\theta}')$ and $(f_{r_\phi} - f_{r_\phi}')$ become composite interaction constants whose terms are inseparable.

The number of force constants can be further reduced to seven if we neglect the bend-bend interaction constants while retaining the stretch-bend interaction constants. The justification of these assumptions is arrived at by studying the force constants found for the related square coplanar and tetrahedral systems.

A detail account of such studies will be presented separately in section 3.4; meanwhile, the results of these studies are assumed in the present section for the isolated-ion analysis of $CuCl_4^{2-}$ ion.

3.3.2 *Experimental Data*

Much thought was devoted to deciding the experimental data to which the force constants were to be fitted. The most detailed spectra[112,113] of Cs_2CuCl_4 exhibit too many bands (as a consequence of factor group effects) for an analysis within the isolated-ion approximation; and there is no general agreement on the band positions reported by other workers who have published less well resolved spectra (refer table 3.1.1). Our own measurement of the far infra-red spectrum of Cs_2CuCl_4 as a mull at room temperature showed bands at 285.4, 256.4, 141.8 and 129.3 cm^{-1}; again, they are not in exact agreement with those in the literature.

As the results of our analysis will ultimately be compared with those of McGinnety's, we eventually used solid state data for Cs_2CuCl_4 rather than solution data which may seem more appropriate for the study of a genuinely isolated $CuCl_4^{2-}$ ion. Referring to tables 3.1.2 and 3.1.3, the frequency of an isolated-ion mode may be taken as the mean of the frequencies of its crystal components. Table 3.3.5 shows the isolated-ion frequencies thus obtained.

TABLE 3.3.5

Frequencies (in cm^{-1}) of isolated-ion modes as the means of the frequencies of crystal components

Isolated-ion Frequency		Crystal Mode Frequency
$\nu(a_1)$	297	297
$\nu(e)$ or $\nu(b_2)$	288	296, 288, 280
$\nu(e)$ or $\nu(b_2)$	255	258, 256, 253, 251
If $\delta(b_2) > \delta(e)$:		
$\delta(b_2)$	150	151, 149
$\delta(e)$	130	141, 136, 126, 123, 120
If $\delta(e) > \delta(b_2)$:		
$\delta(e)$	144	151, 149, 141, 136
$\delta(b_2)$	123	126, 123, 120
$\delta(a_1)$	103	103

Footnote: As in most other measurements of the vibrational spectra of Cs_2CuCl_4, $\delta(b_1)$ cannot be located with certainty.

3.3.3 *Results and Discussion*

As mentioned in the previous section, only six experimental parameters are available for input as the isolated-ion modes of $CuCl_4^{2-}$ ion. However, seven force constants are required in our calculations. The obvious solution to this problem is to arbitrarily assign a value to any one force constant so that the equations can be solved exactly for the other six, within physically reasonable limits. In this work, f_ϕ was chosen to assume a range of arbitrary values.

On the basis of our results of section 3.4, it has become necessary for some, if not all, bend-bend interaction constants to assume small values so that, overall, the force constants are more accurately determined. $f_{\phi\phi}$, the interaction constant between two bond angles at 100.6° with a common bond, and $f_{\theta\phi}$, the interaction constant between bond angle at 129.2° and bond angle at 100.6° with a common bond, were deemed more important than the other bend-bend interaction constants. Hence, a further assumption is made such that

$$f_{\phi\phi} = 0.1 f_\phi \ ;$$
$$f_{\theta\phi} = 0.05(f_\theta + f_\phi)$$

for given values of f_θ and f_ϕ.

This is again justified by observing the relative magnitudes of the force constants found from the related systems.

Given no prior knowledge as to the likely order of the e and b_2 modes, there are four possible assignments:

I $\nu(e) > \nu(b_2) > \delta(b_2) > \delta(e)$

II $\nu(b_2) > \nu(e) > \delta(b_2) > \delta(e)$

III $\nu(e) > \nu(b_2) > \delta(e) > \delta(b_2)$

IV $\nu(b_2) > \nu(e) > \delta(e) > \delta(b_2)$

In each of the assignments above, $\nu(a_1)$ and $\delta(a_1)$ modes are always of the highest and lowest energies respectively, in accordance with experimental evidence.

Exhaustive calculations based on the four assignments showed that real solutions for the six unknowns were obtained over a narrow range of f_ϕ values only. The limits within which the force constants can be placed are further restricted if the following constraints are imposed:

(A) $f_{rr'} > f_{rr}$.

This is always found to be true for square coplanar systems, and can be interpreted in terms of metal-ligand π-bonding[119,125].

(B) $f_\phi > f_\theta$.

We expect that the greater of the two bending force constants should be associated with the smaller bond angle; in square coplanar MX_4^{2-} and MX_4^- species, f_ϕ/f_θ is found to be about 2[119].

(C) $(f_{r\phi} - f_{r\phi'}) > (f_{r\theta} - f_{r\theta'})$.

$(f_{r\theta} - f_{r\theta'})$ vanishes in the limit of square coplanarity, hence it may be expected to decrease relative to $(f_{r\phi} - f_{r\phi'})$ as a tetrahedron is flattened towards D_{4h}.

Tables 3.3.6 - 3.3.9 show the force constants obtained for the four assignments. In each case, the upper and lower limits of f_ϕ for which real solutions could be found are given. However, only the sets of force constants which conform to the artificially imposed constraints are shown in the tables.

In assignments III and IV where $\delta(e)$ modes were placed higher than $\delta(b_2)$ modes, real solutions were found over a larger range of f_ϕ values than those for assignments I and II. However, the force constants obtained are unrealistic in that, among other things, the stretch-bend interaction constants are found to be larger than the primary bending force constants. In assignment III, the ratios $(f_{r\phi} - f_{r\phi}')/f_\phi$ range from 1.06 to 1.16 while $(f_{r\theta} - f_{r\theta}')/f_\theta$ range from 1.58 to 1.56. The corresponding ranges of ratios in assignment IV are 1.09 to 1.13 and 1.72 to 1.35. In their normal coordinate treatment of tetrahedral XY_4 type molecules and ions, including halides and complex halides, using approximated GVFF, Krebs, et al.[133] found that the values of $(f_{r\alpha} - f_{r\alpha}')$ are always smaller than those of $(f_\alpha - f_{\alpha\alpha}')$. On this evidence alone, the force constants derived from assignments III and IV appear to be rather unsatisfactory. Further, the calculated values of $\delta(b_1)$, based on F_{33} element of table 3.3.1, are *ca.* 138.6 cm^{-1} for assignment III and *ca.*156.8 cm^{-1} for assignment IV; the latter assignment is incidentally similar to that of McGinnety's. There is no experimental basis for $\delta(b_1)$ mode to assume this magnitude. McGinnety reassigned the Raman band at 136 cm^{-1} to $\delta(b_1)$, on the basis of his calculations; this is not inconsistent with the original Raman data[112] but would appear likely to be the upper limit for this mode. Thus, assignments III and IV can be discounted on these

TABLE 3.3.6

Experimental frequencies (in cm^{-1}) and calculated force constants (in millidyne $\mathring{A}^{-1}$) for assignment I

(a) Experimental frequencies (in cm^{-1}):

297 $\nu(a_1)$; 103 $\delta(a_1)$; 288 $\nu(e)$; 130 $\delta(e)$;

255 $\nu(b_2)$; 150 $\delta(b_2)$.

(b) Calculated force constants (in millidyne $\mathring{A}^{-1}$)

Real solutions only for $0.104 < f_\phi < 0.114$

f_r	f_{rr}	f_{rr}'	f_θ	f_ϕ	$f_{r\theta} - f_{r\theta}'$	$f_{r\phi} - f_{r\phi}'$
1.2550	0.1878	0.2114	0.1042	0.1070	0.0863	0.0924
1.2595	0.1888	0.2049	0.1039	0.1080	0.0843	0.0983
1.2631	0.1898	0.1992	0.1037	0.1090	0.0822	0.1034
1.2661	0.1911	0.1938	0.1034	0.1100	0.0797	0.1081

TABLE 3.3.7

Experimental frequencies (in cm^{-1}) and calculated force constants (in millidyne $\mathring{A}^{-1}$) for assignment II

(a) Experimental frequencies (in cm^{-1}):

297 $\nu(a_1)$; 103 $\delta(a_1)$; 255 $\nu(b_2)$; 130 $\delta(b_2)$;

288 $\nu(e)$; 150 $\delta(e)$.

(b) Calculated force constants (in millidyne $\mathring{A}^{-1}$):

Real solutions only for $0.104 < f_\phi < 0.114$

f_r	f_{rr}	f_{rr}'	f_θ	f_ϕ	$f_{r\theta} - f_{r\theta}'$	$f_{r\phi} - f_{r\phi}'$
1.2242	0.1200	0.3778	0.1039	0.1080	0.0883	0.0929
1.2268	0.1213	0.3726	0.1037	0.1090	0.0858	0.0974
1.2287	0.1228	0.3676	0.1034	0.1100	0.0829	0.1014
1.2300	0.1246	0.3628	0.1031	0.1110	0.0796	0.1052
1.2305	0.1269	0.3577	0.1029	0.1120	0.0754	0.1087
1.2295	0.1305	0.3515	0.1026	0.1130	0.0691	0.1119

TABLE 3.3.8

Experimental frequencies (in cm^{-1}) and calculated force constants (in millidyne $\mathring{A}^{-1}$) for assignment III

(a) Experimental frequencies (in cm^{-1}):

297 $\nu(a_1)$; 103 $\delta(a_1)$; 288 $\nu(e)$; 144 $\delta(e)$;

255 $\nu(b_2)$; 123 $\delta(b_2)$.

(b) Calculated force constants (in millidyne $\mathring{A}^{-1}$):

Real solutions only for $0.12 < f_\phi < 0.25$

f_r	f_{rr}	f_{rr}'	f_θ	f_ϕ	$f_{r\theta} - f_{r\theta}'$	$f_{r\phi} - f_{r\phi}'$
1.3219	0.1666	0.1869	0.0950	0.1430	0.1505	0.1521
1.3238	0.1667	0.1849	0.0947	0.1440	0.1499	0.1549
1.3256	0.1667	0.1829	0.0945	0.1450	0.1494	0.1576
1.3273	0.1668	0.1810	0.0942	0.1460	0.1488	0.1602
1.3290	0.1669	0.1792	0.0939	0.1470	0.1482	0.1627
1.3305	0.1670	0.1774	0.0937	0.1480	0.1477	0.1652
1.3320	0.1671	0.1758	0.0934	0.1490	0.1471	0.1677
1.3335	0.1672	0.1741	0.0932	0.1500	0.1465	0.1701
1.3348	0.1673	0.1726	0.0929	0.1510	0.1460	0.1724
1.3362	0.1674	0.1711	0.0927	0.1520	0.1454	0.1747
1.3374	0.1675	0.1696	0.0924	0.1530	0.1448	0.1770
1.3387	0.1676	0.1682	0.0922	0.1540	0.1442	0.1792

TABLE 3.3.9

Experimental frequencies (in cm^{-1}) and calculated force constants (in millidyne $\mathring{A}^{-1}$) for assignment IV

(a) Experimental frequencies (in cm^{-1}):

297 $\nu(a_1)$; 103 $\delta(a_1)$; 288 $\nu(b_2)$; 123 $\delta(b_2)$;

255 $\nu(e)$; 144 $\delta(b_2)$.

(b) Calculated force constants (in millidyne $\mathring{A}^{-1}$):

Real solutions only for $0.12 < f_\phi < 0.25$

f_r	f_{rr}	f_{rr}'	f_θ	f_ϕ	$f_{r\theta} - f_{r\theta}'$	$f_{r\phi} - f_{r\phi}'$
1.3033	0.0924	0.3538	0.0906	0.1600	0.1561	0.1745
1.3074	0.0943	0.3460	0.0881	0.1700	0.1489	0.1903
1.3090	0.0965	0.3399	0.0855	0.1800	0.1411	0.2043
1.3087	0.0991	0.3352	0.0830	0.1900	0.1328	0.2168
1.3065	0.1021	0.3313	0.0804	0.2000	0.1237	0.2281
1.3026	0.1057	0.3280	0.0779	0.2100	0.1136	0.2384
1.2967	0.1103	0.3247	0.0753	0.2200	0.1020	0.2478

evidences. It is significant that we used similar frequencies as McGinnety in assignment IV (see table 3.3.9) and yet the force constants derived have appeared to be lacking in credibility. Obviously, inclusion of the stretch-bend interaction constants have brought to the surface problems never before envisaged; the relative magnitudes of the force constants found in the analysis are mainly a consequence of the ordering of the e and b_2 modes as discussed later.

Comparing now the other two assignments, the absolute and relative magnitudes of the force constants for assignment I appear eminently reasonable. As desired, we have $f_{rr'} > f_{rr}$, $f_{\phi} > f_{\theta}$ and $(f_{r\phi} - f_{r\phi'}) > (f_{r\theta} - f_{r\theta'})$, though in each case the difference is quite small. The calculated value of $\delta(b_1)$ mode is *ca.* 118.5 cm^{-1} which is not unreasonable. With assignment II, which is similar to that of McGinnety except for the ordering of $\delta(e)$ and $\delta(b_2)$, we find that $f_{rr'}$ seems to be too large by comparison with f_r and f_{rr}. As in assignment IV, the value of f_r is rather larger while f_{rr} and $f_{rr'}$ are smaller compared with McGinnety's force constants (table 3.1.5), this is a consequence of introducing stretch-bend interaction terms. Even so, the ratio $f_{rr'}/f_{rr}$ is still too large; we know of no precedent for such a ratio exceeding 0.2. The ratio $f_{rr'}/f_{rr}$ is comparable with that found for square coplanar systems[119] (section 3.4), but seems too high for the modest extent of flattening found in Cs_2CuCl_4. McGinnety's objection to assignment I was based upon the poor agreement between the experimental and calculated frequencies; this can be attributed to his neglect of stretch-bend interaction constants. McGinnety expressed some concern over the large ratio

$f_{rr'}/f_{rr}$, and suggested that it might be an artefact arising from the approximations involved. However, this is an inevitable consequence of his assignment; placing $\nu(b_2)$ higher than $\nu(e)$ requires a large value of $f_{rr'}$, whatever assumptions are made concerning stretch-bend and bend-bend interaction.

Thus, assignment I is favoured over all the other assignments. The ordering of $\nu(e)$ and $\nu(b_2)$ modes in this assignment is also in agreement with the infra-red evidence.

3.4 *RELATED SYSTEMS*

In using GVFF for the normal coordinate analysis of isolated $CuCl_4^{2-}$ ion, we were confronted with the problem of having too many force constants for the number of observed frequencies. To assist us in making approximations so that the problem is solvable, we propose that the force constants which fit the spectra of comparable tetrahedral and square coplanar species should afford some guidance concerning the relative magnitudes of the force constants for $CuCl_4^{2-}$ ion. To this end, we initiated a study of the vibrations of such systems in GVFF, the transferability of which ensured that such exercises would be worthwhile.

3.4.1 *Tetrahedral Ion*

The $ZnCl_4^{2-}$ ion should serve very nicely as a model for the hypothetical tetrahedral $CuCl_4^{2-}$ ion. Caesium tetrachlorozincate(II) is isostructural with Cs_2CuCl_4, both belonging to the same space group[5,7]. Except for the extent of distortion of the anions, the structural parameters are quite similar as shown in table 3.4.1.

Wong[134] has recently measured the Raman spectra of single and polycrystalline Cs_2ZnCl_4 and followed up with high pressure studies[135] of the same compound. A normal coordinate analysis was performed on the $ZnCl_4^{2-}$ ion assuming T_d symmetry and using the modified Urey-Bradley force field[136-138]. Using the force constants for the tetrahedral $ZnCl_4^{2-}$ ion obtained by Avery et al.,[110] Wong derived at a set of fundamental modes whose frequencies agree

TABLE 3.4.1

Structural parameters of Cs_2CuCl_4[5] and Cs_2ZnCl_4[7]

Both belong to space group *Pnma*-D_{2h}^{16}

Unit cell dimensions:

	Cs_2ZnCl_4	Cs_2CuCl_4
a	9.7577 Å	9.7599 Å
b	7.4004 Å	7.6091 Å
c	12.9704 Å	12.3967 Å

Anion bond lengths and bond angles:

	M = Zn	M = Cu
M-Cl(1)	2.249 Å	2.244
M-Cl(2)	2.259 Å	2.235
M-Cl(3)	2.252 Å	2.220 Å
Cl(1)-M-Cl(2)	115.34 °	131.2 °
Cl(1)-M-Cl(3)	109.62 °	101.6 °
Cl(2)-M-Cl(3)	106.52 °	99.7 °
Cl(3)-M-Cl(3)	109.03 °	127.1 °

very closely with the observed ones. These are shown in table 3.4.2. As described earlier (figure 3.1.2), the fundamental modes of a tetrahedral MX_4 species belong to the irreducible representations $(a_1 + e + 2t_2)$, all of which are Raman-active while the $2t_2$ modes are also infra-red-active.

TABLE 3.4.2

Calculated frequencies (in cm^{-1}) for $ZnCl_4^{2-}$ ion according to Wong[135]. The force constants are those obtained by Avery et al.[110]

	Calc	Obs	(293°K) *
$\nu(t_2)$	297.3	298.3	s
	297.3	278.0	sh
	297.3		
$\nu(a_1)$	287.0	288.7	s
$\delta(t_2)$	133.4	142.3	m
	133.4	130.8	s
	133.4		
$\delta(e)$	121.2	116.7	s
	121.2	111.0	sh

* The description of band intensities are in accordance with the published spectrum, but provided by us.

We have performed a normal coordinate analysis of the $ZnCl_4^{2-}$ ion in GVFF using the calculated frequencies of Wong (table 3.4.2) as these are appropriate for a regularly tetrahedral symmetry. Since only four frequencies are available, only four force constants can be expected. The F_S matrix elements, which are derived from table 3.3.1 by setting $\theta = \phi = 109.5^{\circ}$, are shown in table 3.4.3. The corresponding G_S matrix elements were obtained from standard tabulations[120], and are not included here.

TABLE 3.4.3

F_S matrix elements for T_d $ZnCl_4^{2-}$ ion

a_1	$F_{11} = f_r + 3f_{rr}$
e	$F_{22} = f_\alpha + f_{\alpha\alpha}' - 2f_{\alpha\alpha}$
t_2	$F_{33} = f_r - f_{rr}$
	$F_{34} = 2^{\frac{1}{2}} r(f_{r\alpha} - f_{r\alpha}')$
	$F_{44} = r^2(f_\alpha - f_{\alpha\alpha}')$

As seen from table 3.4.3, the F_S matrix contains five independent terms: f_r, f_{rr}, $(f_{r\alpha} - f_{r\alpha}')$, $(f_\alpha - f_{\alpha\alpha}')$ and $(f_{\alpha\alpha} - f_{\alpha\alpha}')$. The obvious procedure is to set one of these equal to zero, in which case the two most likely candidates are $(f_{r\alpha} - f_{r\alpha}')$ and $(f_{\alpha\alpha} - f_{\alpha\alpha}')$. Alternatively, if one of the terms is allowed to assume a series of values, then we can find values for the other four which fit the spectrum exactly. Thus, calculations were performed over a range of conceivable values for $(f_{r\alpha} - f_{r\alpha}')$: 0.0 to 0.2 millidyne Å^{-1}. The force constants obtained are shown in table 3.4.4.

TABLE 3.4.4

Force constants for $ZnCl_4^{2-}$ (in millidyne $Å^{-1}$)

with assumed values for $(f_{r\alpha} - f_{r\alpha}')$

$f_{r\alpha} - f_{r\alpha}'$	f_r	f_{rr}	$f_\alpha - f_{\alpha\alpha}'$	$f_{\alpha\alpha} - f_{\alpha\alpha}'$
0.000	1.158	0.188	0.112	0.005
0.025	1.218	0.167	0.104	0.001
0.050	1.269	0.151	0.101	0.000
0.075	1.313	0.136	0.102	0.000
0.100	1.351	0.123	0.104	0.001
0.125	1.385	0.112	0.110	0.004
0.150	1.414	0.102	0.117	0.007
0.175	1.439	0.094	0.126	0.012
0.200	1.459	0.087	0.137	0.017

With $(f_{r\alpha} - f_{r\alpha}')$ assumed to be zero, the force constants obtained are quite comparable with those previously published[122,123,7], allowing for the variations of the experimental frequencies used. As the assumed value of $(f_{r\alpha} - f_{r\alpha}')$ is increased, f_r increases fairly rapidly while f_{rr} falls. The value of $(f_\alpha - f_{\alpha\alpha}')$ remains roughly constant, while $(f_{\alpha\alpha} - f_{\alpha\alpha}')$ is close to zero throughout the range of $(f_{r\alpha} - f_{r\alpha}')$ values considered. Thus, $(f_{\alpha\alpha} - f_{\alpha\alpha}')$ appears to be relatively unimportant; however, this parameter is always so close to zero that the other four will be poorly determined if we try to evaluate them by setting $(f_{\alpha\alpha} - f_{\alpha\alpha}')$ equal to zero. It is noted that f_r and f_{rr} are very sensitive to the chosen value of $(f_{r\alpha} - f_{r\alpha}')$ and it is difficult to decide upon the most probable value of the latter.

Further guidance on this problem is sought from the study of the related square coplanar MX_4^{2-} species as described in the following section.

3.4.2 *Square Coplanar MX_4^{n-} Ions*

A rather extensive study of the vibrational spectra of square coplanar anions MX_4^{n-} (M = Pd, Pt or Au; X = Cℓ, Br or I; n = 1 or 2) was reported by Goggin and Mink[119]. Using where possible solution data which are appropriate for a 'free' ion approximation, they performed a force constant analysis on each MX_4^{n-} species. Their results are shown in table 3.4.6 (a).

The $\underset{\sim}{F}_S$ matrix elements, which can be derived by setting $\theta = 180^\circ$ and $\phi = 90^\circ$ in table 3.3.1, are shown in table 3.4.5; the corresponding $\underset{\sim}{G}_S$ matrix elements were again obtained from standard tabulations[120]. Referring to figure 3.1.2, the irreducible representations of the fundamental modes of a MX_4 species are $(a_{1g} + b_{1g} + b_{2g} + a_{2u} + b_{2u} + 2e_u)$. The a_{1g}, b_{1g} and b_{2g} modes are Raman-active, a_{2u} and e_u modes are infra-red-active while b_{2u} is inactive.

Using the same set of observed frequencies as Goggin and Mink but added to it the calculated b_{2u} frequency (table 3.4.7), we recalculated the force constants for each species assuming $(f_{r\phi} - f_{r\phi}')$ equal to zero. This was an exercise to evaluate the effects on the other force constants if the stretch-bend interaction constant was ignored. The results are shown in table 3.4.6 (b).

TABLE 3.4.5

$\underset{\sim}{F}_S$ matrix elements for D_{4h} MX_4^{n-} ion

a_{1g}	$F_{11} = f_r + 2f_{rr} + f_{rr}'$
a_{2u}	$F_{22} = r^2(f_\theta + f_{\theta\theta})$
b_{1g}	$F_{33} = f_r - 2f_{rr} + f_{rr}'$
b_{2g}	$F_{44} = r^2(f_\phi - 2f_{\phi\phi} + f_{\phi\phi}')$
b_{2u}	$F_{55} = r^2(f_\theta - f_{\theta\theta})$
e_u	$F_{66} = f_r - f_{rr}'$
	$F_{67} = 2^{\frac{1}{2}}r(f_{r\phi} - f_{r\phi}')$
	$F_{77} = r^2(f_\phi - f_{\phi\phi}')$

As seen from table 3.4.6, a direct consequence of ignoring $(f_{r\phi} - f_{r\phi}')$ is to significantly increase the ratio f_{rr}'/f_r. In the real situations, the ratios f_{rr}'/f_r are smaller, and $(f_{r\phi} - f_{r\phi}')$ is always greater than $(f_{\phi\phi} - f_{\phi\phi}')$ by a factor of 2 to 6.

3.4.3 *Conclusion*

The results of the two previous sections show conclusively that in dealing with $CuCl_4^{2-}$ ion, where the extent of distortion is intermediate between a square plane and a tetrahedron, we cannot afford to neglect the stretch-bend interaction constants,

TABLE 3.4.6

(a) Force constants by Goggin and Mink[119]

(b) Force constants by assuming $(f_{r\phi} - f_{r\phi}') = 0$

	$PdCl_4^{2-}$		$PdBr_4^{2-}$		$PtCl_4^{2-}$		$PtBr_4^{2-}$		PtI_4^{2-}		$AuCl_4^-$		$AuBr_4^-$	
	(a)	(b)	(a)	(b)	(a)	(b)	(a)	(b)	(a)	(b)	(a)	(b)	(a)	(b)
f_r	1.53	1.45	1.37	1.23	1.81	1.77	1.63	1.53	1.40	1.26	2.20	2.17	1.85	1.77
f_{rr}	0.08	0.09	0.06	0.07	0.07	0.08	0.06	0.06	0.07	0.07	0.08	0.08	0.08	0.09
f_{rr}'	0.16	0.25	0.15	0.30	0.28	0.32	0.22	0.32	0.24	0.39	0.16	0.21	0.13	0.21
$f_{r\phi} - f_{r\phi}'$	0.08	0.00	0.09	0.00	0.06	0.00	0.09	0.00	0.09	0.00	0.06	0.00	0.08	0.00
$f_\phi - f_{\phi\phi}'$	0.19	0.21	0.15	0.19	0.22	0.23	0.20	0.22	0.17	0.21	0.22	0.23	0.18	0.19
$f_{\phi\phi} - f_{\phi\phi}'$	0.01	0.02	0.01	0.03	0.03	0.04	0.02	0.04	0.01	0.04	0.03	0.04	0.02	0.03
f_θ	0.10	0.10	0.07	0.08	0.13	0.13	0.09	0.10	0.07	0.08	0.12	0.12	0.08	0.09

TABLE 3.4.7

Experimental frequencies (in cm^{-1}) which produced force constants of table 3.4.6 (b)

	$PdCl_4^{2-}$	$PdBr_4^{2-}$	$PtCl_4^{2-}$	$PtBr_4^{2-}$	PtI_4^{2-}	$AuCl_4^-$	$AuBr_4^-$
a_{1g}	300.0	188.0	328.0	205.0	155.0	349.0	214.0
a_{2u}	150.0	114.0	147.0	105.0	85.0	142.0	99.0
b_{1g}	270.0	172.0	305.0	192.0	142.0	325.0	196.0
b_{2g}	176.0	106.0	173.0	113.0	85.0	172.0	106.0
b_{2u}*	98.0	57.0	112.0	65.0	45.0	108.0	61.0
e_u	321.0	243.0	313.0	227.0	180.0	361.0	252.0
e_u	161.0	104.0	165.0	112.0	85.0	166.0	106.0

* calculated values[119]

although there is some justification for ignoring the bend-bend interaction constants. In order that the overall force constants are more accurately determined, small non-zero values could be assumed for the bend-bend interaction constants; the order of magnitude of these should be about 10 percent of the relevant primary bending force constants.

3.5 *SUMMARY OF RESULTS AND CONCLUSION*

The importance of normal coordinate analysis has been emphasised by Mohan et al.[139] We quote: "It is well known that a serious interpretation of the strength of chemical bonds using vibrational spectroscopy can only be provided by normal coordinate analysis. This, in essence, means the calculation of the force constants from the vibrational frequencies." However, the results of such analysis would only be meaningful if all the inherent assumptions and approximations have been closely scrutinised and vindicated. In the GVFF, where the method requires more approximations than other models, there is a dangerous tendency to adopt an over-simplified view of the problem concerned.

We have adopted a cautious and systematic approach throughout this work in deriving at a set of force constants which best describe the vibrations of the $CuCl_4^{2-}$ ion, within an isolated-ion approximation. Assumptions on the relative importance of the force constants in the GVFF were made only after a close examination of those found in the related systems. Consequently, the results obtained form part of the total picture.

The major conclusions to be drawn from this work may be summarised as follows:

(A) To the extent that the crystal modes in Cs_2CuCl_4 can be definitely related to the isolated-ion modes, the ordering of the latter is probably

$$\nu(a_1) > \nu(e) > \nu(b_2) > \delta(b_2) > \delta(e) > \delta(b_1) > \delta(a_1)$$

as in assignment I.

(B) For $CuCl_4^{2-}$ ion, and presumably for related species as well, it is important to include stretch-bend interaction constants in the analysis. Our results have shown that in neglecting these terms, McGinnety[5] had committed himself to a much too simplistic treatment of the problem.

(C) Within the isolated-ion approximation, the general valence force constants of $CuCl_4^{2-}$ are as shown in table 3.5.1 (see also table 3.3.6).

The errors quoted in table 3.5.1 are not to be regarded as absolute errors; they are simply the allowed limits within which reasonable values, within the constraints specified in section 3.3.3, of force constants can be located.

The results we have presented so far may reasonably be challenged on the grounds that the isolated-ion approximation is invalid where we are using single-crystal experimental data. In the crystal, there will be mixing between internal anion modes and lattice modes. There will also be factor group splitting (or correlation splitting), as is evident in Cs_2CuCl_4. These effects may well be sufficient to render our isolated-ion force constants invalid. It may be argued that solution spectra would be more appropriate as input data for a normal coordinate analysis of the isolated ion. Apart from possible problems with ion paring

TABLE 3.5.1

General valence force constants (in millidyne $\mathring{A}^{-1}$) of $CuCl_4^{2-}$ ion, within an isolated-ion approximation

f_r	1.26 ± 0.01
f_{rr}	0.19 ± 0.00
f_{rr}'	0.20 ± 0.01
f_θ	0.10 ± 0.00
$*f_\phi$	0.11 ± 0.00
$f_{r\theta} - f_{r\theta}'$	0.08 ± 0.01
$f_{r\phi} - f_{r\phi}'$	0.10 ± 0.01
$*f_{\theta\phi}$	0.01
$*f_{\phi\phi}$	0.01

* assumed values

and anion-solvent interactions, the exact geometry of the anion in solution is not known. McGinnety[5] calculated the crystal forces acting upon the bonds within a $CuCl_4^{2-}$ ion and, having corrected for these effects and for thermal motion, derived at a value of 2.283 $\mathring{A}$ for the Cu-Cl bond length in a 'free' $CuCl_4^{2-}$ ion. This is significantly longer than the mean Cu-Cl distance in the

crystal. Thus, while the assignment problem has probably been solved, drawing on the support of the infra-red evidence[113], the values of the force constants in the real situations may well be quite different. We therefore undertook a normal coordinate analysis of the complete unit cell (chapter 4). This is justified in that it completes the whole venture of the interpretation of the vibrational spectrum of Cs_2CuCl_4, and that the force constants thus obtained would afford a useful comparison with the results obtained within the isolated-ion approximation.

CHAPTER 4 ANALYSIS OF THE VIBRATIONS OF CAESIUM TETRACHLOROCUPRATE(II) CRYSTAL

4.1 *INTRODUCTION*

Solid state vibrational spectra exhibit unique features which distinguish them from the gaseous and solution spectra. These can be attributed to a different symmetry environment within the crystal and the presence of significant intermolecular forces. Thus, the vibrational selection rules applicable to 'free' molecules or ions are relaxed as exemplified by the observation, in the solid spectra, of previously 'forbidden' bands as weak absorption features. Also, the lowering of site symmetry in the crystal causes single bands, which are intrinsically degenerate, to split into multiplets. The most distinctive feature of solid state spectra, however, is the presence of low-frequency bands which are called lattice modes.

It is convenient to classify the observed vibrational frequencies of solids into two categories:

(A) the internal modes or molecular modes; and

(B) the external modes or lattice modes.

The internal modes arise from the vibrations of atoms relative to one another within a group of atoms, in the crystal, bound together by intramolecular forces that are usually covalent in nature. Accordingly, these modes have frequencies which are very close to those of the free molecules or ions (see section 3.2). The lattice

modes arise from the motions of entire molecules or ions relative to one another in the crystal. The intermolecular forces involved are much weaker than the intramolecular forces since the former are either ionic or Van der Waals in nature. Thus, the lattice modes are at much lower energies than the internal modes.

Any meaningful discussion of crystal vibrations depends on the knowledge of the symmetry present in the crystal. Such information is obtained from X-ray crystallography. Many texts have been written on the subject of crystal symmetry; discussion in this area is thus omitted. The crystallographic data on which the present work was based was obtained from reference 5, but the symmetry elements pertaining to space group D_{2h}^{16} were obtained from International Tables for X-ray Crystallography[140], and Wyckoff notations[141] concerning the atom positions in the unit cell were followed.

There are two qualitative approaches to the analysis of crystal vibrations. These are the site group analysis and the factor group or unit cell analysis[142]. In the site group approach, which was developed by Halford[143] in 1946, intermolecular coupling of vibrations in the crystal is completely ignored. The internal modes are obtained as a result of a lowered site symmetry. In the factor group analysis, complete vibrational coupling in the crystal is assumed. The method considers that only the motions of atoms in a unit cell give rise to the observed frequencies; hence it is sometimes called the unit cell approach.

The $\underset{\sim}{GF}$ matrix method developed by Wilson[144,145] for the study of molecular vibrations has been found to be also applicable to the calculation of optically active lattice frequencies of crystals.

The adaption of the method for this purpose has been described in detail in a paper by Shimanouchi, et al.[146].

In our present work, the analysis of the vibrations of Cs_2CuCl_4 crystal is based fundamentally on the method of Shimanouchi et al[146], but only the unit cell atoms were considered. Thus, the vibrations of the atoms are considered to belong to the irreducible representations of D_{2h}^{16} factor group. This is true in the $k = 0$ approximation (k is the wave vector) when translationally related atoms in each unit cell move in phase. The unit cell is in fact treated as a giant polyatomic molecule, and the $\underset{\sim}{GF}$ matrix method described earlier (section 3.2.3), with slight modification, applies.

In many ways, our approach resembles that described in a paper by Beattie et al. [147] ; however, to suit our purpose, computation was carried out using a series of programs, instead of only one that is all-inclusive, at various stages of the calculations. Computational difficulties are indeed quite considerable in view of the size of the matrices involved. A detail computing procedure is described in appendix III.

As mentioned at the end of the previous chapter, the aim of the present work is primarily to arrive at a physically acceptable set of force constants for Cs_2CuCl_4 corresponding to the assignment of the anion modes established in the isolated-ion analysis. It is also important that an appropriate model force field be defined such that the experimentally observed lattice frequencies and internal mode splittings can be reproduced.

Various features of crystal vibrations pertaining to Cs_2CuCl_4 are also to be investigated; in particular, the extent of mixing of the internal crystal modes is to be carefully examined.

4.2 *STRUCTURE OF UNIT CELL AND MATRIX METHOD*

4.2.1 *Unit Cell Parameters*

The latest reported crystal structure data of Cs_2CuCl_4[5] were used in this work. These are reproduced in table 4.2.1, using standard notations consistent with *Pnma*-D_{2h}^{16} space group[140]. The atom positions in the unit cell were obtained from reference 141 using Wyckoff notations.

The complete set of Cartesian coordinates, with reference to the origin at (0, 0, 0), for the 28 atoms is as shown in table 4.2.2. Figure 4.2.1 is a schematic representation of the unit cell, drawn in perspective, together with the numbering of the atoms used in our calculation; the origin is indicated in the figure.

4.2.2 *Matrix Method*

It is most convenient to work in Cartesian coordinates in dealing with the 28-atom primitive orthorhombic unit cell. Each atom is assigned a set of three displacement vectors, parallel to the unit cell edges (figure 4.2.1). The Cartesian inverse kinetic energy matrix $\underset{\sim}{G}^{c}$ is simply a diagonal matrix (84 × 84) whose non-zero elements are the reciprocal masses of the atoms. The 84 Cartesian coordinates are combined into 84 symmetry coordinates by

TABLE 4.2.1

Crystal structure data of Cs_2CuCl_4 [5]

(orthorhombic, $Pnma - D_{2h}^{16}$)

Unit cell: a = 9.7599 Å

b = 7.6091 Å

c = 12.3967 Å

Position Parameters:

Atom	Position*	x	y	z
Cu	(4c)	0.23054	0.25	0.41806
Cs(1)	(4c)	0.63399	0.25	0.39679
Cs(2)	(4c)	0.00556	0.25	0.67481
Cl(1)	(4c)	0.0054	0.25	0.3812
Cl(2)	(4c)	0.3430	0.25	0.5751
Cl(3)	(8d)	0.2937	-0.0112	0.3556

* Wyckoff notations:

(4c) ± (u ¼ v; u + ½, ¼, ½ − v)

(8) ± (xyz; x + ½, ½ − y, ½ − z; x, ½ − y, z; ½ − x, $\bar{y}$, z + ½)

TABLE 4.2.2

Cartesian coordinates (in Å) of

Cs_2CuCl_4 unit cell atoms

	x	y	z	(N)*
Cu	2.25005	1.90228	5.18256	2
	7.50985	5.70683	7.21414	3
	7.13	1.90228	1.01579	1
	2.6299	5.70683	11.3809	4
Cs(1)	6.18768	1.90228	4.91889	1
	3.57222	5.70683	7.47781	7
	1.3077	1.90228	1.27946	4
	8.45217	5.70683	11.1172	6
Cs(2)	0.054265	1.90228	8.36542	3
	9.70563	5.70683	4.03128	5
	4.93422	1.90228	10.2296	2
	4.82568	5.70683	2.16707	8
Cl(1)	0.052704	1.90228	4.72562	6
	9.7072	5.70683	7.67108	10
	4.93265	1.90228	1.47273	1
	4.82725	5.70683	10.924	13
Cl(2)	3.34765	1.90228	7.12934	5
	6.41225	5.70683	5.26736	9
	8.2276	1.90228	-0.930992	2
	1.5323	5.70683	13.32769	14
Cl(3)	2.86648	-0.085222	4.40827	8
	6.89342	7.69432	7.98843	11
	7.74643	3.88977	1.79008	3
	2.01347	3.71933	10.6066	16
	2.86648	3.88977	4.40827	7
	6.89342	3.71933	7.98843	12
	2.01347	7.69432	10.6066	15
	7.74643	-0.085222	1.79008	4

* N = Designated number of each atom in the unit cell (refer figure 4.2.1).

Figure 4.2.1 SCHEMATIC REPRESENTATION OF THE UNIT CELL OF Cs_2CuCl_4

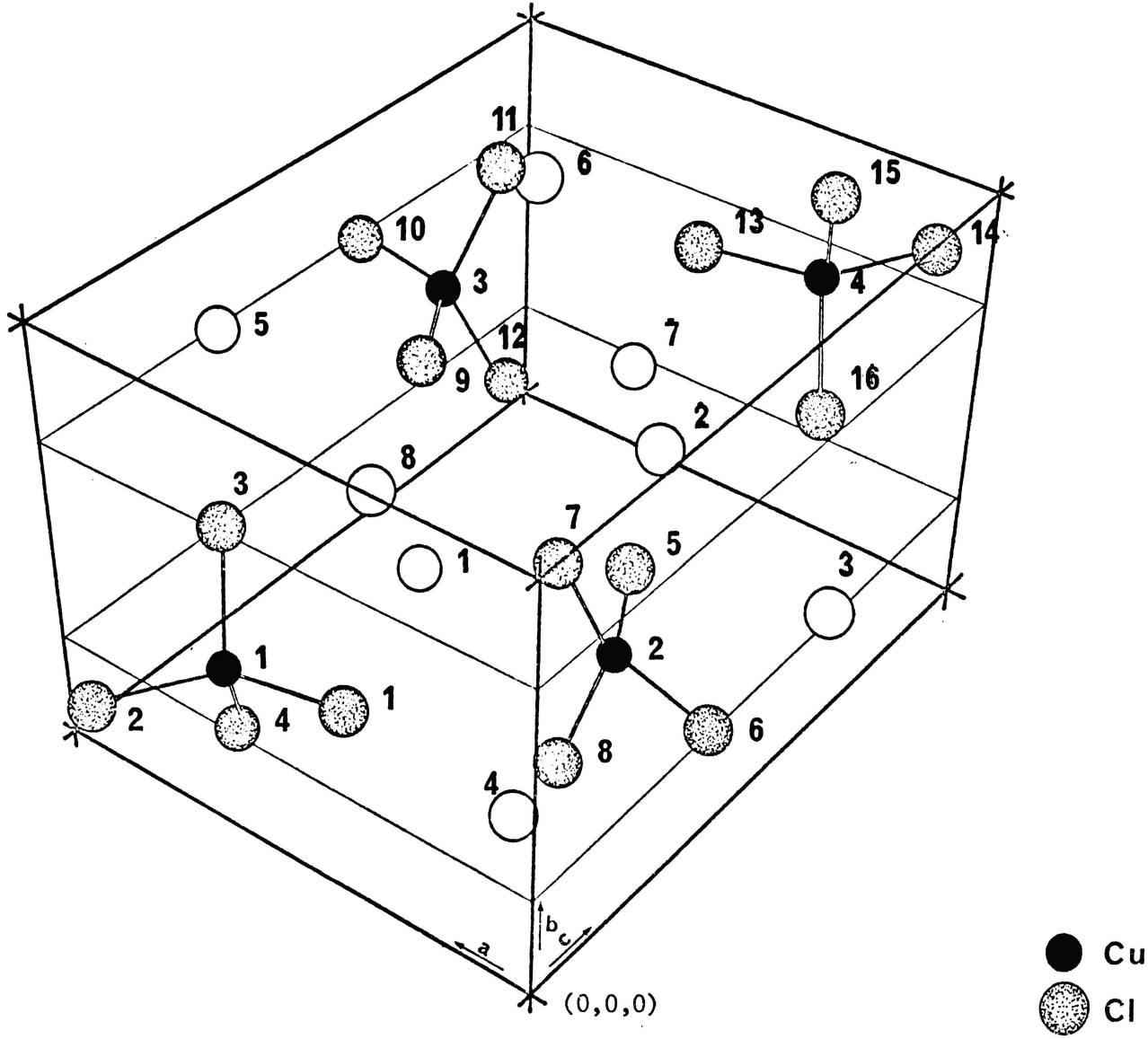

Figure 4.2.1 SCHEMATIC REPRESENTATION OF THE UNIT CELL OF Cs_2CuCl_4

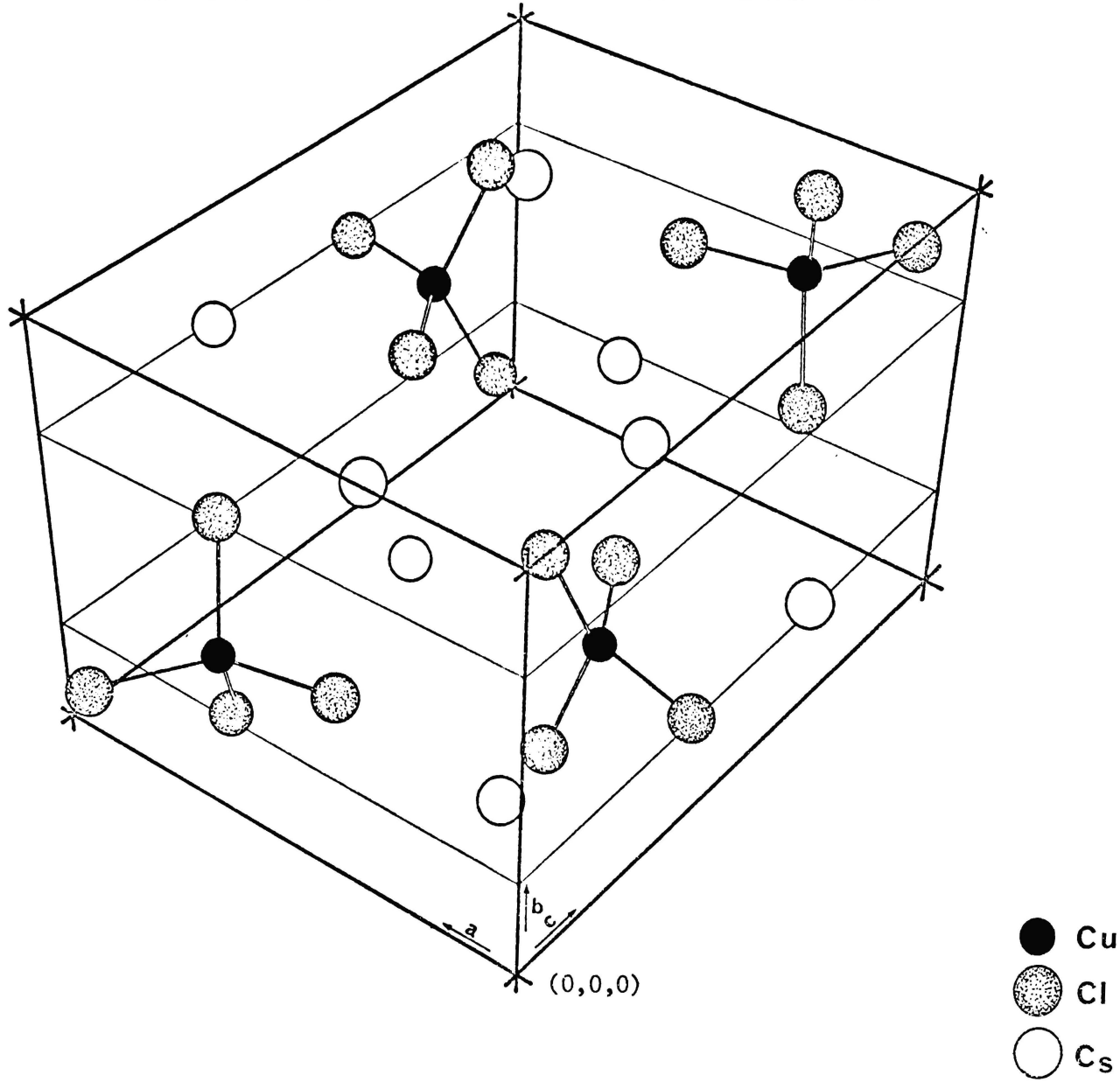

the usual group theoretical methods; the symmetry coordinates are linear combinations of the Cartesian coordinates belonging to irreducible representations of the D_{2h} factor group, in accordance with the results of factor group analysis [112] [113] (appendix II). This process can be described by the following matrix equation:

$$\underset{\sim}{S} = \underset{\sim\sim}{U}\underset{\sim}{X} \qquad (29),$$

where $\underset{\sim}{X}$ is the column vector of Cartesian coordinates, $\underset{\sim}{S}$ is the column vector of symmetry coordinates, and $\underset{\sim}{U}$ is an 84×84 transformation matrix.

The symmetry-adapted inverse kinetic energy matrix $\underset{\sim}{G}^{c}_{s}$ is then obtained from

$$\underset{\sim}{G}^{c}_{s} = \underset{\sim\sim}{U}\underset{\sim}{G}^{c}\underset{\sim}{U}^{t} \qquad (30),$$

where $\underset{\sim}{U}^{t}$ is the transpose of $\underset{\sim}{U}$.

The potential energy matrix in the Cartesian coordinates is set up in terms of the force constant matrix $\underset{\sim}{F}_{i}$. The latter is a square matrix of order q, where q is the number of chosen internal coordinates defined by the potential force field of the unit cell. The Cartesian symmetry-adapted force constant matrix $\underset{\sim}{F}^{c}_{s}$ is then obtained from

$$\underset{\sim}{F}^{c}_{s} = \underset{\sim}{B}^{t}_{s}\underset{\sim}{F}_{i}\underset{\sim}{B}_{s} \qquad (31),$$

where $\underset{\sim}{B}$ is a matrix which transforms internal coordinates into Cartesian coordinates (as in equation (10), chapter 3), and $\underset{\sim}{B}_{s}$ is its symmetry-adapted derivative according to equation (32).

$$\underset{\sim}{B}_S = \underset{\sim}{B}\underset{\sim}{U}^t \qquad (32).$$

In $\underset{\sim}{B}$, as defined earlier in section 3.2.2, the element b_{ij} is equal to the displacement of the ith internal coordinate caused by a small unit displacement of the jth Cartesian coordinate. Thus, the elements of $\underset{\sim}{B}$ can be calculated from the crystallographic atom positions [5].

$\underset{\sim}{F}^{\mathcal{C}}_S$ and $\underset{\sim}{G}^{\mathcal{C}}_S$ are both 84 × 84 matrices, but their product $\underset{\sim}{G}^{\mathcal{C}}_S\underset{\sim}{F}^{\mathcal{C}}_S$ is not symmetric. Symmetrisation of the product matrix is carried out using the method of Shimanouchi et al.[146] as follows:

A diagonal matrix (84 × 84), $(\underset{\sim}{G}^{\mathcal{C}}_S)^{\frac{1}{2}}$, is defined such that its non-zero elements are the square roots of the corresponding elements of the $\underset{\sim}{G}^{\mathcal{C}}_S$ matrix. Thus,

$$(\underset{\sim}{G}^{\mathcal{C}}_S)^{\frac{1}{2}}(\underset{\sim}{G}^{\mathcal{C}}_S)^{\frac{1}{2}} = \underset{\sim}{G}^{\mathcal{C}}_S \qquad (33),$$

and

$$(\underset{\sim}{G}^{\mathcal{C}}_S)^{-\frac{1}{2}}(\underset{\sim}{G}^{\mathcal{C}}_S)^{\frac{1}{2}} = \underset{\sim}{E} \qquad (34),$$

where $\underset{\sim}{E}$ is an identity matrix of the same order. Now,

$$\underset{\sim}{G}^{\mathcal{C}}_S\underset{\sim}{F}^{\mathcal{C}}_S\underset{\sim}{L} = \underset{\sim}{L}\underset{\sim}{\Lambda} \qquad (35),$$

which is an extension of equation (22) of section 3.2.3, and in which $\underset{\sim}{\Lambda}$ is a diagonal matrix whose elements are the eigenvalues of the product matrix $\underset{\sim}{G}^{\mathcal{C}}_S\underset{\sim}{F}^{\mathcal{C}}_S$, and $\underset{\sim}{L}$ is the corresponding eigenvector matrix. Then,

$$(\underset{\sim}{G}^{\mathcal{C}}_S)^{\frac{1}{2}}\underset{\sim}{F}^{\mathcal{C}}_S(\underset{\sim}{G}^{\mathcal{C}}_S)^{\frac{1}{2}}\cdot(\underset{\sim}{G}^{\mathcal{C}}_S)^{-\frac{1}{2}}\underset{\sim}{L} = (\underset{\sim}{G}^{\mathcal{C}}_S)^{-\frac{1}{2}}(\underset{\sim}{G}^{\mathcal{C}}_S\underset{\sim}{F}^{\mathcal{C}}_S\underset{\sim}{L}) = (\underset{\sim}{G}^{\mathcal{C}}_S)^{-\frac{1}{2}}\underset{\sim}{L}\underset{\sim}{\Lambda} \qquad (36).$$

If, we now define

$$\underset{\sim}{L}' = (\underset{\sim}{G}^{\mathcal{C}}_{\mathcal{S}})^{-\frac{1}{2}}\underset{\sim}{L} \qquad (37),$$

equation (36) becomes

$$(\underset{\sim}{G}^{\mathcal{C}}_{\mathcal{S}})^{\frac{1}{2}}\underset{\sim}{F}^{\mathcal{C}}_{\mathcal{S}}(\underset{\sim}{G}^{\mathcal{C}}_{\mathcal{S}})^{\frac{1}{2}}\underset{\sim}{L}' = \underset{\sim}{L}'\underset{\sim}{\Lambda} \qquad (38).$$

The matrix $(\underset{\sim}{G}^{\mathcal{C}}_{\mathcal{S}})^{\frac{1}{2}}\underset{\sim}{F}^{\mathcal{C}}_{\mathcal{S}}(\underset{\sim}{G}^{\mathcal{C}}_{\mathcal{S}})^{\frac{1}{2}}$ is symmetric and the same $\underset{\sim}{\Lambda}$, c.f. equation (35), is obtained, from which the frequencies of the crystal modes are obtained using equation (20).

The original eigenvector matrix, $\underset{\sim}{L}$, is obtained from

$$\underset{\sim}{L} = (\underset{\sim}{G}^{\mathcal{C}}_{\mathcal{S}})^{\frac{1}{2}}\underset{\sim}{L}' \qquad (39).$$

4.2.3 *Matrix Data*

Before proceeding to the actual calculations as described in appendix III, various matrix data had to be constructed, and some of these stored as data files for computation. The important programs used in this work are given in appendix IV.

$\underset{\sim}{S}$ Matrix

The derivation of the 84 symmetry coordinates which form the elements of the column vector $\underset{\sim}{S}$ is given in appendix V.

$\underset{\sim}{X}$ Matrix

The order in which the 84 Cartesian displacement vectors appear in the column matrix $\underset{\sim}{X}$ is given in appendix VI.

$\underset{\sim}{U}$ and $\underset{\sim}{U}^{t}$ Matrices

The $\underset{\sim}{U}$ matrix (84 × 84) was obtained from equation (29) while its transpose $\underset{\sim}{U}^{t}$ was obtained using program TRN; the latter

was stored as a data file UTXL.DAT.

$\underset{\sim}{R}$ Matrix

This is a column vector of chosen internal coordinates in accordance with the potential force field defined in Section 4.3.1. The order in which the q elements appear is given in appendix VII.

$\underset{\sim}{B}_s$ and $\underset{\sim}{B}_s^t$ Matrices

The elements b_{ij} of $\underset{\sim}{B}$ matrix ($q \times 84$) corresponding to the chosen internal coordinates (as in $\underset{\sim}{R}$ matrix) were determined using the method shown in appendix VIII. These were calculated from the atom coordinates of table 4.2.2. The $\underset{\sim}{B}_s$ matrix ($q \times 84$) was obtained by equation (32) and its transpose $\underset{\sim}{B}_s^t$ by program TRN; these were stored as data files BSXL.DAT and BSTXL.DAT respectively as (84×84) matrices by filling the empty rows and columns with zero elements.

$\underset{\sim}{G}_s^c$ Matrix

The non-zero elements of the diagonal matrix $\underset{\sim}{G}^c$ (84×84) are given in appendix IX. The symmetry-adapted $\underset{\sim}{G}_s^c$ matrix (84×84) was obtained from equation (30); to economise on space this was stored as a row matrix. Thus, $(\underset{\sim}{G}_s^c)'$ matrix (1×84) consists of 84 non-zero elements $(g_s^c)_i'$ which correspond directly to the elements $(g_s^c)_{ii}$ of $\underset{\sim}{G}_s^c$ matrix (84×84). The row matrix data file was named GCSXL.DAT.

4.3 *RESULTS AND DISCUSSION*

4.3.1 *Unit Cell Force Field*

Our aim here was to define a potential function, for the unit cell of Cs_2CuCl_4, which would allow us to obtain good agreement between observed and calculated frequencies. This essentially means the choice of internal coordinates, $\underset{\sim}{R}$, the number of which is arbitrary, and their associated force constants, $\underset{\sim}{F_i}$. We aimed at including as many internal coordinates as were required to make the set kinematically complete; to economise on computer time, the number had to be restricted to those considered to be most important.

A realistic force field for the unit cell of Cs_2CuCl_4 should include contributions from the following sources:

(A) intramolecular potential due to $CuCl_4^{2-}$ anions;

(B) anion site symmetry perturbation;

(C) cation-anion interaction; and

(D) anion-anion interaction.

(A) Intramolecular Potential

Referring to figure 4.2.1, the unit cell of Cs_2CuCl_4 contains four distinguishable $CuCl_4^{2-}$ anions. The set of internal coordinates must then include the ten coordinates for each anion, so that the $\underset{\sim}{F_i}$ matrix includes the primary and interaction force constants previously discussed in chapter 3 (see also $\underset{\sim}{F_R}$ matrix in appendix I), four times over. These coordinates were, however, appropriate only to an idealised

D_{2d} symmetry. The $\underset{\sim}{B}$ matrix, whereby $\underset{\sim}{F_i}$ would be transformed into $\underset{\sim}{F_s^C}$ using equation (31), was constructed from the crystallographic atom positions and reflects the C_s site symmetry. Thus, in setting up the valence force constants of the anions, such lowering of anion symmetry in the crystal must be duely considered.

(B) Site Symmetry Perturbation

To take into account the effects of actual site symmetry, we made distinctions between the primary force constants associated with different bond lengths and bond angles in the anion; the interaction force constants were not deemed to be greatly affected. We propose the following relationships

(i) $$f_r \propto r^{-3} \qquad (40).$$

The primary force constant associated with a stretching coordinate is inversely proportional to the cube of Cu-Cℓ bond distance. This relationship is invariably true in diatomic molecules where the quadratic force constants are related to the equilibrium bond lengths by Badger's rule[126]: $k_e = a/(r_e-d)^3$, a and b are chosen parameters. For polyatomic molecules or ions, this relationship appears to be an acceptable approximation.

(ii) $$f_\alpha \propto (\sin\alpha)^{\frac{1}{2}} \qquad (41).$$

The primary force constant associated with a bending coordinate is directly proportional to the square root of $\sin\alpha$, where α is the Cℓ-Cu-Cℓ bond angle. This relationship

is rather arbitrary; it is, however, in line with the relative magnitudes of $f_\theta(\theta = 129.2^\circ)$ and $f_\phi(\phi = 100.6^\circ)$ found in the isolated-ion analysis (refer table 3.5.1).

(C) Cation-anion Interaction

This was considered in the form of Cs ... Cℓ displacements in a central force field (CFF) formalism. In addition, we included interaction constants associated with Δr(Cu-Cℓ$_a$) and Δq(Cs ... Cℓ$_a$) coordinates, where Cℓ$_a$ was a common atom, as off-diagonal terms in the $F_{\sim i}$ matrix. These were intuitively thought to be of some importance to achieve factor group splittings of the stretching mode frequencies. We selected Cs ... Cℓ contacts of less than 3.57 Å, the sum of the ionic radiiof Cs^+ and $C\ell^-$, allocating them force constant terms according to their symmetries in the unit cell.

Thus, for instance, $f_{Cs \ldots C\ell}(m)$ implies the force constant associated with Δq(Cs ... Cℓ) coordinate lying in a mirror plane; the atom positions correspond to those of 4(*c*) by Wyckoff's notations (table 4.2.1). Conversely, $f_{Cs \ldots C\ell}(1)$ implies the force constant associated with Δq(Cs ... Cℓ) coordinate not lying in a mirror plane; the Cs atom positions are 4(*c*) while the Cℓ atom positions are 8(*d*). These central force constants were further differentiated by their variations in Cs ... Cℓ distances, e.g. $f_{Cs \ldots C\ell}(m)$ and $f_{Cs \ldots C\ell}(m')$ are force constant terms associated with Δq(Cs ... Cℓ) coordinates of same symmetry but different Cs ... Cℓ distances.

There were a total of 24 such force constants (table 4.3.1), some atoms from adjacent cells having been included to define

the complete set of internal coordinates. Table 4.3.2 shows the corresponding Cu-Cℓ ... Cs stretching interaction constants defined in four different sets according to the associated Cu-Cℓ ... Cs angles. Thus, $f_{Cu_i\text{-}Cl_j \ldots Cs_k}(\alpha)$ is defined as the force constant associated with the internal coordinates $\Delta r(Cu_i\text{-}Cl_j)$ and $\Delta q(Cs_k \ldots Cl_j)$ with $Cu_i\text{-}Cl_j \ldots Cs_k$ angle equal to α°. The set of interaction constants was set up symmetrically as off-diagonal elements of the $\underset{\sim}{F}_i$ matrix, totalling 48.

(D) Anion-anion Interaction

This was considered in the form of Cℓ ... Cℓ displacements in CFF formalism. Sixteen shortest Cℓ ... Cℓ contacts between different anions were selected and allocated force constant terms $f_{Cl \ldots Cl}(l)$ and $f_{Cl \ldots Cl}(l')$ (table 4.3.3); the convention used in labelling these force constants is the same as in (C). The next shortest Cℓ ... Cℓ distance is *ca.* 0.04 Å away.

The complete $\underset{\sim}{F}_i$ matrix, then, assumed a dimension of 80 × 80. Our neglect of the longer-range interactions meant that the set of coordinates was not kinematically complete, and some low-frequency lattice modes might remain unaccounted for. However, we are mainly interested in the anion modes which are not likely to be greatly affected by such longer-range crystal interactions. Accordingly, interactions of the types Cu ... Cu and Cu ... Cs were not considered. Likewise, Cs ... Cs interactions which could be important in pinpointing the lattice modes but otherwise unimportant were not included.

TABLE 4.3.1

Selected Cs ... Cℓ central force constants and the associated internal coordinates r_i

Force constant	r_i	q(Å)	i
$f_{Cs \ldots C\ell}^{(m)}$	$\Delta q(Cs_2 \ldots C\ell_2)$	3.5177	41
	$\Delta q(Cs_3 \ldots C\ell_5)$	3.5177	42
	$\Delta q(Cs_5 \ldots C\ell_9)$	3.5177	43
	$\Delta q(Cs_8 \ldots C\ell_{14})$	3.5177	44
$f_{Cs \ldots C\ell}^{(m')}$	$\Delta q(Cs_3^* \ldots C\ell_2)$	3.4827	45
	$\Delta q(Cs_2 \ldots C\ell_5)$	3.4827	46
	$\Delta q(Cs_8 \ldots C\ell_9)$	3.4827	47
	$\Delta q(Cs_5^* \ldots C\ell_{14})$	3.4827	48
$f_{Cs \ldots C\ell}^{(l)}$	$\Delta q(Cs_5 \ldots C\ell_3)$	3.4876	49
	$\Delta q(Cs_5^* \ldots C\ell_4)$	3.4876	50
	$\Delta q(Cs_8 \ldots C\ell_7)$	3.4876	51
	$\Delta q(Cs_8^* \ldots C\ell_8)$	3.4876	52
	$\Delta q(Cs_2^* \ldots C\ell_{11})$	3.4876	53
	$\Delta q(Cs_2 \ldots C\ell_{12})$	3.4876	54
	$\Delta q(Cs_3^* \ldots C\ell_{15})$	3.4876	55
	$\Delta q(Cs_3 \ldots C\ell_{16})$	3.4876	56

Table 4.3.1 continued

$f_{Cs \ldots Cl}(l')$	$\Delta q(Cs_8 \ldots Cl_3)$	3.4604	57
	$\Delta q(Cs_8^* \ldots Cl_4)$	3.4604	58
	$\Delta q(Cs_5^* \ldots Cl_7)$	3.4604	59
	$\Delta q(Cs_5^* \ldots Cl_8)$	3.4604	60
	$\Delta q(Cs_3^* \ldots Cl_{11})$	3.4604	61
	$\Delta q(Cs_3^* \ldots Cl_{12})$	3.4604	62
	$\Delta q(Cs_2^* \ldots Cl_{15})$	3.4604	63
	$\Delta q(Cs_2 \ldots Cl_{16})$	3.4604	64

q = Cs ... Cl distance

A_i^* = Atom from neighbouring cell translationally related to A_i.

TABLE 4.3.2

Cu-Cℓ ... Cs interaction force constants and the associated internal coordinates

Force constant

$f_{Cu-C\ell \ldots Cs}^{(\alpha)}$

$\Delta r(Cu_1-C\ell_2)\ \Delta q(Cs_2 \ldots C\ell_2)$ $\quad \alpha = 81.16^\circ$

$\Delta r(Cu_2-C\ell_5)\ \Delta q(Cs_3 \ldots C\ell_5)$ $\quad \alpha = 81.16^\circ$

$\Delta r(Cu_3-C\ell_9)\ \Delta q(Cs_5 \ldots C\ell_9)$ $\quad \alpha = 81.16^\circ$

$\Delta r(Cu_4-C\ell_{14})\ \Delta q(Cs_8 \ldots C\ell_{14})$ $\quad \alpha = 81.16^\circ$

$f_{Cu-C\ell \ldots Cs}^{(\beta)}$

$\Delta r(Cu_1-C\ell_2)\ \Delta q(Cs_3 \ldots C\ell_2)$ $\quad \beta = 177.69^\circ$

$\Delta r(Cu_2-C\ell_5)\ \Delta q(Cs_2 \ldots C\ell_5)$ $\quad \beta = 177.69^\circ$

$\Delta r(Cu_3-C\ell_9)\ \Delta q(Cs_8 \ldots C\ell_9)$ $\quad \beta = 177.69^\circ$

$\Delta r(Cu_4-C\ell_{14})\ \Delta q(Cs_5 \ldots C\ell_{14})$ $\quad \beta = 177.69^\circ$

$f_{Cu-C\ell \ldots Cs}^{(\gamma)}$

$\Delta r(Cu_1-C\ell_3)\ \Delta q(Cs_5 \ldots C\ell_3)$ $\quad \gamma = 148.83^\circ$

$\Delta r(Cu_1-C\ell_4)\ \Delta q(Cs_5 \ldots C\ell_4)$ $\quad \gamma = 148.83^\circ$

$\Delta r(Cu_2-C\ell_7)\ \Delta q(Cs_8 \ldots C\ell_7)$ $\quad \gamma = 148.83^\circ$

$\Delta r(Cu_2-C\ell_8)\ \Delta q(Cs_8 \ldots C\ell_8)$ $\quad \gamma = 148.83^\circ$

$\Delta r(Cu_3-C\ell_{11})\ \Delta q(Cs_2 \ldots C\ell_{11})$ $\quad \gamma = 148.83^\circ$

$\Delta r(Cu_3-C\ell_{12})\ \Delta q(Cs_2 \ldots C\ell_{12})$ $\quad \gamma = 148.83^\circ$

$\Delta r(Cu_4-C\ell_{15})\ \Delta q(Cs_3 \ldots C\ell_{15})$ $\quad \gamma = 148.83^\circ$

$\Delta r(Cu_4-C\ell_{16})\ \Delta q(Cs_3 \ldots C\ell_{16})$ $\quad \gamma = 148.83^\circ$

Table 4.3.2 continued

$$f_{Cu\text{-}C\ell \ \ldots \ Cs}{}^{(\delta)} \quad \begin{cases} \Delta r(Cu_1\text{-}C\ell_3)\ \Delta q(Cs_8 \ \ldots \ C\ell_3) & \delta = 105.88^{\circ} \\ \Delta r(Cu_1\text{-}C\ell_4)\ \Delta q(Cs_8 \ \ldots \ C\ell_4) & \delta = 105.88^{\circ} \\ \Delta r(Cu_2\text{-}C\ell_7)\ \Delta q(Cs_5 \ \ldots C\ell_7)) & \delta = 105.88^{\circ} \\ \Delta r(Cu_2\text{-}C\ell_8)\ \Delta q(Cs_5 \ \ldots \ C\ell_8) & \delta = 105.88^{\circ} \\ \Delta r(Cu_3\text{-}C\ell_{11})\Delta q(Cs_3 \ \ldots \ C\ell_{11}) & \delta = 105.88^{\circ} \\ \Delta r(Cu_3\text{-}C\ell_{12})\Delta q(Cs_3 \ \ldots \ C\ell_{12}) & \delta = 105.88^{\circ} \\ \Delta r(Cu_4\text{-}C\ell_{15})\Delta q(Cs_2 \ \ldots \ C\ell_{15}) & \delta = 105.88^{\circ} \\ \Delta r(Cu_4\text{-}C\ell_{16})\Delta q(Cs_2 \ \ldots \ C\ell_{16}) & \delta = 105.88^{\circ} \end{cases}$$

Footnote: r is referred to here as a Cu-Cℓ bond stretching coordinate and is not to be confused with the elements r_i of $\underset{\sim}{R}$ matrix (appendix VII).

TABLE 4.3.3

Cℓ ... Cℓ central force constants and the associated internal coordinates r_i

Force constant	r_i	t(Å)	i
$f_{C\ell \ldots C\ell}^{(l)}$	$\Delta t(C\ell_1 \ldots C\ell_7)$	4.1032	65
	$\Delta t(C\ell_1 \ldots C\ell_8)$	4.1032	66
	$\Delta t(C\ell_{13} \ldots C\ell_{11})$	4.1032	67
	$\Delta t(C\ell_{13} \ldots C\ell_{12})$	4.1032	68
	$\Delta t(C\ell_6 \ldots C\ell_3^*)$	4.1032	69
	$\Delta t(C\ell_6 \ldots C\ell_4^*)$	4.1032	70
	$\Delta t(C\ell_{10} \ldots C\ell_{15}^*)$	4.1032	71
	$\Delta t(C\ell_{10} \ldots C\ell_{16}^*)$	4.1032	72
$f_{C\ell \ldots C\ell}^{(l')}$	$\Delta t(C\ell_9 \ldots C\ell_7)$	4.0758	73
	$\Delta t(C\ell_9 \ldots C\ell_8^*)$	4.0758	74
	$\Delta t(C\ell_5 \ldots C\ell_{11}^*)$	4.0758	75
	$\Delta t(C\ell_5 \ldots C\ell_{12})$	4.0758	76
	$\Delta t(C\ell_2 \ldots C\ell_{15}^*)$	4.0758	77
	$\Delta t(C\ell_2 \ldots C\ell_{16})$	4.0758	78
	$\Delta t(C\ell_{14} \ldots C\ell_3)$	4.0758	79
	$\Delta t(C\ell_{14} \ldots C\ell_4^*)$	4.0758	80

t = Cℓ ... Cℓ distance

A_i^* = Atom from neighbouring cell translationally related to A_i.

Thus, the potential energy of the unit cell of Cs_2CuCl_4 in this work was defined as:

$$2V = \sum_{k=1}^{4} \left[\sum f_{ii} (\Delta r_i)^2 + \sum_{i \neq j} f_{ij} (\Delta r_i)(\Delta r_j) \right]_k$$

$$+ \sum k_{ii} (\Delta q_i)^2 + \sum k'_{ij} (\Delta r_i)(\Delta q_j)$$

$$+ \sum l_{ii} (\Delta t_i)^2 \qquad (42);$$

where

f_{ii} = valence force constants (anion)

f_{ij} = valence interaction constants (anion)

k_{ii} = central force constants associated with Cs ... Cl displacements

k'_{ij} = interaction constants associated with coordinates $\Delta r(\text{Cu-Cl}_a) \Delta q(\text{Cs ... Cl}_a)$

r = Cu-Cl bond distance or Cl-Cu-Cl bond angle

q = Cs ... Cl distance

t = Cl ... Cl distance

4.3.2 *Site Group Analysis*

The valence force constants of table 3.5.1 as obtained from the isolated-ion analysis were first used to set up the F_i matrix with no external force constants. Thus, the F_i matrix consisted of 40 × 40 elements diagonally blocked out, with 10 × 10 elements to each block (see F_R matrix, appendix I). As individual values were required as input for each force constant appearing in the F_i matrix, $f_{r\theta}'$ and $f_{r\phi}'$ were given zero values while $f_{r\theta}$ and $f_{r\phi}$ assumed the values of the composite force constants $(f_{r\theta} - f_{r\theta}')$ and $(f_{r\phi} - f_{r\phi}')$, respectively. Such a procedure was unquestionably legitimate since the condition of the F_i matrix required that the same composite terms appeared in the final F_s matrix (similar to table 3.3.1) regardless of any variation in the individual contributions of $f_{r\theta}$, $f_{r\theta}'$, $f_{r\phi}$ and $f_{r\phi}'$ to the totals.

As described in section 4.3.1, the primary valence force constants were adjusted using relationships (40) and (41) so that they were appropriate to the actual C_s site symmetry. The crystallographic bond distances and bond angles were employed in making the adjustments; the value of f_r from the isolated-ion analysis was associated with the average Cu-Cℓ bond distance of 2.22975 Å.

The new set of force constants is shown in table 4.3.4. These produced 36 anion crystal modes which could be correlated with $6A'$ and $3A''$ site group vibrations (table 4.3.5).

The frequencies of the site group modes obtained were very similar to those from the isolated-ion analysis (table 3.3.6 (a)). The slight discrepancies could be attributed to the rounding-off errors of the force constants; in the isolated-ion analysis, the

TABLE 4.3.4

$CuCl_4^{2-}$ anion force constants

(in millidyne $\mathring{A}^{-1}$) from site group analysis

$f_r(Cu\text{-}Cl_1)$	1.2361
$f_r(Cu\text{-}Cl_2)$	1.2511
$f_r(Cu\text{-}Cl_3)$	1.2767
f_{rr}	0.19
f_{rr}'	0.20
$f_\theta(Cl_1\text{-}Cu\text{-}Cl_2)$	0.1008
$f_\theta(Cl_3\text{-}Cu\text{-}Cl_3)$	0.0992
$f_\phi(Cl_1\text{-}Cu\text{-}Cl_3)$	0.1105
$f_\phi(Cl_2\text{-}Cu\text{-}Cl_3)$	0.1095
$(f_{r\theta} - f_{r\theta}')$	0.08
$(f_{r\phi} - f_{r\phi}')$	0.10
$f_{\theta\phi}$	0.01
$f_{\phi\phi}$	0.01

Footnote: The Cl atoms are numbered as in table 3.4.1

TABLE 4.3.5

Calculated frequencies (in cm^{-1}) of the site group modes of Cs_2CuCl_4

Site (C_s)	cm^{-1}	Unit cell (D_{2h})	Ion (D_{2d})
A'	296.89	$a_g + b_{2g} + b_{1u} + b_{3u}$	$\nu(a_1)$
	287.06	$a_g + b_{2g} + b_{1u} + b_{3u}$	$\nu(e)$
	255.18	$a_g + b_{2g} + b_{1u} + b_{3u}$	$\nu(b_2)$
	142.15	$a_g + b_{2g} + b_{1u} + b_{3u}$	$\delta(b_2)$
	128.00	$a_g + b_{2g} + b_{1u} + b_{3u}$	$\delta(e)$
	98.47	$a_g + b_{2g} + b_{1u} + b_{3u}$	$\delta(a_1)$
A''	290.40	$b_{1g} + b_{3g} + a_u + b_{2u}$	$\nu(e)$
	122.52	$b_{1g} + b_{3g} + a_u + b_{2u}$	$\delta(e)$
	115.23	$b_{1g} + b_{3g} + a_u + b_{2u}$	$\delta(b_1)$

force constants were calculated to four decimal places whereas the input force constants in the site group analysis were only to two decimal places (table 3.5.1). In view of the good agreement between the two sets of frequencies, and that the site group modes were calculated from the anion force constants by setting up the appropriate $\underset{\sim}{F}_i$ matrix, we have also demonstrated that the approximation (equation (28)) made concerning the F_{12} element of the $\underset{\sim}{F}_s$ matrix of D_{2d} $CuCl_4^{2-}$ ion is indeed quite close to reality.

The significant effect of site symmetry on the anion modes was the removal of the degeneracy of *e* vibrations. As seen from table 4.3.5, the $\nu(e)$ anion mode was split by *ca.* 3.3 cm^{-1} and the $\delta(e)$ mode by *ca.* 5.5 cm^{-1}. No factor group splitting was obtained; this would only be achieved through a complete analysis of the unit cell in which crystal interactions are duely considered.

4.3.3 *Unit Cell Analysis*

The vibrational analysis of the unit cell of Cs_2CuCl_4 was performed using the potential force field defined in equation (42) and on the assumptions of intermolecular interactions discussed in section 4.3.1. Our preliminary study of the vibrations of Cs_2CuCl_4 in the isolated-ion approximation has led us to conclude that, insofar as the crystal modes could be definitely related to the isolated-ion modes, the ordering of the latter was

$$\nu(a_1) > \nu(e) > \nu(b_2) > \delta(b_2) > \delta(e) > \delta(b_1) > \delta(a_1)$$

This assignment, although contradicting that of Beattie et al.[112], was supported by the infra-red evidence[113]. Our aim then was to obtain a set of force constants which produced crystal mode frequencies close to the observed ones and in agreement with the assignment of the anion modes above. To this end, the defined force field must be able to account satisfactorily for the observed factor group splittings.

In our calculations, the weak band observed in the Raman at 253 cm^{-1} (with both b_{1g} and b_{3g} components) was ignored; a detailed discussion of the observed vibrational frequencies has already been presented in section 3.1.3. In addition, a b_{1g} band observed at

105 cm^{-1} was considered too weak to be positively assigned with any confidence, and was hence ignored.

Before proceeding to setting up a complete $\underset{\sim}{F}_i$ matrix, some preliminary investigation of the effects of external force constants on the internal modes was carried out. This was necessary for two important reasons

(A) to determine the appropriate values of the external force constants; and

(B) to gain an understanding on how these force constants effected factor group splittings.

The set of force constants obtained from the site group analysis was used as the initial approximate values of the internal force constants in the crystal. As explained earlier, cation-anion interactions in the unit cell were considered by means of including Cs ... Cℓ central force constants in the $\underset{\sim}{F}_i$ matrix. Twenty-four such force constants were included (table 4.3.1); a value of 0.1 millidyne $Å^{-1}$, which is similar to that used by Wong[135] in the analysis of Cs_2ZnCl_4, produced 24 lattice modes of frequencies between 90 - 30 cm^{-1}.

It was assumed that the highest frequency lattice modes were predominantly Cs ... Cℓ stretching in character. Thus, in setting these central force constants, we aimed at producing the observed lattice modes of 86 cm^{-1} (b_{2g}) and 83 cm^{-1} (b_{1u} or b_{3u}) (refer tables 3.1.2 and 3.1.3). We first varied the values of $f_{Cs \ldots Cl}$ according to the Cs ... Cℓ distances involved; the shorter the distance the larger the value of $f_{Cs \ldots Cl}$ was assumed. However, it was found that, using this method, the calculated crystal mode frequencies were not entirely consistent with the observed pattern

of factor group splittings. Better results were obtained by merely distinguishing these force constants by the symmetries of their associated internal coordinates. With $f_{Cs \ldots C\ell}(m, m')$ equal to 0.1 millidyne Å^{-1} and $f_{Cs \ldots C\ell}(l, l')$ equal to 0.2 millidyne Å^{-1}, the two highest frequency lattice modes were correctly placed at *ca.* 88 cm^{-1} (b_{2g}) and 80 cm^{-1} (b_{1u} and b_{3u}). It was not expected that such long-range crystal interaction constants should vary according to Badger's rule. Hence, only empirical adjustments of these force constants were made with the sole aim of arriving at consistency with the experimental data.

An important result of these calculations was that inclusion of Cs ... Cℓ force constants drove the internal modes to significantly higher frequencies. Tentative adjustments of the internal force constants were subsequently made so that the calculated frequencies were more in line with the observed ones. The overall adjustment of all these force constants would have to await the use of a complete $\underset{\sim}{F}_i$ matrix (80 × 80) in the final calculations.

Preliminary examination of the effects of Cu-Cℓ ... Cs stretching interaction constants on the internal modes was also carried out at this stage. Calculations were performed by using small values (*ca.* 0.01 millidyne Å^{-1}) of such off-diagonal terms (table 4.3.2) in the $\underset{\sim}{F}_i$ matrix consisting of internal force constants as well as the 24 Cs ... Cℓ central force constants. It was found that only the crystal modes of isolated-ion stretching parentage were affected; generally the effect was to lower the frequencies of

these modes by *ca.* 3 cm^{-1}. Of the four sets of interaction constants, $f_{Cu\text{-}C\ell \ldots Cs}(\beta)$, which has the largest Cu-Cℓ ... Cs angle, was most significant, followed by $f_{Cu\text{-}C\ell \ldots Cs}(\gamma, \delta)$. The effect of $f_{Cu\text{-}C\ell \ldots Cs}(\alpha)$, which has an acute Cu-Cℓ ... Cs angle, on the internal modes was minimal. These were thus ignored in later calculations.

We then considered the effects of anion-anion interactions on the internal modes. If, in addition to the internal force constants, 16 Cℓ ... Cℓ central force constants (table 4.3.3) were included in the $F_{\sim i}$ matrix, the resultant lattice modes would be largely due to such anion-anion interactions only. Using $f_{C\ell \ldots C\ell}(l)$ of 0.2 millidyne $\mathring{A}^{-1}$ and $f_{C\ell \ldots C\ell}(l')$ of 0.4 millidyne $\mathring{A}^{-1}$, compared with the single value of 0.3 millidyne $\mathring{A}^{-1}$ used by Wong[135] in the analysis of $Cs_2ZnC\ell_4$, 16 lattice modes of frequencies between 45 - 10 cm^{-1} were obtained. Empirical adjustments of $f_{C\ell \ldots C\ell}$ according to Cℓ ... Cℓ distances helped in some way towards achieving the desired factor group splittings. As there was no other legitimate criterion by which to estimate the correct values of $f_{C\ell \ldots C\ell}$ - the observed lattice modes of average frequencies most probably reflect crystal interactions of diverse nature - no serious attempt was made at this stage. A better estimation of the values of $f_{C\ell \ldots C\ell}$ could only be obtained when the overall adjustments of the force constants, using a complete $F_{\sim i}$ matrix, were made later.

One of the effects of the Cℓ ... Cℓ force constants on the internal modes was, again, to increase the frequencies of the latter, but only marginally. Thus, anion-anion interactions

appear to play a lesser role than cation-anion interactions in modifying the anion force constants.

The final calculations were performed by setting up the full 80 × 80 $\underset{\sim}{F}_i$ matrix consisting of all internal and external force constants. In each calculation, the $\underset{\sim}{F}_s^c$ matrix was checked to ensure that it was properly symmetry-blocked. After a few manual adjustments of the force constants, we settled for the set shown in table 4.3.6. In table 4.3.7, we give the crystal mode frequencies calculated from these force constants alongside the experimental[112,113] values.

The only major difficulty in relating the crystal modes to their isolated-ion parentage is that all these modes are mixed to a greater or lesser extent. This is especially damaging in the region 110 - 140 cm^{-1} where the crystal modes arising from $\delta(e)$ and $\delta(b_1)$ apparently overlap; while those of a_g, b_{2g}, b_{1u} and b_{3u} symmetries can only come from $\delta(e)$, the others are inextricably jumbled.

That mixing of the internal modes is wide-spread is evident from the following exercises:

(A) Increasing f_{rr} valence interaction force constant by 0.1 millidyne $Å^{-1}$ caused $\nu(a_1)$ crystal components to increase and $\nu(b_2)$ crystal components to decrease as predicted by the $\underset{\sim}{F}_s$ matrix elements (table 3.3.1) of the $CuCl_4^{2-}$ anion. However, in this case, it was found that the $\nu(e)$ crystal components of the same symmetries (a_g, b_{2g}, b_{1u}, b_{3u}) increased slightly as well, even though the anion $\underset{\sim}{F}_s$ matrix elements of

TABLE 4.3.6

Force constants (in millidyne $\mathring{A}^{-1}$) from unit cell analysis of Cs_2CuCl_4

Internal valence force constants*:

1	$f_r(Cu\text{-}Cl_1)$	1.1380
2	$f_r(Cu\text{-}Cl_2)$	1.1518
3	$f_r(Cu\text{-}Cl_3)$	1.1754
4	f_{rr}	0.1700
5	f_{rr}'	0.1870
6	$f_\theta(Cl_1\text{-}Cu\text{-}Cl_2)$	0.0635
7	$f_\theta(Cl_3\text{-}Cu\text{-}Cl_3)$	0.0625
8	$f_\phi(Cl_1\text{-}Cu\text{-}Cl_3)$	0.0753
9	$f_\phi(Cl_2\text{-}Cu\text{-}Cl_3)$	0.0746
10	$(f_{r\theta} - f_{r\theta}')$	0.0500
11	$(f_{r\phi} - f_{r\phi}')$	0.0570
12	$f_{\theta\theta}$	0.0
13	$f_{\theta\phi}$	0.01
14	$f_{\phi\phi}$	0.01
15	$f_{\phi\phi}'$	0.0

Table 4.3.6 continued

External central force constants:

16	$f_{Cs \ldots Cl}(m)$	0.10
17	$f_{Cs \ldots Cl}(m')$	0.10
18	$f_{Cs \ldots Cl}(l)$	0.20
19	$f_{Cs \ldots Cl}(l')$	0.20
20	$f_{Cl \ldots Cl}(l)$	0.02
21	$f_{Cl \ldots Cl}(l')$	0.04

Valence-central interaction force constants:

22	$f_{Cu-Cl \ldots Cs}(\alpha)$	0.00
23	$f_{Cu-Cl \ldots Cs}(\beta)$	0.03
24	$f_{Cu-Cl \ldots Cs}(\gamma)$	0.01
25	$f_{Cu-Cl \ldots Cs}(\delta)$	0.01

* similar notations to those in table 4.3.4 are adopted here

TABLE 4.3.7

Calculated and observed crystal mode frequencies (in cm^{-1})

Ion (D_{2d})	Unit Cell (D_{2h})	Calc	Obs
		Internal Modes	
$\nu(a_1)$	b_{2g}	295.70	
	a_g	295.46	297
	b_{1u}	292.98	
	b_{3u}	292.69	
$\nu(e)$	b_{2u}	293.73	296
	b_{1g}	293.66	
	a_u	293.65	
	b_{3g}	293.58	
	b_{1u}	285.24	288
	b_{3u}	285.23	
	b_{2g}	284.52	
	a_g	284.49	280
$\nu(b_2)$	b_{1u}	257.43	258
	b_{3u}	257.39	
	b_{2g}	255.41	256
	a_g	255.37	251
$\delta(b_2)$	b_{3u}	151.48	151
	a_g	151.38	149
	b_{2g}	144.91	
	b_{1u}	144.62	

Table 4.3.7 continued

$\delta(e) + \delta(b_1)$	a_u	135.35	
	b_{3g}	134.94	141
	b_{2u}	128.19	136
	b_{1g}	128.00	136
	b_{1g}	116.02	
	b_{2u}	114.43	
	b_{3g}	113.27	
	a_u	110.64	
$\delta(e)$	b_{3u}	124.55	
	b_{1u}	123.42	123
	a_g	120.16	120
	b_{2g}	115.69	126
$\delta(a_1)$	a_g	110.78	103
	b_{2g}	109.51	103
	b_{1u}	106.05	
	b_{3u}	104.29	
		External Modes	
	b_{2g}	91.43	86
	b_{3u}	83.55	83
	b_{1u}	82.57	
	a_g	76.88	76
	b_{1g}	75.23	
	b_{2u}	74.19	79

Table 4.3.7 continued

b_{3g}	73.36	71
a_u	72.25	
b_{1u}	72.03	
b_{2g}	66.53	
b_{3u}	65.47	
b_{1g}	63.31	
b_{2u}	61.53	61
a_g	57.51	62
a_g	52.91	58
a_u	51.18	
b_{2g}	51.01	
b_{3g}	50.33	
b_{1u}	48.59	
b_{3u}	47.58	
b_{1u}	38.66	
a_u	37.36	
a_g	35.50	51
b_{2g}	35.18	
b_{2u}	31.47	
b_{3g}	28.20	38
b_{3u}	24.23	
9 others	< 20.00	

Footnote: Since the b_{1u} and b_{3u} modes were not differentiated in the original paper [113], assignments in these symmetries are those which give the best agreement with the calculations.

e symmetry include no f_{rr} term. Obviously, crystal modes arising from $\nu(e)$ isolated-ion mode possess some $\nu(a_1)$ character.

(B) Increasing f_θ, a force constant associated with $\delta(b_2)$ anion mode, resulted in an increase in the frequencies of $\delta(e)$ crystal components as well. Likewise, increasing f_ϕ, a force constant associated with $\delta(e)$, caused the frequencies of the $\delta(b_2)$ crystal components to increase. It is evident that crystal modes of these anion parentage are quite extensively mixed.

(C) Increasing the value of $f_{\phi\phi}$ should, on examining the appropriate $\underset{\sim}{F}_s$ matrix elements of the anion, decrease the frequency of the $\delta(b_1)$ anion mode hence the frequencies of its crystal components. However, it was found that all the bending frequencies between 110 - 140 cm^{-1} of b_{1g}, b_{3g}, a_u and b_{2u} symmetries decreased simultaneously, giving no clear-cut indication as to whether they are of $\delta(e)$ or $\delta(b_1)$ origin. These modes are again quite extensively mixed.

The results of the above investigation into the extent of mixing of the crystal modes thus revealed that no definite correlation of these modes to their isolated-ion parentage was possible without forcing the issue slightly. There is evidence, however, that the stretching modes are much less interferred with than the bending modes. This gives much credibility to the stretching force constants obtained; insofar as the bending force constants are

concerned, the calculated frequencies they produced are in satisfactory agreement with the observed ones showing no alarming signs of their being incorrectly determined.

The observed factor group splitting of 8 cm^{-1} between b_{2u} and (b_{1u} or b_{3u}) crystal components of $\nu(e)$ isolated-ion mode was successfully reproduced by our potential force field. A splitting of 9.2 cm^{-1} was obtained between a_g and b_{2u} components of the same anion mode compared with the observed splitting of 16 cm^{-1}. Similarly, the calculated splitting between a_g and (b_{1u} or b_{3u}) components of $\nu(b_2)$ was only 2 cm^{-1} compared with the observed splitting of 7 cm^{-1}; and hardly any splitting was obtained between the a_g and b_{2g} components of the same mode. The discrepancies in the last few areas should not be significant enough to discredit our defined force field, bearing in mind the extent of mixing of the crystal modes is not fully understood except for its wide-spread nature.

The overall agreement between the calculated and observed frequencies is quite satisfactory, as seen from table 4.3.7. This is particularly remarkable in view of the fact that the harmonic approximation inherent in the force constant analysis is not entirely appropriate where anharmonicity is probably closer to the real situation in the crystal. That the Raman band at 253 cm^{-1} could be a combination band is an evidence of such anharmonicity (see section 3.2.5). No doubt better agreement could be obtained using a more elaborate refinement procedure, such as is normally performed in normal coordinate analyses. However, we did not think that such refinement would be worth the expenditure of computer time which would be entailed, bearing in

mind that many of the predicted bands have not been observed, and some of the crystal mode assignments are doubtful. In any event, it is unlikely that the force constants in table 4.3.6 would be substantially changed by such refinement.

Compared with table 3.5.1, the relative magnitudes of the anion force constants of table 4.3.6 are quite similar. However, the latter force constants are significantly smaller. This arises mainly from the Cs ... Cℓ central force constants introduced into $\underset{\sim}{F}_i$ matrix; their effect is to drive the internal anion modes to higher frequencies, though this is partially relieved by the inclusion of Cu-Cℓ ... Cs interaction constants. This observation is consistent with the fact that the crystal modes in tetraalkylammonium tetrachlorocuprates(II) appear at lower frequencies[1,90] since, in this case, the cations become larger, and the lattice interactions become less important.

The Cℓ ... Cℓ interaction terms have a smaller but still substantial effect on the internal crystal modes. Nine of the 45 expected lattice modes (in addition to the three acoustic modes) turn up in the calculations to have zero frequencies; this arises, as discussed before, from the limitation we have imposed on the size of $\underset{\sim}{F}_i$ matrix by neglecting most of the longer-range lattice interactions. This could no doubt be rectified by introducing more Cℓ ... Cℓ and Cs ... Cℓ (and perhaps Cs ... Cs) force constants into $\underset{\sim}{F}_i$, but the anion force constants are unlikely to be greatly affected.

The factor group splitting is largely produced by the culmination of site symmetry perturbation, cation-anion interactions and anion-anion interactions, with the first two playing the more important role.

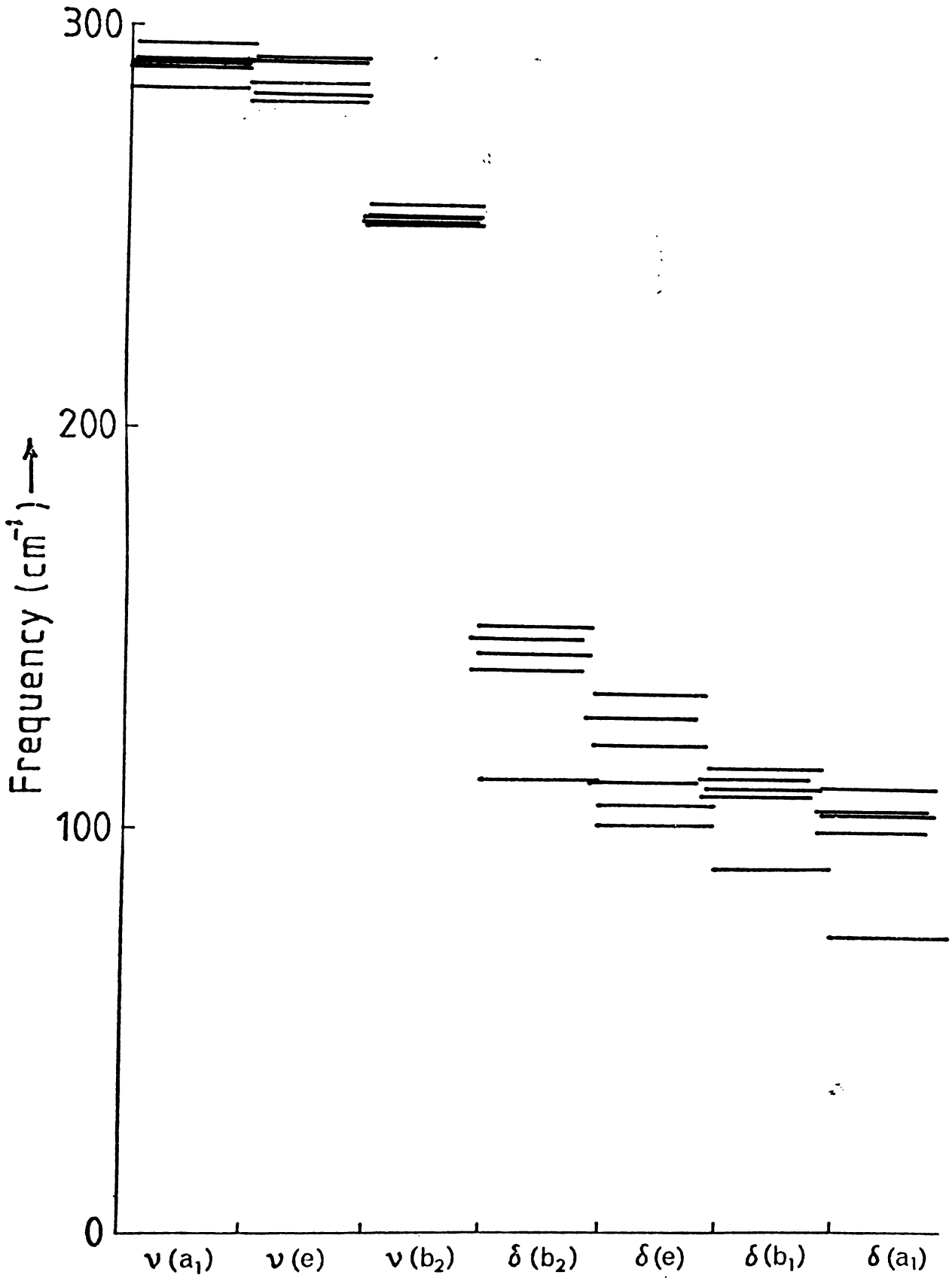
(c) Site Symmetry Perturbation
plus Cation-Anion Interactions
plus Anion-Anion Interactions
300
200
100
0
Frequency (cm⁻¹)
ν (a1)
ν (e)
ν (b2)
δ (b2)
δ (e)
δ (b1)
δ (a1)

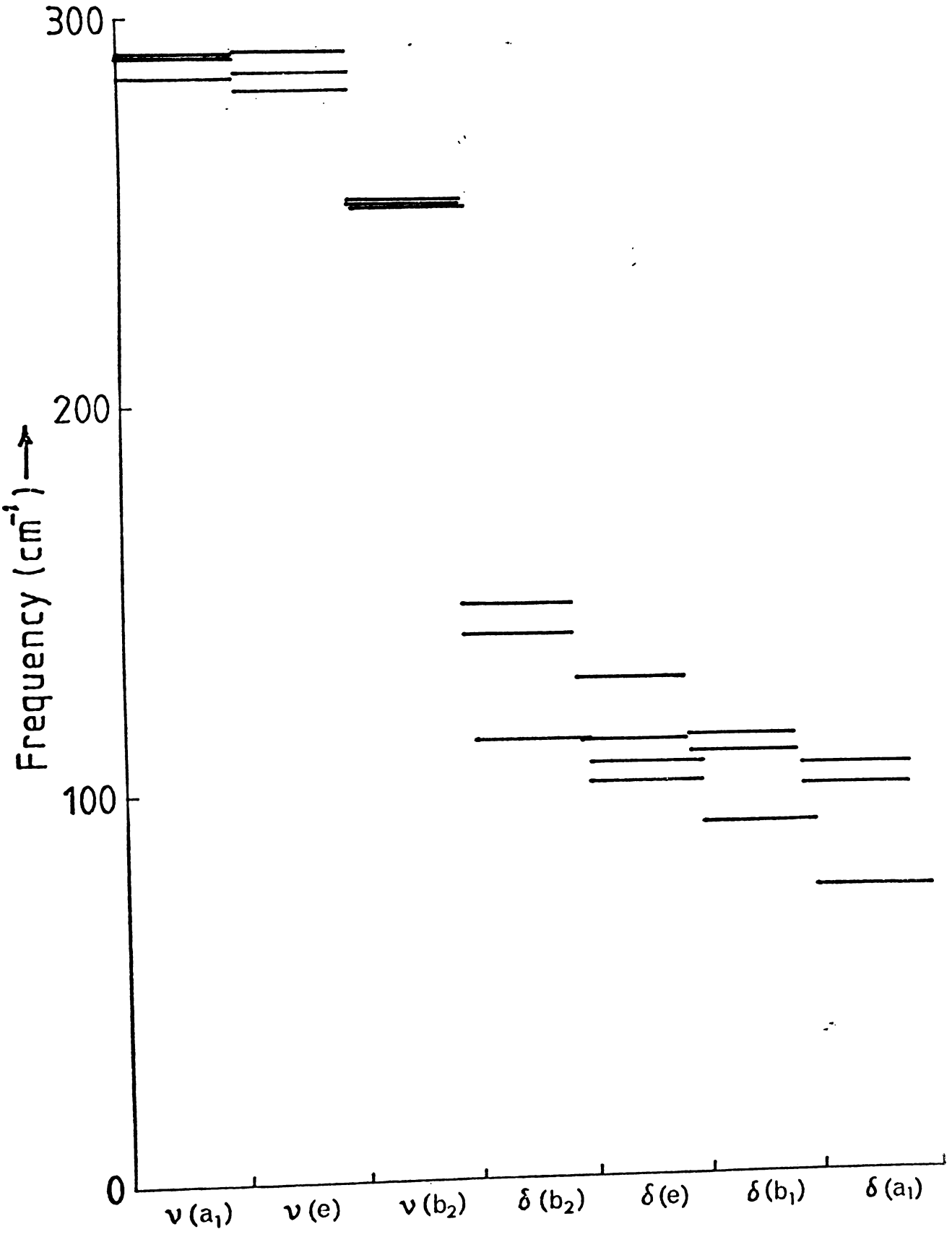
(b) Site Symmetry Perturbation
plus Cation-Anion Interactions
300
200
100
0
Frequency (cm⁻¹)
ν (a1)
ν (e)
ν (b2)
δ (b2)
δ (e)
δ (b1)
δ (a1)

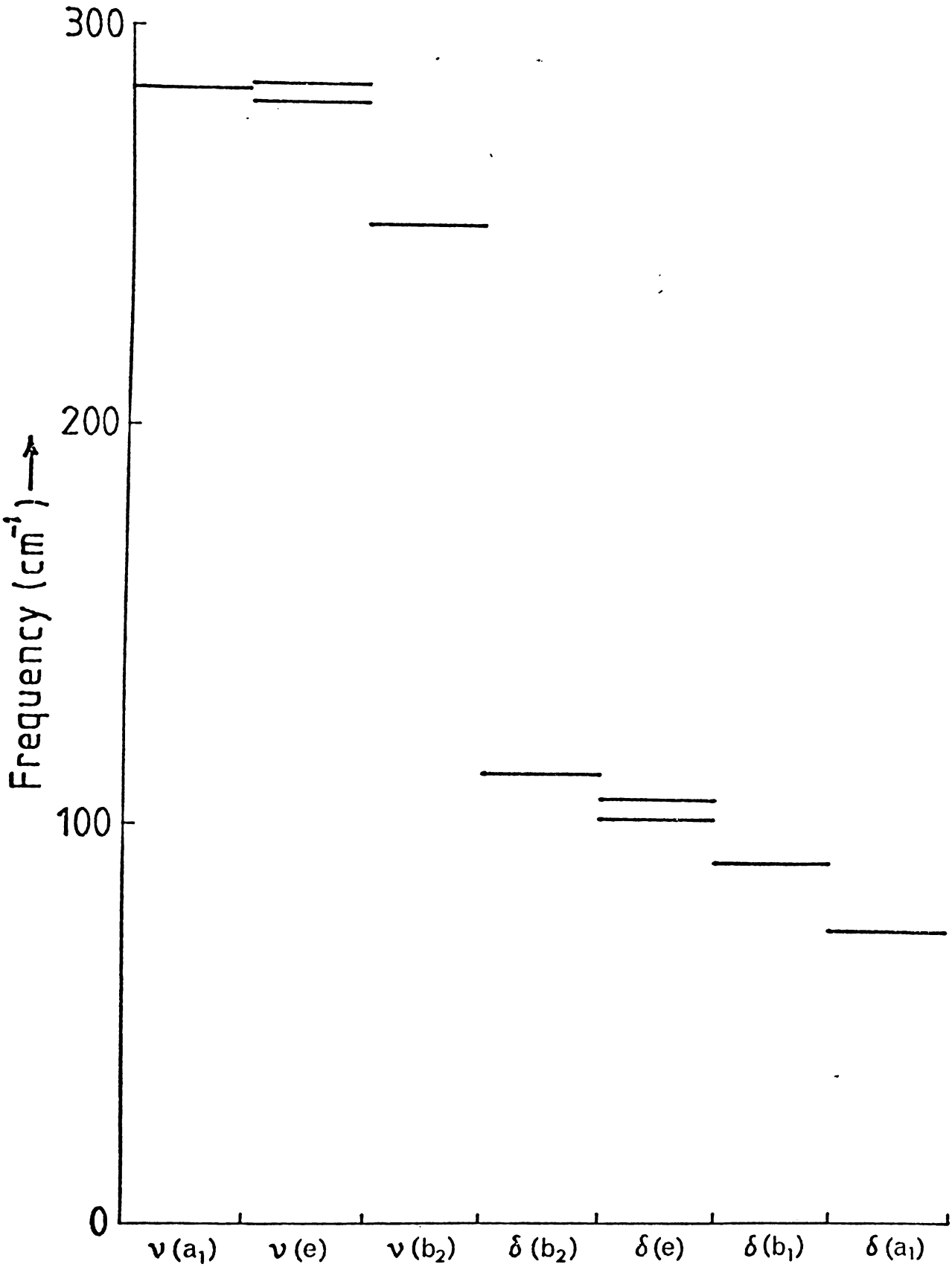
(a) Site Symmetry Perturbation
300
200
100
0
Frequency (cm⁻¹)
ν (a1)
ν (e)
ν (b2)
δ (b2)
δ (e)
δ (b1)
δ (a1)

This is graphically demonstrated in figure 4.3.1 (a), (b), (c).

To sum up, the set of force constants obtained from this work is physically satisfactory for reasons discussed in chapter 3, and the frequencies they produce are in good agreement with experimental evidence[112,113]. While this is by no means the unique solution*, our judicious choice of the initial $\underset{\sim}{F}_i$ matrix provided a basis towards a sensible solution, corresponding to a physically meaningful force field.

4.3.4 *Alternative Infra-red Assignment*

It was pointed out in section 3.1.3 that the table of infra-red data for Cs_2CuCl_4 in the original paper[113] was incorrectly labelled, most probably due to a printing error. At the early stage before the mistake was discovered, a unit cell analysis was carried out on Cs_2CuCl_4 using the Raman data of Beattie et al. (table 3.1.2) and Dunsmuir and Lane's infra-red data as they appeared in the original paper (table 3.1.3, with crystal mode symmetries b_{1u} and b_{2u} interchanged). Some rather interesting and instructive results have emerged from this work; a discussion of these is presented in this section.

Two possible assignments were considered in the unit cell analysis based on the results of isolated-ion analysis. They were assignments I and II of section 3.3.3. A similar method to that described in section 4.3.3 was followed, but some changes to the

* In principle, for a secular determinant of order N, there exists as many as N different matrices $\underset{\sim}{F}$ which can reproduce the observed frequencies[127].

unit cell force field were made. These are described below.

For simplicity, no site group perturbation was considered; the internal force constants were then appropriate only to D_{2d} symmetry. Site group splittings were nevertheless obtained because of the nature of the $\underset{\sim}{B}$ matrix elements; these were, however, of smaller magnitude than those calculated in section 4.3.2.

The 24 Cs ... Cℓ contacts were allocated a common force constant $f_{\text{Cs ... C}\ell}$. Likewise, the 16 Cℓ ... Cℓ contacts between different anions were given the same force constant $f_{\text{C}\ell\text{ ... C}\ell}$. In addition, the Cu-C$\ell$ ... Cs off-diagonal terms were ignored.

To account for the observed factor group splittings, an additional feature was included in the force field. This took into consideration the effect of dipolar coupling which represents part of long-range Coulomb interactions[148]. Various workers have made use of such dipolar interaction models with some degree of success[149-151]. To simulate the effect of dipolar coupling, we inserted into $\underset{\sim}{F_i}$ off-diagonal terms between symmetrically equivalent coordinates on different anions. Three interaction terms of this kind were allowed for: $f_{\mu r}$ (between Cu-Cℓ bonds), $f_{\mu\phi}$ (between the smaller interbond angles of *ca.* 100°) and $f_{\mu\theta}$ (between the greater bond angles of *ca.* 130°).

A similar procedure to that in section 4.3.3 was carried out to obtain the force constants which produced a good fit with the observed frequencies for both assignments I and II. The final values are shown in table 4.3.8. In table 4.3.9, we give the internal crystal mode frequencies calculated from these force

TABLE 4.3.8

Force constants (in millidyne Å^{-1}) from unit cell analysis of Cs_2CuCl_4 using the alternative infra-red assignment, with assignments I and II (see section 3.3.3) for isolated-ion modes

	I	II
f_r	1.205	1.180
f_{rr}	0.180	0.116
f_{rr}'	0.195	0.340
f_θ	0.080	0.080
f_ϕ	0.121	0.130
$(f_{r\theta} - f_{r\theta}')$	0.070	0.079
$(f_{r\phi} - f_{r\phi}')$	0.101	0.109
$f_{\theta\theta}$	0.0 *	0.0 *
$f_{\theta\phi}$	0.018	0.019
$f_{\phi\phi}$	0.010	0.011
$f_{\phi\phi}'$	0.0 *	0.0 *
$f_{Cs \ldots Cl}$	0.100	0.100
$f_{Cl \ldots Cl}$	0.040	0.040
$f_{\mu r}$	-0.010	-0.010
$f_{\mu\phi}$	-0.006	-0.006
$f_{\mu\theta}$	-0.001	-0.001

* Assumed values

TABLE 4.3.9

Calculated and observed crystal mode frequencies (in cm^{-1}) for Cs_2CuCl_4. Calculated values are those obtained from the force constants in Table 4.3.8; observed values are taken from references 112 and 113

Assignment		I			II		
		calc	obs		calc	obs	
$\nu(a_1)$	b_{2g}	300.3		b_{2g}	299.0		$\nu(a_1)$
	b_{1u}	297.6	296	b_{1u}	296.5	296	
	b_{3u}	297.5		b_{3u}	296.3		
	a_g	296.8	297	a_g	295.5	297	
$\nu(e)$	b_{1u}	287.8		b_{3u}	289.0	288	$\nu(b_2)$
	b_{3u}	287.7	288	b_{1u}	288.7		
	a_u	286.9		b_{2g}	286.6		
	b_{2g}	286.9		a_g	281.1	280	
	b_{1g}	286.8					
	b_{3g}	286.7					
	b_{2u}	280.4					
	a_g	280.4	280				

Table 4.3.9 continued

$\nu(b_2)$	b_{3u}	260.7	258	b_{3u}	258.2	258	$\nu(e)$
	b_{1u}	260.4		b_{1u}	258.2		
	b_{2g}	258.3	256	b_{2g}	257.5	256	
	a_g	252.2	251	a_u	257.5		
				b_{1g}	257.3		
				b_{3g}	257.2	253?	
				b_{2u}	250.5		
				a_g	250.3	251	
$\delta(b_2)$	b_{3u}	151.1	151	b_{2g}	153.3		$\delta(b_2)$
	b_{2g}	150.7		b_{3u}	152.8	151	
	b_{1u}	148.7		b_{1u}	151.3		
	a_g	146.7	149	a_g	149.4	149	
$\delta(e)$	b_{3u}	141.8		b_{3u}	142.6		$\delta(e)$
	b_{1u}	138.9	136	b_{1u}	138.7	136	
	b_{2g}	133.8	126	b_{2g}	134.2	126	
	a_g	121.6	120	a_g	121.7	120	
$\delta(e)$ + $\delta(b_1)$	a_u	142.4		a_u	145.1		$\delta(e)$ + $\delta(b_1)$
	b_{3g}	141.1	141	b_{3g}	144.1	141	
	b_{1g}	137.0	136	b_{1g}	140.4		
	b_{2u}	135.5		b_{2u}	138.2		
	b_{3g}	133.9		b_{3g}	137.4		
	b_{1g}	133.8		b_{1g}	136.8	136	
	a_u	129.3		a_u	132.9		
	b_{2u}	127.5	123	b_{2u}	131.0	123	

Table 4.3.9 continued

$\delta(a_1)$	b_{2g}	133.3		b_{2g}	113.4		$\delta(a_1)$
	b_{1u}	112.6		b_{1u}	112.9		
	b_{3u}	107.7		b_{3u}	108.2		
	a_g	104.7	103	a_g	104.8	103	

constants alongside the experimental values. The observed infra-red band at 296 cm^{-1} (now b_{1u}) was ascribed to one of the crystal components of $\nu(a_1)$ rather than $\nu(e)$ or $\nu(b_2)$. With assignment I, the weak band observed in the Raman spectrum at 253 cm^{-1} (with both b_{1g} and b_{3g} components) was ignored for similar reasons to those put forward in section 4.3.3; with assignment II, this band was regarded as the b_{3g} component of $\nu(e)$. With both assignments, a weak b_{1g} Raman band at 105 cm^{-1} was ignored. It should be noted that no distinction was made between b_{2u} and b_{3u} (or b_{1u} and b_{3u} in section 4.3.3) crystal modes in the original paper[113]; our assignments in these symmetries are those which gave the best agreement with the calculations.

The major difficulty in relating the crystal modes to their isolated-ion parentage was again the wide-spread mixing of the former; otherwise, with either of the isolated-ion assignments I and II, it is possible to devise assignments of the observed crystal modes which fit the calculated values to within a mean error of about 2 cm^{-1}, as shown in table 4.3.9. As with the isolated-ion calculation, the force constants found on the basis of assignment I are much more satisfactory than those obtained with assignment II.

The agreement between calculated and observed frequencies obtained in this section is clearly more impressive than that obtained in section 4.3.3; and yet the alternative infra-red assignment adopted here is contradictory to experimental evidence. In his normal coordinate anlaysis of $CuCl_4^{2-}$ ion, McGinnety rejected one assignment in favour of another on the grounds that the latter produced a better fit with the observed frequencies. It has

emerged from this work that such a criterion should not rank as the most important; other considerations such as the nature of the force field and the quality of the derived force constants should be higher in priorities.

The unit cell force field defined in thissection is unsatisfactory in that the neglect of site group perturbation and Cu-Cℓ ... Cs interactions may have significantly altered the final values of the force constants; in particular, it is doubtful whether inclusion in the $\underset{\sim}{F}_i$ matrix of off-diagonal terms between symmetrically equivalent coordinates on different anions to simulate dipolar coupling is mathematically correct. The valence force field of McGinnety can be challenged on the grounds that the neglect of stretch-bend interactions was made without justification. More importantly, the force constants derived from his assignment of the isolated-ion modes raise more doubts than they have answered.

4.3.5 *Conclusions*

The major conclusions to be drawn from this work may be summarised as follows:

(A) The results of unit cell analysis of Cs_2CuCl_4 further support the ordering of the isolated-ion modes as derived in chapter 3. There is now solid evidence pointing to the Raman single crystal frequencies of Beattie et al. being incorrectly assigned. The appropriate assignment is probably as shown in table 4.3.7, notwithstanding the confusion arising from the mixing of the internal modes.

(B) The isolated-ion approximation affords a useful guide to the relative magnitudes of the anion force constants in Cs_2CuCl_4, but the introduction of lattice terms, particularly Cs ... Cl stretching force constants has a considerable effect on the crystal modes, and the force constants obtained on the basis of our isolated-ion analysis are likely to be too large. Such approximation could, nevertheless, prove to be quite useful in the analysis of vibrations of chlorocuprates(II) with bulky cations, such as in tetraethylammonium tetrachlorocuprate(II), where cation-anion interactions in the crystal are less significant.

(C) It is apparent now normal coordinate analysis aimed singly at producing a good fit between the calculated and the observed frequencies does not necessarily provide conclusive evidence in support of a particular assignment of the vibrational modes. However, such analysis is useful, when more elaborate experimental methods have failed to establish the correct assignment, if it also considers other requirements, the most important of which is that the force constants obtained must be physically acceptable.

(D) On the basis of the agreement between the calculated and observed frequencies, the set of force constants as presented in table 4.3.6 constitute genuine parameters to which the physical and chemical properties of Cs_2CuCl_4 could be related. As far as we are aware, this is the first report of a full force constant analysis of a chlorocuprate(II)

compound; as such, it paves the way for a potentially fruitful field of research along the same line.

(E) It has been demonstrated that the potential force field as defined in equation (42), in the $k = 0$ approximation, is a competent model force field in a study of this kind. Almost similar force fields have been found to be useful in the studies of vibrations of hexagonal lithium iodate crystal[152] and Mg_2SiO_4[149].

The last conclusion is undeniably encouraging in that such a force field is potentially applicable to the analysis of crystal vibrations of analogous compounds. A logical extension of this work then was an investigation into the normal coordinate analysis of the unit cell of Cs_2ZnCl_4 which belongs to the same space group as Cs_2CuCl_4, and for which almost complete vibrational data[113,134,135] are available. The results of such an investigation are detailed in the following chapter.

CHAPTER 5 ANALYSIS OF THE VIBRATIONS OF CAESIUM TETRACHLOROZINCATE(II) CRYSTAL

5.1 *INTRODUCTION*

The vibrational spectra of tetrachlorozincate(II), $ZnCl_4^{2-}$, have been widely studied over the last fifteen years. The reasons are two-fold. Firstly, it forms part of a systematic study of the spectral properties of tetrahedral tetrahalogeno-metallates(II). Secondly, the Zn^{2+} ion, being of d^{10} configuration, is not subject to the Jahn-Teller effect and hence $ZnCl_4^{2-}$ ions are expected to be regularly tetrahedral (T_d); this provides a direct comparison with the analogous transition metal tetrahalides which may suffer tetragonal distortions.

Until recently, the vibrational spectra of $ZnCl_4^{2-}$ ions have largely been measured on their solid salts with bulky organic cations and also caesium cations (table 5.1.1). The only reported solution infra-red was on the organic salt of $ZnCl_4^{2-}$ with Aliquat 336 cation[153] in benzene. Raman spectra of aqueous solution and tri-n-butyl phosphate extracts containing excess of chloride have also been reported, and the observed bands were attributed to the $ZnCl_4^{2-}$ species[154]. The only other solution Raman spectrum was that of $(Et_4N)_2ZnCl_4$ in nitromethane[110]. As seen from table 5.1.1, several infra-red bands have been observed in the Zn-Cl stretching region although only one is expected for a T_d $ZnCl_4^{2-}$ ion. In some cases[89], the infra-red forbidden ν_2 band has disputably been

TABLE 5.1.1

Vibrational frequencies (in cm^{-1}) of $ZnCl_4^{2-}$ from the literature

Cation	ν_3	ν_1	ν_4	ν_2	Technique	Reference
Et_4N^+	281 m 273 s	-	-	-	IR solid	[109] (1963)
Ph_3MeAs^+	291 sh 283 m 265 s	-	-	-	IR solid	[109] (1963)
Cs^+	292 s 285 m	-	-	-	IR solid	[109] (1963)
Et_4N^+	277 s	-	130 m	80 w(?)	IR solid	[89] (1964)
Me_4N^+	276 s	-	133 m	84 w(?)	IR solid	[89] (1964)
A-336N^+	340 s(?) 303 s(?)	-	118 s(?)	-	IR benzene	[153] (1969)

Table 5.1.1 continued

-	306		275		104		79		R H2O	[154] (1963)
Cs^+	298	m	288	s	130	w	116	w	R solid	[155] (1966)
Et_4N^+	-		276	s	126	w,sh	-		R solid	[110] (1968)
Et_4N^+	-		274	m,pol	-		-		R $MeNO_2$	[110] (1968)
Cs^+	298.3		288.7		142.3		116.7		R solid	[134] (1976)
	278				130.8		111			

Footnote: ν_1 = symmetric stretch (a_1)

ν_2 = symmetric deformation (e)

ν_3, ν_4 = asymmetric stretch and asymmetric deformation $(2t_2)$

observed. This indicates the lifting of the degeneracy of t_2 vibrations; thus, the interpretation of the spectra in terms of tetrahedral $ZnCl_4^{2-}$ ion is not entirely appropriate.

In 1969, Beattie et al.[112] reported the single-crystal Raman spectrum of Cs_2ZnCl_4 which provides a conclusive evidence of the splitting of the degenerate anion modes. This work has now been superceded by that of Wong[134] who observed all the 18 expected internal modes in the Raman and assigned them unambiguously (table 5.1.2). The corresponding single-crystal infra-red spectrum has also been reported (table 5.1.3).[113]

In the absence of accurate structural parameters, Beattie et al.[112] interpreted their Raman spectrum of Cs_2ZnCl_4 in terms of D_{2d} distortions in the $ZnCl_4^{2-}$ anions. Wong[135] followed up his Raman studies[134] of the compound with a normal coordinate analysis of the $ZnCl_4^{2-}$ anion in C_s symmetry, using the modified Urey-Bradley force field[136-138], and taking into account the interaction between the two closest Cs^+ ions and the $ZnCl_4^{2-}$ ion. A set of force constants was derived, for which he obtained an excellent fit between the calculated and the observed frequencies. However, it is doubtful that these force constants as defined by the modified UBFF would be useful in the comparative study of other tetrachlorometallates(II); in particular, the force field may not be suitable for reasons discussed in section 3.2.4.

The crystal structure of Cs_2ZnCl_4 has now been published[7], and the compound is shown to be isomorphous with Cs_2CuCl_4. In this section, we report the full unit cell analysis of Cs_2ZnCl_4,

TABLE 5.1.2

Single-crystal Raman measurements for Cs_2ZnCl_4 and assignments of internal modes [134]

Frequency (cm^{-1})	Crystal Mode (D_{2h})	Internal Mode (C_s)*
298.3	$a_g + b_{1g} + b_{2g} + b_{3g}$	$a' + a''$ $(2t_2)$
289	$a_g + b_{2g}$	a' (a_1)
278	$a_g + b_{2g}$	a' (t_2)
142.8	b_{2g}	a' (t_2)
142.1	a_g	
130.9	b_{1g}	a'' (t_2)
130.3	b_{3g}	
129.7	b_{2g}	a' (t_2)
129.0	a_g	
116	$a_g + b_{2g}$	a' (e)
112	$b_{1g} + b_{3g}$	a'' (e)
	External Mode	
85.1	b_{2g}	
78	b_{3g}	

Table 5.1.2 continued

76.5	a_g
68	b_{3g}
65.6	a_g
61	a_g
48	b_{2g}
47	a_g
45	a_g
43.5	b_{1g}
43	b_{3g}
38	b_{2g}
36	b_{1g}
34	a_g
31	b_{2g}
24.6	a_g
22	b_{1g}
21	b_{2g}
19	b_{3g}

* The internal modes are classified into the symmetry species of C_s point group but correlated with T_d point group in brackets.

TABLE 5.1.3

Polarised infra-red reflectance data for Cs_2ZnCl_4 [113]

Frequency (cm^{-1})	Crystal Mode (D_{2h})	Internal Mode (C_s)
302	b_{3u}	a' (t_2)
300	b_{1u}	
296	b_{2u}	a'' (t_2)
288	$b_{1u} + b_{3u}$	a' (t_2)
147	b_{3u}	a' (t_2)
139	b_{3u}	a' (t_2)
132	b_{1u}	
134	b_{2u}	a'' (t_2)
114	b_{3u}	a' (e)
110	b_{2u}	a'' (e)

Table 5.1.3 continued

	External Mode
90	b_{3u}
87	b_{1u}
77	b_{2u}
75	b_{3u}
67	$b_{1u} + b_{3u}$
60	b_{2u}
55	b_{3u}

using a similar method to that of chapter 4. The potential force field is again as defined in equation (42) but the parameters used are those pertaining to the compound under study. Thus, the internal force constants obtained will be as defined in the GVFF which in our opinion has greater merits over the UBFF for a study of this kind.

5.2 *STRUCTURE OF UNIT CELL*

The crystal structure data of Cs_2ZnCl_4 were obtained from reference 7. These are reproduced in table 5.2.1. The complete set of Cartesian coordinates with reference to the origin at (0, 0, 0) for the 28 atoms is as shown in table 5.2.2. The general appearance of the unit cell of Cs_2ZnCl_4 is similar to that shown in figure 4.2.1 which applies strictly to Cs_2CuCl_4; however, the numbering of the atoms is the same as before.

TABLE 5.2.1

Crystal structure data of Cs_2ZnCl_4 [7]

(orthorhombic, *Pnma*-D_{2h}^{16})

Unit cell: a = 9.7577 Å

b = 7.4004 Å

c = 12.9704 Å

Position Parameters:

Atom	Position*	x	y	z
Zn	(4*c*)	0.23516	0.25	0.42142
Cs(1)	(4*c*)	0.64076	0.25	0.39875
Cs(2)	(4*c*)	-0.02191	0.25	0.67595
Cl(1)	(4*c*)	0.00590	0.25	0.40300
Cl(2)	(4*c*)	0.31150	0.25	0.58580
Cl(3)	(8*d*)	0.32380	0.0022	0.34590

* Wyckoff notations; similar to those in table 4.2.1.

TABLE 5.2.2

Cartesian coordinates (in Å) of

Cs_2ZnCl_4 unit cell atoms

	x	y	z	(N)
Zn	2.29462	1.8501	5.46599	2
	7.46308	5.5503	7.50441	3
	7.17347	1.8501	1.01921	1
	2.58423	5.5503	11.95119	4
Cs(1)	6.25234	1.8501	5.17195	1
	3.50536	5.5503	7.79845	7
	1.37349	1.8501	1.31325	4
	8.38421	5.5503	11.65715	6
Cs(2)	9.54391	1.8501	8.76734	3
	0.21379	5.5503	4.20306	5
	4.66506	1.8501	10.68826	2
	5.09264	5.5503	2.28214	8
Cl(1)	0.05757	1.8501	5.22707	6
	9.70013	5.5503	7.74333	10
	4.93642	1.8501	1.25813	1
	4.82128	5.5503	11.71227	13
Cl(2)	3.03952	1.8501	7.59806	5
	6.71818	5.5503	5.37234	9
	7.91837	1.8501	-1.11286	2
	1.82933	5.5503	14.08326	14
Cl(3)	3.15954	0.01628	4.48646	8
	6.59816	7.38412	8.48394	11
	8.03839	3.68392	1.99874	3
	1.71931	3.71648	10.97166	16
	3.15954	3.68392	4.48646	7
	6.59816	3.71648	8.48394	12
	1.71931	7.38412	10.97166	15
	8.03839	0.01628	1.99874	4

5.3 *RESULTS AND DISCUSSION*

5.3.1 *Unit Cell Force Field*

As mentioned earlier, this is essentially similar to that of section 4.3.1. The internal force constants were first set up assuming T_d symmetry for the anions in the unit cell; the primary stretching and bending force constants were then adjusted, as described before, so that they were appropriate to the C_s site symmetry. The relevant external force constants pertaining to the present study are as shown in tables 5.3.1 - 5.3.3. Referring to table 5.3.3, 8 additional Cℓ ... Cℓ central force constants compared to those of unit cell analysis of Cs_2CuCl_4 were included, making a total of 24. The reason is all these Cℓ ... Cℓ contacts are quite similar in their interatomic distances and it does not appear sensible to neglect any of them. The next shortest Cℓ ... Cℓ distance is *ca.* 1 Å away. The final $\underset{\sim}{F}_i$ matrix assumed a dimension of 88 × 88. Hence, matrix multiplications were necessarily performed on square matrices of order 88 (refer appendix III). The symmetry-blocked $\underset{\sim}{F}^c_s$ matrix should still be of the order 84.

TABLE 5.3.1

Selected Cs ... Cℓ central force constants and the associated internal coordinates r_i

Force Constant	r_i	q(Å)	i
$f_{Cs \ldots C\ell}^{(m)}$	$\Delta q(Cs_2 \ldots C\ell_2)$	3.4571	41
	$\Delta q(Cs_3 \ldots C\ell_5)$	3.4571	42
	$\Delta q(Cs_5 \ldots C\ell_9)$	3.4571	43
	$\Delta q(Cs_8 \ldots C\ell_{14})$	3.4571	44
$f_{Cs \ldots C\ell}^{(m')}$	$\Delta q(Cs_3^* \ldots C\ell_2)$	3.4917	45
	$\Delta q(Cs_2 \ldots C\ell_5)$	3.4917	46
	$\Delta q(Cs_8 \ldots C\ell_9)$	3.4917	47
	$\Delta q(Cs_5^* \ldots C\ell_{14})$	3.4917	48
$f_{Cs \ldots C\ell}^{(l)}$	$\Delta q(Cs_5 \ldots C\ell_3)$	3.4755	49
	$\Delta q(Cs_5 \ldots C\ell_4)$	3.4755	50
	$\Delta q(Cs_8 \ldots C\ell_7)$	3.4755	51
	$\Delta q(Cs_8^* \ldots C\ell_8)$	3.4755	52
	$\Delta q(Cs_2^* \ldots C\ell_{11})$	3.4755	53
	$\Delta q(Cs_2 \ldots C\ell_{12})$	3.4755	54
	$\Delta q(Cs_3 \ldots C\ell_{15})$	3.4755	55
	$\Delta q(Cs_3 \ldots C\ell_{16})$	3.4755	56

Table 5.3.1 continued

$f_{Cs \ldots Cl}(l')$	$\Delta q(Cs_8 \ldots Cl_3)$	3.4987	57
	$\Delta q(Cs_8^* \ldots Cl_4)$	3.4987	58
	$\Delta q(Cs_5^* \ldots Cl_7)$	3.4987	59
	$\Delta q(Cs_5^* \ldots Cl_8)$	3.4987	60
	$\Delta q(Cs_3^* \ldots Cl_{11})$	3.4987	61
	$\Delta q(Cs_3^* \ldots Cl_{12})$	3.4987	62
	$\Delta q(Cs_2^* \ldots Cl_{15})$	3.4987	63
	$\Delta q(Cs_2^* \ldots Cl_{16})$	3.4987	64

q = Cs ... Cl distance

A_i^* = Atom from neighbouring cell translationally related to A_i.

TABLE 5.3.2

Zn-Cℓ ... Cs interaction force constants and the associated internal coordinates

Force constant

$f_{Zn\text{-}C\ell \ \ldots \ Cs}^{(\alpha)}$

$\Delta r(Zn_1\text{-}C\ell_2)\ \Delta q(Cs_2 \ \ldots \ C\ell_2)$ $\quad \alpha = 90.51^{\circ}$

$\Delta r(Zn_2\text{-}C\ell_5)\ \Delta q(Cs_3 \ \ldots \ C\ell_5)$ $\quad \alpha = 90.51^{\circ}$

$\Delta r(Zn_3\text{-}C\ell_9)\ \Delta q(Cs_5 \ \ldots \ C\ell_9)$ $\quad \alpha = 90.51^{\circ}$

$\Delta r(Zn_4\text{-}C\ell_{14})\Delta q(Cs_8 \ \ldots \ C\ell_{14})$ $\quad \alpha = 90.51^{\circ}$

$f_{Zn\text{-}C\ell \ \ldots \ Cs}^{(\beta)}$

$\Delta r(Zn_1\text{-}C\ell_2)\ \Delta q(Cs_3 \ \ldots \ C\ell_2)$ $\quad \beta = 171.51^{\circ}$

$\Delta r(Zn_2\text{-}C\ell_5)\ \Delta q(Cs_2 \ \ldots \ C\ell_5)$ $\quad \beta = 171.51^{\circ}$

$\Delta r(Zn_3\text{-}C\ell_9)\ \Delta q(Cs_8 \ \ldots \ C\ell_9)$ $\quad \beta = 171.51^{\circ}$

$\Delta r(Zn_4\text{-}C\ell_{14})\Delta q(Cs_5 \ \ldots \ C\ell_{14})$ $\quad \beta = 171.51^{\circ}$

$f_{Zn\text{-}C\ell \ \ldots \ Cs}^{(\gamma)}$

$\Delta r(Zn_1\text{-}C\ell_3)\ \Delta q(Cs_5 \ \ldots \ C\ell_3)$ $\quad \gamma = 157.95^{\circ}$

$\Delta r(Zn_1\text{-}C\ell_4)\ \Delta q(Cs_5 \ \ldots \ C\ell_4)$ $\quad \gamma = 157.95^{\circ}$

$\Delta r(Zn_2\text{-}C\ell_7)\ \Delta q(Cs_8 \ \ldots \ C\ell_7)$ $\quad \gamma = 157.95^{\circ}$

$\Delta r(Zn_2\text{-}C\ell_8)\ \Delta q(Cs_8 \ \ldots \ C\ell_8)$ $\quad \gamma = 157.95^{\circ}$

$\Delta r(Zn_3\text{-}C\ell_{11})\Delta q(Cs_2 \ \ldots \ C\ell_{11})$ $\quad \gamma = 157.95^{\circ}$

$\Delta r(Zn_3\text{-}C\ell_{12})\Delta q(Cs_2 \ \ldots \ C\ell_{12})$ $\quad \gamma = 157.95^{\circ}$

$\Delta r(Zn_4\text{-}C\ell_{15})\Delta q(Cs_3 \ \ldots \ C\ell_{15})$ $\quad \gamma = 157.95^{\circ}$

$\Delta r(Zn_4\text{-}C\ell_{16})\Delta q(Cs_3 \ \ldots \ C\ell_{16})$ $\quad \gamma = 157.95^{\circ}$

Table 5.3.2 continued

$f_{Zn\text{-}C\ell \ \ldots \ Cs}{}^{(\delta)}$

$$\begin{cases} \Delta r(Zn_1\text{-}C\ell_3)\ \Delta q(Cs_8 \ \ldots \ C\ell_3) & \delta = 98.41^{\circ} \\ \Delta r(Zn_1\text{-}C\ell_4)\ \Delta q(Cs_8 \ \ldots \ C\ell_4) & \delta = 98.41^{\circ} \\ \Delta r(Zn_2\text{-}C\ell_7)\ \Delta q(Cs_5 \ \ldots \ C\ell_7) & \delta = 98.41^{\circ} \\ \Delta r(Zn_2\text{-}C\ell_8)\ \Delta q(Cs_5 \ \ldots \ C\ell_8) & \delta = 98.41^{\circ} \\ \Delta r(Zn_3\text{-}C\ell_{11})\Delta q(Cs_3 \ \ldots \ C\ell_{11}) & \delta = 98.41^{\circ} \\ \Delta r(Zn_3\text{-}C\ell_{12})\Delta q(Cs_3 \ \ldots \ C\ell_{12}) & \delta = 98.41^{\circ} \\ \Delta r(Zn_4\text{-}C\ell_{15})\Delta q(Cs_2 \ \ldots \ C\ell_{15}) & \delta = 98.41^{\circ} \\ \Delta r(Zn_4\text{-}C\ell_{16})\Delta q(Cs_2 \ \ldots \ C\ell_{16}) & \delta = 98.41^{\circ} \end{cases}$$

TABLE 5.3.3

Cℓ ... Cℓ central force constants and the associated internal coordinates r_i

Force constant	r_i	t(Å)	i
$f_{C\ell \ldots C\ell}^{(l)}$	$\Delta t(C\ell_2 - C\ell_{15}^*)$	4.1149	65
	$\Delta t(C\ell_2 - C\ell_{16})$	4.1149	66
	$\Delta t(C\ell_{14} - C\ell_3)$	4.1149	67
	$\Delta t(C\ell_{14} - C\ell_4^*)$	4.1149	68
	$\Delta t(C\ell_5 - C\ell_{11}^*)$	4.1149	69
	$\Delta t(C\ell_5 - C\ell_{12})$	4.1149	70
	$\Delta t(C\ell_9 - C\ell_7)$	4.1149	71
	$\Delta t(C\ell_9 - C\ell_8^*)$	4.1149	72
$f_{C\ell \ldots C\ell}^{(l')}$	$\Delta t(C\ell_9 - C\ell_3)$	4.0752	73
	$\Delta t(C\ell_9 - C\ell_4^*)$	4.0752	74
	$\Delta t(C\ell_5 - C\ell_{15}^*)$	4.0752	75
	$\Delta t(C\ell_5 - C\ell_{16})$	4.0752	76
	$\Delta t(C\ell_2 - C\ell_{11}^*)$	4.0752	77
	$\Delta t(C\ell_2 - C\ell_{12})$	4.0752	78
	$\Delta t(C\ell_{14} - C\ell_7)$	4.0752	79
	$\Delta t(C\ell_{14} - C\ell_8^*)$	4.0752	80

Table 5.3.3 continued

$f_{Cl \ldots Cl}^{(2'')}$	$\Delta t(Cl_6 - Cl_3^*)$	4.1161	81
	$\Delta t(Cl_6 - Cl_4^*)$	4.1161	82
	$\Delta t(Cl_1 - Cl_7)$	4.1161	83
	$\Delta t(Cl_1 - Cl_8)$	4.1161	84
	$\Delta t(Cl_{10} - Cl_{15}^*)$	4.1161	85
	$\Delta t(Cl_{10} - Cl_{16}^*)$	4.1161	86
	$\Delta t(Cl_{13} - Cl_{11})$	4.1161	87
	$\Delta t(Cl_{13} - Cl_{12})$	4.1161	88

t = Cl ... Cl distance

A_i^* = Atom from neighbouring cell translationally related to A_i

5.3.2 *Unit Cell Analysis*

The calculated frequencies were fitted with the experimental values of Wong[134] and of Dunsmuir and Lane[113] (tables 5.1.2 and 5.1.3). The initial approximate values of the internal force constants were obtained from one of the sets derived from the isolated-ion analysis of $ZnCl_4^{2-}$ (table 3.4.4); specifically, the set of force constants with f_r equal to 1.218 millidyne $Å^{-1}$ were chosen since these appear compatible with the force constants of Cs_2CuCl_4.

The calculations were carried out using the same method as in chapter 4, and the force constants were adjusted manually to obtain a good fit. As usual, in each calculation the F^C_S matrix was checked to ensure that it was properly symmetry-blocked. The final force constants which we deemed satisfactory are given in table 5.3.4. In table 5.3.5 we give the crystal mode frequencies calculated from these force constants, alongside the experimental values.

The overall agreement between the calculated and the observed frequencies is quite satisfactory as seen from table 5.3.5. As in the study of Cs_2CuCl_4, we have not been able to account for all the expected lattice frequencies owing to the limitations inherent in our defined force field. However, the highest frequencies, *ca.* 10 of them, agree closely with the experimental values, indicating that the values obtained for the Cs ... Cl and Cl ... Cl interaction constants are reasonable.

Referring to tables 5.1.2 and 5.1.3, it is seen that the Raman-active crystal components at 289 cm^{-1} ($a_g + b_{2g}$), which arise from the $\nu(t_2)$ isolated-ion mode, appear to have no counterparts in the infra-red; instead, the infra-red bands at 288 cm^{-1} ($b_{1u} + b_{3u}$) are stated

TABLE 5.3.4

Force constants (in millidyne $\mathring{A}^{-1}$) from unit cell analysis of Cs_2ZnCl_4

Internal valence force constants:

1	f_r (Zn-Cl$_1$)	1.1963
2	f_r (Zn-Cl$_2$)	1.1804
3	f_r (Zn-Cl$_3$)	1.1915
4	f_{rr}	0.1500
5	f_ϕ (Cl$_1$-Zn-Cl$_2$)	0.0821
6	f_ϕ (Cl$_3$-Zn-Cl$_3$)	0.0798
7	f_ϕ (Cl$_1$-Zn-Cl$_3$)	0.0800
8	f_ϕ (Cl$_2$-Zn-Cl$_3$)	0.0789
9	$f_{r\phi}$-$f_{r\phi}'$	0.0300
10	$f_{\phi\phi}$	0.0100
11	$f_{\phi\phi}'$	0.0

External central force constants:

12	$f_{Cs \ldots Cl^{(m)}}$	0.15
13	$f_{Cs \ldots Cl^{(m')}}$	0.15
14	$f_{Cs \ldots Cl^{(l)}}$	0.15
15	$f_{Cs \ldots Cl^{(l')}}$	0.15
16	$f_{Cl \ldots Cl^{(l)}}$	0.01
17	$f_{Cl \ldots Cl^{(l')}}$	0.02
18	$f_{Cl \ldots Cl^{(l'')}}$	0.01

Table 5.3.4 continued

Valence-central interaction force constants:

19	$f_{Cu-Cl \ldots Cs}(\gamma)$	0.01
20	$f_{Cu-Cl \ldots Cs}(\beta)$	0.04
21	$f_{Cu-Cl \ldots Cs}(\gamma)$	0.02
22	$f_{Cu-Cl \ldots Cs}(\delta)$	0.01

TABLE 5.3.5

Calculated and observed crystal mode frequencies (in cm^{-1})

Ion (T_d)	Unit Cell (D_{2h})	Calc	Obs
		Internal Modes	
$\nu(t_2)$	a_g	298.10	298.3
	b_{1u}	297.79	300.0
	b_{2g}	297.44	298.3
	b_{3u}	297.03	302.0
	b_{1g}	294.11	298.3
	a_u	294.08	
	b_{2u}	294.07	296.0
	b_{3g}	294.07	298.3
$\nu(a_1) + \nu(t_2)$	b_{3u}	291.51	288.0
	b_{2g}	291.10	289.0
	b_{1u}	290.52	288.0
	a_g	290.27	289.0
	a_g	283.66	278.0
	b_{1u}	283.42	
	b_{2g}	283.02	278.0
	b_{3u}	282.77	

Table 5.3.5 continued

$\delta(t_2)$	b_{1u}	145.75	
	b_{3u}	144.29	147.0
	a_g	142.73	142.1
	b_{2g}	139.00	142.8
$\delta(t_2) + \delta(e)$	a_g	132.59	129.0
	b_{3u}	128.42	139.0
	a_u	128.24	
	b_{3g}	127.75	130.3
	b_{2g}	127.45	129.7
	b_{1u}	126.63	132.0
	b_{2u}	124.69	134.0
	b_{1g}	123.83	130.9

Table 5.3.5 continued

$\delta(e)$	a_g	120.05	116.0
	b_{2g}	119.86	116.0
	b_{1u}	116.05	
	b_{3u}	115.23	114.0
	b_{2u}	111.38	110.0
	b_{3g}	111.24	112.0
	b_{1g}	109.02	112.0
	a_u	105.83	
		External Modes	
	b_{3u}	88.33	90.0
	b_{2g}	85.85	85.1
	b_{1u}	77.05	87.0
	a_g	76.48	76.5
	b_{1u}	70.75	67.0
	b_{3u}	69.09	75.0
	b_{1g}	68.09	
	b_{2u}	67.53	77.0

Table 5.3.5 continued

b_{3g}	66.88	78.0
a_u	66.59	
a_g	65.93	65.6
b_{2g}	63.32	48.0
b_{3u}	54.76	67.0
b_{1u}	52.91	
b_{1g}	50.91	43.5
b_{2g}	49.56	38.0
a_g	49.16	61.0
b_{2u}	48.69	60.0
a_u	48.19	
b_{1u}	44.03	
b_{3g}	40.74	68.0
b_{2g}	42.71	31.0
a_g	32.77	47.0
b_{2g}	30.57	21.0

Table 5.3.5 continued

a_u	28.55	
b_{1g}	26.23	36.0
b_{3u}	22.52	55.0
9 others	<20.00	

to be of $\nu(t_2)$ origin. Our investigation reveals that within each symmetry all the stretching crystal modes are mixed, being extremely sensitive to the changes in the values of f_r and f_{rr}; the order of these modes interchanges rather readily with slight variations in the force constants. While the exact mechanism is not understood, it appears that the Raman bands at *ca.* 280 and 290 cm^{-1} are either broadened out in the infra-red so that only one maximum is observed in each symmetry (b_{1u} or b_{3u}), or that the order of the bands as they appear in the Raman are somehow reversed in the infra-red. It is significant that Beattie et al.[112], in reporting their Raman powder spectrum of Cs_2ZnCl_4, noted the close relative intensities of modes at 299 and 290 cm^{-1}. They suggested that these modes had mixed under the low site symmetry, indicating a departure from the gas-phase or isolated-ion approximation. Such mixing of the stretching modes is now confirmed; in addition, it was found that the crystal modes of frequencies between *ca.* 120-140 cm^{-1} are also quite extensively mixed. These modes are therefore collectively assigned as the components arising from $\delta(t_2) + \delta(e)$ isolated-ion modes in table 5.3.5.

The splitting of the internal modes is largely produced by the site-symmetry perturbation. In comparison, the lattice interactions we have considered appear to play a lesser role. This is perhaps as expected since the lowering of anion symmetry from T_d to C_s as in Cs_2ZnCl_4 is relatively more severe than from D_{2d} to C_s as in Cs_2CuCl_4.

The set of force constants obtained for Cs_2ZnCl_4 are physically sensible as apparent from their relative magnitudes; in particular, these force constants compare logically with those of Cs_2CuCl_4 (table 4.3.6), giving rise to meaningful correlation of the physical properties of the two compounds.

5.4 *CONCLUSIONS*

There have been several previous attempted force constant analyses of $ZnCl_4^{2-}$ ion, but no unit cell analysis has yet been reported. Krebs et al.[133] made use of rather imprecise frequency data for their analysis of T_d $ZnCl_4^{2-}$ ion in the GVFF; the force constants thus obtained are not to be considered reliable. Basile et al.[123] defined four force constants, f_r, f_{rr}, f_ϕ and $f_{\phi\phi}$ to fit four observed frequencies and obtained values of 1.21, 0.12, 0.06 and 0.01 millidyne Å^{-1}, respectively. Since the solution frequency data were used in the calculations, these force constants probably represent the true parameters for a 'free' $ZnCl_4^{2-}$ ion; however, as mentioned before, the neglect of $f_{r\alpha}$ is a serious flaw, and hence the accuracy of the final values is subject to grave doubts. McGinnety[7] adopted an even simpler treatment by defining only three force constants, f_r, f_{rr} and f_ϕ, in his GVFF and obtained values of 1.15, 0.18 and 0.10* millidyne Å^{-1}. By far the best force constant analysis performed on the $ZnCl_4^{2-}$ ion is that by Wong[135] who assumes that the distortion of the anion in the Cs_2ZnCl_4 crystal is entirely due to the pressure exerted by two Cs^+ ions within the vicinity of a chlorine atom. Excellent agreement between the calculated and the observed frequencies was obtained and the splitting of the internal modes was accounted for. However, Wong has chosen to use the modified Urey-Bradley force field in his analysis; the force constants he obtained are thus not directly

*In the original paper, the value of f_ϕ is given as 0.53 millidyne Å^{-1}; this is obviously an error, and the correct value should be 0.10 which is $0.53/r^2$, where r is the average Zn-Cl bond length in Å.

comparable to ours. It is perhaps worth mentioning that Wong obtained for the Zn-Cℓ stretching force constant a value of *ca.* 1.0 millidyne Å^{-1}; this seems to be on the small side especially when compared with the force constants of the GVFF.

In view of the limited information made available from these earlier works, our results have shown that the unit cell approach to the vibrational analysis could be both fruitful and satisfying. The set of force constants we have obtained appear realistic. In particular, we have been able to demonstrate the mixing of crystal modes which is a feature suggested from the experimental observation but could not be feasibly demonstrated in practice. All these serve to strengthen our confidence in the general applicability of the potential force field as defined in equation (42) to the study of the vibrations of similar compounds.

REFERENCES

1. D.W. Smith, *Coord. Chem. Rev.*, 21, 93 (1976).

2. W.E. Hatfield and R. Whyman, *Transition Met. Chem.*, 5, 147 (1969).

3. R. Colton and J.H. Canterford, *Halides of the First Row Transition Metals*, Wiley-Interscience, London (1969).

4. R. Colton, *MTP International Review of Science, Inorganic Chemistry Ser. 1*, Vol 5, Butterworths, 299 (1972).

5. J.A. McGinnety, *J. Am. Chem. Soc.*, 94, 8406 (1972).

6. J.A. McGinnety, *Acta Crystallogr. Sect. B*, 28, 2845 (1972).

7. J.A. McGinnety, *Inorg. Chem.*, 13, 1057 (1974).

8. R.L. Harlow, W.J. Wells, G.W. Watt and S.H. Simonsen, *Inorg. Chem.*, 13, 2106 (1974).

9. L.P. Battaglia, A.B. Corradi, G. Marcotrigiano, L. Menabue and G.C. Pellacani, *Inorg. Chem.*, 18, 148 (1979)

10. M.R. Udupa and B. Krebs, *Inorg. Chim. Acta*, 33, 241 (1979).

11. J.W. Weenk, A.L. Spek, *Cryst. Struct. Commun.*, 5, 805 (1976).

12. G. Marcotrigiano, L. Menabue and G.C. Pellacani, *J. Coord. Chem.*, 5, 189 (1976).

13. G. Marcotrigiano, L. Menabue and G.C. Pellacani, *Transition Met. Chem.*, 3, 108 (1978).

14. G. Marcotrigiano, L. Menabue and G.C. Pellacani, *Inorg. Chem.*, 15, 2333 (1976).

15. L. Menabue and G.C. Pellacani, *J. Chem. Soc., Dalton Trans.*, 455 (1976).

16. A.R. Siedle, G.A. Candela, T.F. Finnegan, R.P. Van Duyne, T. Cape, G.F. Kokoszka and P.M. Woyciesjes, *Chem. Commun.*, 69 (1978).

17 R.D. Willett, *J. Chem. Phys.*, 41, 2243 (1964).

18. J.P. Steadman and R.D. Willett, *Inorg. Chim. Acta*, 4, 367 (1970).

19. F. Barendregt and H. Schenck, *Physica*, 49, 465 (1970).

20. D.N. Anderson and R.D. Willett, *Inorg. Chim. Acta*, 8, 167 (1974).

21. K.P. Larsen, *Acta Chem. Scand., Ser. A*, 28, 194 (1974).

22. G.B. Birrell and B. Zaslow, *J. Inorg. Nucl. Chem.*, 34, 1751 (1972).

23. B. Morosin, P. Fallon and J.S. Valentine, *Acta Crystallogr., Sect. B*, 31, 2220 (1975).

24. G.L. Ferguson and B. Zaslow, *Acta Crystallogr., Sect. B*, 27, 849 (1971).

25. D.W. Smith, *J. Chem. Soc. (A)*, 1498 (1970).

26 R.D. Willett, J.A. Haugen, J. Lesback and J. Morrey, *Inorg. Chem.*, 13, 2510 (1974)

27. J. Petzelt, *J. Phys. Chem. Solids*, 36, 1005 (1975).

28 D.R. Hill and D.W. Smith, *J. Inorg. Nucl. Chem.*, 36, 466 (1974).

29. R.L. Harlow and S.H. Simonsen, *Abstracts of Papers, Am. Chem. Soc.*, Inorg. 81, March 20-25, (1977).

30. W.E. Estes, J.R. Wasson, J.W. Hall and W.E. Hatfield, *Inorg. Chem.*, 17, 3657 (1978).

31. M. Textor, E. Dubler and H.R. Oswald, *Inorg. Chem.*, 13, 1361 (1974).

32. R.D. Willett and C. Chow, *Acta Crystallogr., Sect. B*, 30, 207 (1974).

33. A.F. Wells, *J. Chem. Soc.*, 1662 (1947).

34. A.W. Schuetler, R.A. Jacobson and R.E. Rundle, *Inorg. Chem.*, 5, 277 (1966).

35. C.J. Kroese, W.J.A. Maaskant and G.C. Verschoor, *Acta Crystallogr., Sect. B*, 30, 1053 (1974).

36. M.A. Khan and M.J. Schwing-Weill, *Inorg. Chem.*, 15, 2202 (1976).

37. Z. Biela and J. Gazo, *Chem. Zvesti*, 30, 42 (1976).

38. M.J. Schwing-Weill, *Bull. Soc. Chim. Fr.*, 3, 823 (1973).

39. R.P. Eswein, E.S. Howald, R.A. Howald and D.P. Keeton, *J. Inorg. Nucl. Chem.*, 29, 437 (1967).

40. C. Furlani and G. Morpurgo, *Theor. Chim. Acta*, 1, 102 (1963).

41. W. Ludwig and M. Textor, *Helv. Chim. Acta*, 54, 1143 (1971).

42. R.D. Willett, O.L. Liles and C. Michelson, *Inorg. Chem.*, 6, 1885 (1967).

43. J. Sykora, E. Horvath and J. Gazo, *Z. Chem.* (Ger.), 18, 346 (1978).

44. J. Sykora, E. Horvath and J. Gazo, *Z. Anorg. Allg. Chem.* (Ger.), 442, 245 (1978).

45. R.D. Braun, *Fresenius' Z. Anal. Chem.*, 285, 47 (1977).

46. Y. Sasaki, M. Takizawa, K. Umemoto and N. Matsuura, *Nippon Kagaku Kaishi* (Jpn.), 983 (1977).

47. M. Machtinger, M.J. Vuaille and B. Tremillon, *J. Electroanal. Chem. Interfacial Electrochem.* (Fr.), 83, 273 (1977).

48. U.K.A. Klein and D.J. Miller, *Ber. Bunsengens. Phys. Chem.*, 80, 113 (1976).

49. M. Moreno, *J. Phys. C*, 9, 3277 (1976).

50. M. Moreno, *Chem. Phys. Lett.*, 45, 479 (1977).

51. S. Lahiry, J. Banerjee and H.O. Gupta, *Proc. Nucl. Phys. Solid State Phys. Symp.*, 17C, 304 (1974).

52. S. Lahiry, J. Sharma, G.D. Sootha and H.O. Gupta, *Phys. Status Solidi A*, 46, 153 (1978).

53. P. Bloembergen, *Physica B + C*, 85, 51 (1976).

54. T. Iwashita and N. Uryu, *J. Phys. Soc. Jpn.*, 39, 905 (1975).

55. N. Fogel and T.J. Nolan, *Am. Chem. Soc. Symp.*, Inorg. 121 (1975).

56. T.J. Nolan, H. Haralson, J.L. McAdams and N. Fogel, *J. Chem. Soc., Dalton Trans.*, 1608 (1977).

57. H.T. Witteveen, *Physica*, 71, 204 (1974).

58. J.R. Ferraro, *J. Coord. Chem.*, 5, 101 (1976).

59. A.T. Sherren and J.R. Ferraro, *Inorg. Chim. Acta*, 22, 43 (1977).

60. P.J. Wang and H.G. Drickamer, *J. Chem. Phys.*, 59, 559 (1973).

61. L.V. Soboleva and M.G. Vasil'eva, *Zh. Neorg.Khim.* (Russ), 22, 1293 (1977).

62. S. Sawada, S. Hirotsu, T. Suzuki, M. Takashige and Y. Shiroishi, *Izv. Akad. Nauk SSSR.Ser. Fiz.* (Russ.), 41, 501 (1977).

63. I. Yahara, N. Kaneshima, T. Kuga, H. Kubo and K. Hirakawa, *Kyushu Daigaku Kogaku Shuho* (Jpn.), 48, 803 (1975).

64. L.D. Khoi, P. Veillet and J.P. Renard, *Solid State Commun.*, 24, 313 (1977).

65. P.E. Schipper, *J. Am. Chem. Soc.*, 98, 7938 (1976).

66. D.W. Smith, *Inorg. Chim. Acta*, 22, 107 (1977).

67. D.A. Cruse and M. Gerloch, *J. Chem. Soc., Dalton Trans.*, 1617 (1977).

68. J.M. Smit, C. Haas and W.C. Nieuwpoort, *Theor. Chim. Acta*, 43, 277 (1977).

69. M. Barber, J.D. Clark and A. Hinchliffe, *J. Chem. Soc., Faraday Trans. 2*, 74, 681 (1978).

70. L. Helmholz and R.F. Kruh, *J. Am. Chem. Soc.*, 74, 1176 (1952).

71. B. Morosin and E.L. Lingafelter, *J. Phys. Chem.*, 65, 50 (1961).

72. G.B. Deacon and F.B. Taylor, *J. Chem. Soc. (A)*, 463 (1966).

73. G.B. Deacon, J.H.S. Green and F.B. Taylor, *Aust. J. Chem.*, 20, 2069 (1967).

74. T.K. Yeoh, *M.Sc. thesis*, University of Waikato, Hamilton, New Zealand (1976).

75. D.W. Smith and T.K. Yeoh, *Aust. J. Chem.*, 32, 691 (1979).

76. R. Boca, *Chem. Zvesti*, 30, 13 (1976).

77. L.A. Il'yukevich and G.A. Shagisultanova, *Zh. Neorg. Khim.*, 8, 2308 (1963).

78. P.S. Gentile, T.A. Shankoff and J. Carlotto, *J. Inorg. Nucl. Chem.*, 29, 1397 (1967).

79. K.N. Raymond, *Chem. Commun.*, 1294 (1969).

80. S.A. Goldfield and K.N. Raymond, *Inorg. Chem.*, 10, 2604 (1971).

81. H.T. Witteveen, D.L. Jongejan and V. Brandwijk, *Mat. Res. Bull.*, 9, 345 (1974).

82. Z. Biela, T. Obert, M. Melnik and J. Gazo, *Chem. Zvesti*, 29, 56 (1975).

83. Z. Kompisova and J. Gazo, *Z. Chem.* (Ger.), 5, 344 (1965).

84. Z. Biela, T. Obert and J. Gazo, *Chem. Zvesti*, 30, 52 (1976).

85. C.E. Zaspel and J.E. Drumheller, *Phys. Rev. B*, 16, 1771 (1977).

86. R. Clay, J. Murray-Rust and P. Murray-Rust, *Acta Crystallogr., Sect. B*, 31, 289 (1975).

87. J. Lamotte-Brasseur, *Bull. Soc. R. Sci. Liege*, 41, 331 (1972).

88. D.W. Smith, *Struct. Bonding (Berlin)*, 12, 49 (1972).

89. A. Sabatini and L. Sacconi, *J. Am. Chem. Soc.*, 86, 17 (1964).

90. J.T.R. Dunsmuir and A.P. Lane, *J. Chem. Soc. (A)*, 2781 (1971).

91. F. Basolo, *Coord. Chem. Rev.*, 3, 213 (1968).

92. B.N. Figgis and C.M. Harris, *J. Chem. Soc.*, 855 (1959).

93. S. Mitra, *Ind. J. Pure Appl. Physics*, 2, 333 (1964).

94. M. Sharnoff, *J. Chem. Phys.*, 42, 3383 (1965).

95. A. Bose, S. Lahiri and U.S. Ghosh, *J. Phys. Chem. Solids*, 26, 1747 (1965).

96. A. Bose, S. Mitra and R. Rai, *Ind. J. Phys.*, 42, 357 (1965).

97. M. Gerloch, *J. Chem. Soc. (A)*, 2023 (1968).

98. B.N. Figgis, M. Gerloch, J. Lewis and R.L. Slade, *J. Chem. Soc. (A)*, 2028 (1968).

99. J. Ferguson, *J. Chem. Phys.*, 40, 3406 (1964).

100. M. Sharnoff and C.W. Reimann, *J. Chem. Phys.*, 43, 2993 (1965).

101. B.D. Bird and P. Day, *J. Chem Phys.*, 49, 392 (1968).

102. P.Day, *Proc. Chem Soc.*, 18 (1964).

103. W.E. Hatfield and T.S. Piper, *Inorg. Chem.*, 3, 841 (1964).

104. P. Day and C.K. Jorgensen, *J. Chem. Soc.*, 6226 (1964).

105. D.W. Smith, *J. Chem. Soc. (A)*, 2900 (1970).

106. L.L. Lohr and W.N. Lipscomb, *Inorg. Chem.*, 3, 911 (1963).

107. J. Demyunck, A. Veillard and U. Wahlgren, *J. Am. Chem. Soc.*, 95, 5563 (1973).

108. D.M. Adams and P.J. Lock, *J. Chem. Soc. (A)*, 620 (1967).

109. R.J.H. Clark and T.M. Dunn, *J. Chem Soc.*, 1198 (1963).

110. J.S. Avery, C.D. Burbridge and D.M.L. Goodgame, *Spectrochim Acta A*, 24, 1721 (1968).

111. A.R. Chughtai and R.N. Keller, *J. Inorg. Nucl. Chem.*, 31, 633 (1969).

112. I.R. Beattie, T.R. Gilson and G.A. Ozin, *J. Chem. Soc. (A)*, 534 (1969).

113. J.T.R. Dunsmuir and A.P. Lane, *J. Chem. Soc. (A)*, 404 (1971).

114. A.B. Blake and F.A. Cotton, *Inorg. Chem.*, 2, 906 (1963).

115. A.B. Blake and F.A. Cotton, *Inorg. Chem.*, 3, 5 (1964).

116. G.N. Papatheodorou, *J. Inorg. Nucl. Chem.*, 35, 465 (1973).

117. H. Hartmann, W. Strehlow and H. Haas, *Z. Naturforsch.*, 23, 2029 (1968).

118. D.E. Scaife, *Aust. J. Chem.*, 24, 1993 (1971).

119. P.L. Goggin and J. Mink, *J. Chem. Soc., Dalton Trans.*, 1479 (1974).

120. K. Nakamoto, *Infra-red Spectra of Inorganic and Coordination Compounds*, 2nd Edn., Wiley-Interscience, New York, part I (1970).

121. R.D. Willett, J.R. Ferraro and M. Choca, *Inorg. Chem.*, 13, 2919 (1974).

122. A. Muller and B. Krebs, *J. Mol. Spec.*, 24, 180 (1967).

123. L.J. Basile, J.R. Ferraro, P. LaBonville and M.C. Walls, *Coord. Chem. Rev.*, 11, 21 (1973).

124. E.B. Wilson, J.C. Decius and P.C. Cross, *Molecular Vibrations*, McGraw-Hill, New York (1955).

125. L.H. Jones, *Coord. Chem. Rev.*, 1, 351 (1966).

126. T. Shimanouchi, *Physical Chemistry An Advanced Treatise*, Academic Press, New York/London, vol. IV, 233 (1970).

127. G. Turrel, *Infra-red and Raman Spectra of Crystals*, Academic Press, New York/London, Chapter 1 (1972).

128. L.A. Woodward, *Introduction to the Theory of Molecular Vibrations and Vibrational Spectroscopy*, Oxford University Press, London, part I (1972).

129. P. Gans, *Vibrating Molecules*, William Clowes & Sons Limited, London (1971).

130. J.K.G. Watson, *J. Mol. Spec.*, 41, 229 (1972).

131. H.C. Urey and C.A. Bradley, *Phys. Rev.*, 38, 1969 (1931).

132. T. Shimanouchi, *J. Chem. Phys.*, 17, 245, 743, 848 (1949)

133. B. Krebs, A. Müller and A. Fadini, *J. Mol. Spec.*, 24, 198 (1967).

134. P.T.T. Wong, *J. Chem. Phys.*, 64, 2186 (1976).

135. P.T.T. Wong, *J. Chem. Phys.*, 66, 2347 (1977).

136. I. Nakagowa and T. Shimanouchi, *Spectrochim. Acta*, 18, 101 (1962).

137. Y. Morino, K. Kuchitan and T. Shimanouchi, *J. Chem. Phys.*, 20, 726 (1952).

138. J. Overend and J.R. Scherer, *J. Chem. Phys.*, 32, 1296 (1960).

139. N. Mohan, S.J. Cyvin and A. Muller, *Coord. Chem. Rev.*, 21, 221 (1976).

140. *International Tables for X-Ray Crystallography*, The Kynoch Press, vol. 1, 151 (1969).

141. R.W.G. Wyckoff, *Crystal Structures*, 2nd Edn., John Wiley and Sons, vol. 3, 99 (1963).

142. R.L. Carter, *J. Chem. Ed.*, 48, 297 (1971).

143. R.S. Halford, *J. Chem. Phys.*, 14, 8 (1946).

144. E.B. Wilson, *J. Chem. Phys.*, 7, 1047 (1939).

145. E.B. Wilson, *J. Chem. Phys.*, 9, 76 (1941).

146. T. Shimanouchi, M. Tsuboi and T. Miyazawa, *J. Chem. Phys.*, 35, 1597 (1961).

147. I.R. Beattie, N. Cheetham, M. Gardner and D.E. Rogers, *J. Chem. Soc. (A)*, 2240 (1971).

148. R. French, *J. Chem Phys.*, 58, 5067 (1973).

149. V. Devarajan and E. Funck, *J. Chem. Phys.*, 62, 3406 (1975).

150. J.C. Decius, *J. Chem. Phys.*, 23, 1290 (1955).

151. L.C. Kravitz, J.D. Kingsley and E.L. Elkin, *J. Chem. Phys.*, 49, 4600 (1968).

152. J.M. Crettez, J.P. Misset and E. Coquet, *J. Chem. Phys.*, 70, 4194 (1979).

153. M.L. Good, C.C. Chang, D.W. Wertz and J.R. Durig, *Spectrochim. Acta (A)*, 25, 1303 (1969).

154. D.F.C. Morris, E.L. Short and D.N. Waters, *J. Inorg. Nucl. Chem.*, 25, 975 (1963).

155. C.O. Quicksall and T.G. Spiro, *Inorg. Chem.*, 5, 2232 (1966).

APPENDIX I DERIVATION OF THE F_S MATRIX OF D_{2d} $CuCl_4^{2-}$ ION

References: 120, 124, 126, 129

In section 3.2.1, an expression for the potential energy of a vibrating molecule, in the harmonic approximation, was derived:

$$2V = \underset{\sim}{R}^t \underset{\sim}{F} \underset{\sim}{R} \qquad (7).$$

This is now written as

$$2V = \underset{\sim}{R}^t \underset{\sim}{F}_R \underset{\sim}{R} \qquad (43),$$

where $\underset{\sim}{R}$ is a column matrix of internal displacement coordinates Δr_i, and $\underset{\sim}{R}^t$ its transpose; $\underset{\sim}{F}_R$ is the $\underset{\sim}{F}$ matrix associated with these internal coordinates.

Defining now $\underset{\sim}{S}$ as a column matrix of symmetry coordinates s_i and $\underset{\sim}{U}$ a transformation matrix such that

$$\underset{\sim}{S} = \underset{\sim}{U}\underset{\sim}{R} \qquad (44),$$

then

$$\underset{\sim}{R} = \underset{\sim}{U}^t \underset{\sim}{S} \qquad (45),$$

$$2V = \underset{\sim}{S}^t \underset{\sim}{U} \underset{\sim}{F}_R \underset{\sim}{U}^t \underset{\sim}{S} \qquad (46).$$

Equation (46) can be written as

$$2V = \underset{\sim}{S}^t \underset{\sim}{F}_S \underset{\sim}{S} \qquad (47),$$

where $\underset{\sim}{F}_S$, the $\underset{\sim}{F}$ matrix associated with the symmetry coordinates, is defined as

$$\underset{\sim}{F}_S = \underset{\sim}{U}\underset{\sim}{F}_R\underset{\sim}{U}^t \qquad (48).$$

Consider now a D_{2d} $CuCl_4^{2-}$ ion with the atoms labelled as in the figure below:

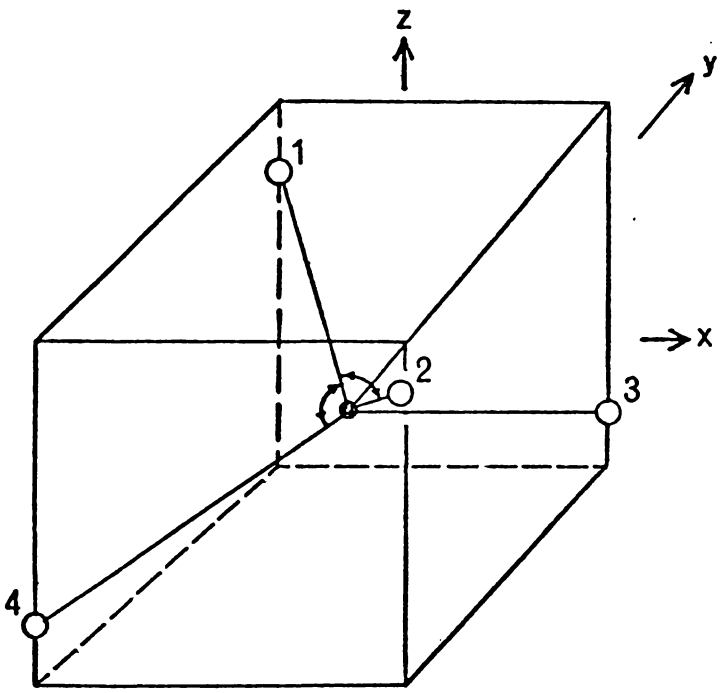

The complete set of internal displacement coordinates Δr_i are defined as follows:

$$\Delta r_1 = \Delta r(\text{Cu-Cl}_1)$$

$$\Delta r_2 = \Delta r(\text{Cu-Cl}_2)$$

$$\Delta r_3 = \Delta r(\text{Cu-Cl}_3)$$

$\Delta r_4 = \Delta r(Cu\text{-}Cl_4)$

$\Delta r_5 = \Delta\phi(Cl_1\text{-}Cu\text{-}Cl_2) \qquad (\phi > 109.5^\circ)$

$\Delta r_6 = \Delta\phi(Cl_3\text{-}Cu\text{-}Cl_4) \qquad (\phi > 109.5^\circ)$

$\Delta r_7 = \Delta\phi(Cl_1\text{-}Cu\text{-}Cl_3) \qquad (\phi < 109.5^\circ)$

$\Delta r_8 = \Delta\phi(Cl_1\text{-}Cu\text{-}Cl_4) \qquad (\phi < 109.5^\circ)$

$\Delta r_9 = \Delta\phi(Cl_2\text{-}Cu\text{-}Cl_3) \qquad (\phi < 109.5^\circ)$

$\Delta r_{10} = \Delta\phi(Cl_2\text{-}Cu\text{-}Cl_4) \qquad (\phi < 109.5^\circ)$

A total of 10 internal coordinates have been defined although only 9 fundamental modes are expected from the vibrational representations ($2a_1 + 2e + b_1 + 2b_2$). Thus, there exists one redundant coordinate which has to be eliminated.

Group theoretical methods produce the following symmetry coordinates:

$a1 \qquad s_1 = 2^{-1}(\Delta r_1 + \Delta r_2 + \Delta r_3 + \Delta r_4)$

$s_2 = 2^{-\frac{1}{2}}(\Delta r_5 + \Delta r_6)$

$s_3 = 2^{-1}(\Delta r_7 + \Delta r_8 + \Delta r_9 + \Delta r_{10})$

$e \qquad s_4 = 2^{-\frac{1}{2}}(\Delta r_1 - \Delta r_2)$

$s_5 = 2^{-\frac{1}{2}}(\Delta r_3 - \Delta r_4)$

$s_6 = 2^{-\frac{1}{2}}(\Delta r_7 - \Delta r_{10})$

$s_7 = 2^{-\frac{1}{2}}(\Delta r_8 - \Delta r_9)$

b_1 $\quad s_8 = 2^{-1}(\Delta r_7 + \Delta r_{10} - \Delta r_8 - \Delta r_9)$

b_2 $\quad s_9 = 2^{-1}(\Delta r_1 + \Delta r_2 - \Delta r_3 - \Delta r_4)$

$\quad s_{10} = 2^{-\frac{1}{2}}(\Delta r_5 - \Delta r_6)$

Since there should only be $2a_1$ vibrations, a redundancy condition exists in this symmetry.

In a tetrahedral molecule, the redundant symmetry coordinate is $6^{-\frac{1}{2}}(\Delta r_5 + \Delta r_6 + \Delta r_7 + \Delta r_8 + \Delta r_9 + \Delta r_{10})$ (reference 120, p.54-55) For a D_{2d} molecule, the redundant coordinate is, by intuition, of the form:

$$s' = a'(\Delta r_5 + \Delta r_6) + b'(\Delta r_7 + \Delta r_8 + \Delta r_9 + \Delta r_{10}) \qquad (49),$$

where a' and b' are positive coefficients such that

$$2(a')^2 + 4(b')^2 = 1 \qquad (50),$$

as required by the normalisation condition.

Defining, now,

$$\underset{\sim}{G}_s = \underset{\sim}{U}\underset{\sim}{G}_R\underset{\sim}{U}^t \qquad (51),$$

(c.f. equation (48)) where $\underset{\sim}{G}_R$ is the $\underset{\sim}{G}$ matrix associated with the internal coordinates and $\underset{\sim}{G}_s$ is the $\underset{\sim}{G}$ matrix associated with the symmetry coordinates.

Note that all the $\underset{\sim}{G}_s$ matrix elements related to the redundant coordinate s' become zero. If $\underset{\sim}{\beta}'$ is a column vector representing the coeffecients of s', i.e. $\underset{\sim}{R}^t\underset{\sim}{\beta}' = [s']$, then

$$\underset{\sim}{G_R}\beta' = [0].$$

The elements of $\underset{\sim}{G_R}\beta'$ take the form

$$p\rho^2\mu_{C\ell} + q\rho^2\mu_{Cu} \qquad (52),$$

where $\rho = {}^1/_r(Cu\text{-}C\ell)$, reciprocal bond length; and $\mu_x = \frac{1}{M_x}$, reciprocal mass; p and q are trigonometric functions.

In equation (52), $p\rho^2\mu_{C\ell}$ and $q\rho^2\mu_{Cu}$ are both zero; more precisely, the sums of coefficients p and q for an element of $\underset{\sim}{G_R}\beta'$ are each equal to zero since the redundancy condition is dependent on the molecular geometry and not on the masses of the atoms. Only that part of the $\underset{\sim}{G_R}$ matrix containing Δr_5 to Δr_{10} need be considered; the redundancy arises because it is impossible to simultaneously increase all the $\Delta\phi_{C\ell_i\text{-}Cu\text{-}C\ell_j}$, there being some trigonometric relation between them.

Thus, for the redundant coordinate s', the redundancy is expressed by:

$$\begin{bmatrix} g_{\Delta r_5\Delta r_5} & g_{\Delta r_5\Delta r_6} & \cdots\cdots\cdots & g_{\Delta r_5\Delta r_{10}} \\ & g_{\Delta r_6\Delta r_6} & & g_{\Delta r_6\Delta r_{10}} \\ & & \ddots & \vdots \\ \text{SYMMETRIC} & & & g_{\Delta r_{10}\Delta r_{10}} \end{bmatrix} \begin{bmatrix} a' \\ a' \\ b' \\ b' \\ b' \\ b' \end{bmatrix} = \begin{bmatrix} 0 \\ 0 \\ 0 \\ 0 \\ 0 \\ 0 \end{bmatrix} \qquad (53),$$

where $g_{\Delta r_i \Delta r_j}$ is the $\underset{\sim}{G}_R$ matrix element between the internal coordinates Δr_i and Δr_j.

Only one element of $\underset{\sim}{G}_R\beta'$ is needed to find the relationship between the coefficients a' and b' in s'. Thus,

$$a'g_{\Delta r_5 \Delta r_5} + a'g_{\Delta r_5 \Delta r_6} + b'g_{\Delta r_5 \Delta r_7} + b'g_{\Delta r_5 \Delta r_8}$$

$$+ b'g_{\Delta r_5 \Delta r_9} + b'g_{\Delta r_5 \Delta r_{10}} = 0.$$

The $g_{\Delta r_i \Delta r_j}$ are obtained from table 3.3.4, and the $\underset{\sim}{G}_R\beta'$ element above is in the form of equation (52).

The redundancy condition may be obtained by summing the coefficients of, say, $\rho^2\mu_{C\ell}$ and equating it to zero:

$$2a' + 4b'\cos\psi = 0 \qquad (54),$$

where $\cos\psi$ is as defined in table 3.3.3.

Solving equations (54) and (50), we obtain

$$a' = -\cos\psi/(2\cos^2\psi + 1)^{\frac{1}{2}}$$

$$b' = {}^1/_2(2\cos^2\psi + 1)^{\frac{1}{2}}.$$

Thus, s' is now obtained, orthogonal to which there must exist a non-redundant coordinate s such that

$$s = a(\Delta r_5 + \Delta r_6) - b(\Delta r_7 + \Delta r_8 + \Delta r_9 + \Delta r_{10}) \qquad (55),$$

where a and b are positive coefficients, and

$$2a^2 + 4b^2 = 1 \qquad (56),$$

the normalisation condition.

The orthogonality condition for equations (49) and (55) requires that

$$2aa' + 4bb' = 0 \qquad (57).$$

Solving equation (56) and (57), we obtain

$$a = [2(1 + 2\cos^2\psi)]^{-\frac{1}{2}} \qquad (58)$$

$$b = \cos\psi[2(1 + 2\cos^2\psi)]^{-\frac{1}{2}} \qquad (59).$$

The non-redundant coordinate s is thus obtained.

The symmetry coordinates for a_1 vibrations are now written as follows:

a_1 $\quad s_1 = 2^{-1}(\Delta r_1 + \Delta r_2 + \Delta r_3 + \Delta r_4)$

$$s_2 = a(\Delta r_5 + \Delta r_6) - b(\Delta r_7 + \Delta r_8 + \Delta r_9 + \Delta r_{10})$$

$$s_3 = a'(\Delta r_5 + \Delta r_6) - b'(\Delta r_7 + \Delta r_8 + \Delta r_9 + \Delta r_{10})$$

Define, now, $\underset{\sim}{F}_R$ matrix as follows:

$$\begin{bmatrix} f_{\Delta r_1\Delta r_1} & f_{\Delta r_1\Delta r_2} & \cdots\cdots\cdots\cdots & f_{\Delta r_1\Delta r_{10}} \\ & f_{\Delta r_2\Delta r_2} & & f_{\Delta r_2\Delta r_{10}} \\ \text{SYMMETRIC} & & \ddots\ddots\ddots & \vdots \\ & & & f_{\Delta r_{10}\Delta r_{10}} \end{bmatrix}$$

Using the notations of force constants as in table 3.3.2, the above F_R matrix is synonymous to the following:

$$\begin{bmatrix}
f_r & f_{rr}' & f_{rr} & f_{rr} & f_{r\theta} & f_{r\theta}' & f_{r\phi} & f_{r\phi} & f_{r\phi}' & f_{r\phi}' \\
 & f_r & f_{rr} & f_{rr} & f_{r\theta} & f_{r\theta}' & f_{r\phi}' & f_{r\phi}' & f_{r\phi} & f_{r\phi} \\
 & & f_r & f_{rr}' & f_{r\theta}' & f_{r\theta} & f_{r\phi} & f_{r\phi}' & f_{r\phi} & f_{r\phi}' \\
 & & & f_r & f_{r\theta}' & f_{r\theta} & f_{r\phi}' & f_{r\phi} & f_{r\phi}' & f_{r\phi} \\
 & & & & f_\theta & f_{\theta\theta} & f_{\theta\phi} & f_{\theta\phi} & f_{\theta\phi} & f_{\theta\phi} \\
 & & & & & f_\theta & f_{\theta\phi} & f_{\theta\phi} & f_{\theta\phi} & f_{\theta\phi} \\
\text{SYMMETRIC} & & & & & & f_\phi & f_{\phi\phi} & f_{\phi\phi} & f_{\phi\phi}' \\
 & & & & & & & f_\phi & f_{\phi\phi}' & f_{\phi\phi} \\
 & & & & & & & & f_\phi & f_{\phi\phi} \\
 & & & & & & & & & f_\phi
\end{bmatrix}$$

Applying equation (44), U is obtained. And applying equation (48), F_S matrix is obtained as a 10 × 10 matrix in which the elements $f_{3,j}$ (j = 1 to 10) and $f_{i,3}$ (i = 1 to 10) are zero. The F_S matrix is block diagonalised: $a_1(3 \times 3)$, $e(4 \times 4)$, $b_1(1 \times 1)$ and $b_2(2 \times 2)$. The e block can be further reduced to a 2 × 2 block. The elements of the final F_S matrix, with the redundancy removed, are as shown in table 3.3.1.

APPENDIX II FACTOR GROUP ANALYSIS FOR Cs_2CuCl_4 (*Pnma*-D_{2h}^{16})

D_{2h}	n	n_i	n_l	T
a_g	13	6	7	0
b_{1g}	8	3	5	0
b_{2g}	13	6	7	0
b_{3g}	8	3	5	0
a_u	8	3	5	0
b_{1u}	13	6	6	1
b_{2u}	8	3	4	1
b_{3u}	13	6	6	1

n = total number of crystal modes

n_i = number of internal anion modes

n_l = number of lattice modes

T = number of acoustic modes

APPENDIX III COMPUTING PROCEDURE FOR THE UNIT CELL ANALYSIS OF Cs_2CuCl_4

All computation was carried out on a PDP 11/70 computer at the University of Waikato on a RSTS/E system. The programs were written in FORTRAN language, compiled and linked using a RSTS/E compiler and linker. The subroutine EIGEN was obtained from the Computer Centre at the University of Waikato as a standard package program but was originally written at the Australian National University.

Only one program, MATMLT, was written to perform matrix multiplication of square matrices of order N, $N \leq 100$. Thus, if $\underset{\sim}{A}$ is a matrix of dimension $m \times n$, $m < n \leq N$, then the matrix is input as $\underset{\sim}{A}'(n \times n)$ by filling up the $m + 1$, $m + 2$, ..., n rows with zero elements.

The following diagram provides a step-by-step description of computing procedure which calculates and prints out, for a given set of force constants, frequencies (in cm^{-1}) of the 84 crystal modes in the order $13a_g$, $8b_{1g}$, $13b_{2g}$, $8b_{3g}$, $8a_u$, $13b_{1u}$, $8b_{2u}$ and $13b_{3u}$, as well as the corresponding eigenvector matrix.

Block 1

Nineteen force constants (in millidyne Å^{-1}) are required as inputs in the order: f_r, f_{rr}, $f_{rr'}$, f_θ, f_ϕ, $f_{r\theta}$, $f_{r\theta'}$, $f_{r\phi}$, $f_{r\phi'}$, $f_{\theta\theta}$, $f_{\theta\phi}$, $f_{\phi\phi}$, $f_{\phi\phi'}$, $f_{Cs \ldots C\ell}(m)$, $f_{Cs \ldots C\ell}(m')$, $f_{Cs \ldots C\ell}(l)$, $f_{Cs \ldots C\ell}(l')$, $f_{C\ell \ldots C\ell}(l)$ and $f_{C\ell \ldots C\ell}(l')$.

All data assume floating point format, and up to three decimal places are acceptable. Name of data file created, say KTS.DAT, is typed in from the keyboard.

BLOCK 1

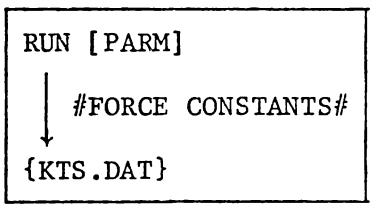

BLOCK 2

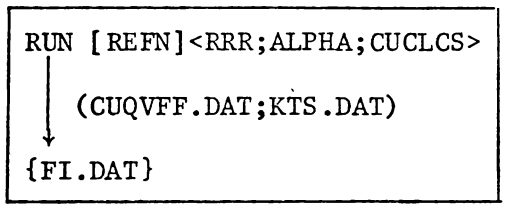

BLOCK 3

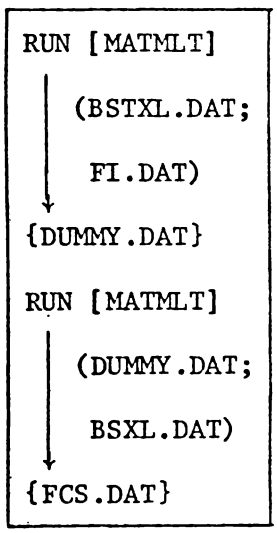

BLOCK 4

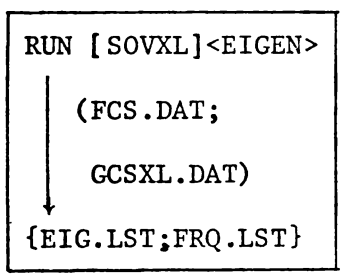

[ ] PROGRAM NAME

< > SUBROUTINE NAME

INPUT DATA

( ) INPUT FILE NAME

{ } OUTPUT FILE NAME

Block 2

A previously created array format CUQVFF.DAT, which sets up four blocks of 10 × 10 symmetrical array of internal force constants, is input together with the data file created in block 1. The subroutines, RRR and ALPHA, alter the primary stretching and bending force constants according to equations (40) and (41) to simulate site symmetry perturbations, while the third subroutine, CUCLCS, sets up the off-diagonal Cu-Cℓ ... Cs interaction terms. The name of the force constant matrix created, say FI.DAT, is typed in from the keyboard.

Block 3

Matrix calculations are carried out here using program MATMLT. Previously created data files BSTXL.DAT, FI.DAT and BSXL.DAT are required as inputs. The name of the $\underset{\sim}{F}^{\mathcal{C}}_{S}$ matrix created, say FCS.DAT, is typed in from the keyboard.

Block 4.

Computation of the eigenvalues is carried out here using subroutine EIGEN. Previously created data files FCS.DAT and GCSXL.DAT, the latter of which is a row matrix whose elements are the diagonal elements of $\underset{\sim}{G}^{\mathcal{C}}_{S}$ matrix, are required as inputs. The eigenvalues of $(\underset{\sim}{G}^{\mathcal{C}}_{S})^{\frac{1}{2}}\underset{\sim}{F}^{\mathcal{C}}_{S}(\underset{\sim}{G}^{\mathcal{C}}_{S})^{\frac{1}{2}}$ and the corresponding frequencies in cm^{-1} were evaluated. Names of output files, say FRQ.LST for the frequencies and EIG.LST for the eigenvector matrix corresponding to $\underset{\sim}{G}^{\mathcal{C}}_{S}\underset{\sim}{F}^{\mathcal{C}}_{S}$ of the secular determinant, are typed in from the keyboard.

APPENDIX IV MAJOR COMPUTER PROGRAMS

PARM.FOR

```
C     THIS PROGRAM CREATES A FORCE CONSTANT DATA FILE FOR THE
C     UNIT CELL ANALYSIS OF CAESIUM TETRACHLOROCUPRATE(II).
C
C     DATA REQUIRED: 13 GENERAL VALENCE FORCE CONSTANTS
C                    (ORDER AS DESCRIBED IN APPENDIX III)
C                    6 EXTERNAL CENTRAL FORCE CONSTANTS
C     (ALL UNITS IN MILLIDYNE/A)
C     CCCCCCCCCCCCCCCCCCCCCCCCCCCCCCCCCCCCCCCCCCCCCCCCCCCCCCCCC
C
      DIMENSION DUM(19)
      TYPE 10
10    FORMAT(' ENTER DATA FILE NAME---',$)
      CALL ASSIGN(3,,-1,'NEW')
      DO 30 I=1,13
      TYPE 20,I
20    FORMAT(' ENTER DATA',I3,'---',$)
      ACCEPT 40,DUM(I)
30    CONTINUE
      TYPE 31
31    FORMAT(' ENTER CS-CL(M) INTERACTION CONSTANT---',$)
      ACCEPT 40,DUM(14)
      TYPE 32
32    FORMAT(' ENTER CS-CL(M)* INTERACTION CONSTANT---',$)
      ACCEPT 40,DUM(15)
      TYPE 33
33    FORMAT(' ENTER CS-CL(L) INTERACTION CONSTANT---',$)
      ACCEPT 40,DUM(16)
      TYPE 34
34    FORMAT(' ENTER CS-CL(L)* INTERACTION CONSTANT---',$)
      ACCEPT 40,DUM(17)
      TYPE 35
35    FORMAT(' ENTER CL-CL(L) INTERACTION CONSTANT---',$)
      ACCEPT 40,DUM(18)
      TYPE 36
36    FORMAT(' ENTER CL-CL(L)* INTERACTION CONSTANT---',$)
      ACCEPT 40,DUM(19)
40    FORMAT(F6.3)
      WRITE (3) DUM
      STOP
      END

Ready
```

```
C       THIS PROGRAM SETS UP A FI-MATRIX WITHIN THE
C       UNIT CELL FORCE FIELD (EQUATION (42)) OF
C       CAESIUM TETRACHLOROCUPRATE(II).
C
C       R, THE AVERAGE COPPER-CHLORINE BOND DISTANCE
C       = 2.22975 MILLIDYNE/A.
C
C       SUBROUTINES REQUIRED:
C       RRR, CUCLCS, ALPHA.
C       CCCCCCCCCCCCCCCCCCCCCCCCCCCCCCCCCCCCCCCCCCCCCC
C
        COMMON/FMAT/FI(84,84)
        DIMENSION K(10,10),DATA(13)
        DIMENSION DUM(19)
        TYPE 10
10      FORMAT(' ENTER OVFF ARRAY FILE NAME ---',$)
        CALL ASSIGN(2,,-1,'RDO')
        TYPE 20
20      FORMAT(' AND FI MATRIX FILE NAME ---',$)
        CALL ASSIGN(3,,-1,'NEW')
        DO 24 I=1,84
        DO 24 J=1,84
24      FI(I,J)=0.0
        TYPE 1
1       FORMAT(' ENTER DATA FILE NAME---',$)
        CALL ASSIGN(4,,-1,'RDO')
        READ(4) DUM
        DO 3  I=1,13
3       DATA(I)=DUM(I)
        CSCLM=DUM(14)
        CSCLMD=DUM(15)
        CSCLL=DUM(16)
        CSCLLD=DUM(17)
        CLCLL=DUM(18)
        CLCLLD=DUM(19)
        R=2.22975
        DO 21 I=4,5
21      DATA(I)=(R**2)*DATA(I)
        DO 22 I=10,13
22      DATA(I)=(R**2)*DATA(I)
        DO 23 I=6,9
23      DATA(I)=R*DATA(I)
        DO 25 I=1,10
25      READ (2) (K(I,J),J=1,10)
        DO 62 I=1,4
        I10=(I-1)*10
        DO 62 J=1,10
        DO 62 L=1,10
        FI(I10+J,I10+L)=DATA(K(J,L))
62      CONTINUE
        DO 63 I=41,44
63      FI(I,I)=CSCLM
        DO 64 I=45,48
64      FI(I,I)=CSCLMD
```

```
      DO 66 I=49,56
66    FI(I,I)=CSCLL
      DO 68 I=57,64
68    FI(I,I)=CSCLLD
      DO 75 J=65,72
75    FI(J,J)=CLCLL
      DO 77 J=73,80
77    FI(J,J)=CLCLLD
      FR=DATA(1)
      CALL RRR(FR,R)
      FA=DATA(4)
      FB=DATA(5)
      THETA=129.15
      PHI=100.65
      CALL ALPHA(FA,FB,THETA,PHI)
      CALL CUCLCS
      DO 310 I=1,84
310   WRITE(3) (FI(I,J),J=1,84)
      STOP
      END
```

```
      SUBROUTINE RRR(FR,V)
      COMMON/FMAT/FI(84,84)
      REAL R(3)
C     IN THE FOLLOWING THREE LINES, THE PRIMARY VALENCE
C     STRETCHING FORCE CONSTANTS ARE ADJUSTED ACCORDING
C     TO EQUATION (40) OF THESIS.
C
      R(1)=FR*(V/2.244)**3
      R(2)=FR*(V/2.235)**3
      R(3)=FR*(V/2.220)**3
      DO 70 I=1,31,10
      FI(I,I)=R(1)
70    CONTINUE
      DO 80 I=2,32,10
      FI(I,I)=R(2)
80    CONTINUE
      DO 90 J=1,2
      DO 90 I=J+2,J+32,10
      FI(I,I)=R(3)
90    CONTINUE
      RETURN
      END
```

```
      SUBROUTINE CUCLCS
      COMMON/FMAT/FI(84,84)
      REAL PARA(4)
C     THIS SUBROUTINE SETS UP 48 SYMMETRICAL OFF-DIAGONAL
C     TERMS (IN MILLIDYNE/A) IN A FORCE CONSTANT MATRIX.
C     REFER TABLE 4.3.2 OF THESIS.
C
      TYPE 10
10    FORMAT(' ENTER FALPHA,FBETA,FDELTA,FGAMMA----',$)
      ACCEPT 30,PARA
30    FORMAT(4F6.3)
      J=41
      DO 100 I=2,32,10
      FI(I,J)=PARA(1)
      FI(J,I)=PARA(1)
      J=J+1
100   CONTINUE
      J=45
      DO 200 I=2,32,10
      FI(I,J)=PARA(2)
      FI(J,I)=PARA(2)
      J=J+1
200   CONTINUE
      J=49
      DO 300 I=3,33,10
      FI(I,J)=PARA(3)
      FI(J,I)=PARA(3)
      J=J+1
      FI(I+1,J)=PARA(3)
      FI(J,I+1)=PARA(3)
      J=J+1
300   CONTINUE
      J=57
      DO 400 I=3,33,10
      FI(I,J)=PARA(4)
      FI(J,I)=PARA(4)
      J=J+1
      FI(I+1,J)=PARA(4)
      FI(J,I+1)=PARA(4)
      J=J+1
400   CONTINUE
      RETURN
      END
```

```
      SUBROUTINE ALPHA(FA,FB,THETA,PHI)
      COMMON/FMAT/FI(84,84)
      REAL A(4)
C     IN THE FOLLOWING FOUR LINES, THE PRIMARY VALENCE
C     BENDING FORCE CONSTANTS ARE ADJUSTED ACCORDING
C     TO EQUATION (41) OF THESIS.
C
      A(1)=FA*SQRT((SIN(131.2*PI/180)/SIN(THETA*PI/180)))
      A(2)=FA*SQRT((SIN(127.1*PI/180)/SIN(THETA*PI/180)))
      A(3)=FB*SQRT((SIN(101.6*PI/180)/SIN(PHI*PI/180)))
      A(4)=FB*SQRT((SIN(99.7*PI/180)/SIN(PHI*PI/180)))
      DO 50 I=5,35,10
50    FI(I,I)=A(1)
      DO 60 I=6,36,10
60    FI(I,I)=A(2)
      DO 70 J=1,2
      DO 70 I=J+6,J+36,10
70    FI(I,I)=A(3)
      DO 80 J=1,2
      DO 80 I=J+8,J+38,10
80    FI(I,I)=A(4)
      RETURN
      END
```

MATMLT.FOR

```
C       THIS PROGRAM PERFORMS MULTIPLICATION BETWEEN
C       MATRICES OF ORDER N.
C
C       MULTIPLY MATRIX A BY MATRIX B GIVING MATRIX C.
C       ASSUME MATRICES ARE STORED IN DISK FILES ROWWISE.
C       CCCCCCCCCCCCCCCCCCCCCCCCCCCCCCCCCCCCCCCCCCCCCCC
C
      COMMON /SIZE/N
      DIMENSION B(84,84),A(84),C(84)
      N=84
      TYPE 10
10    FORMAT(/,' C = A * B')
      TYPE 20
20    FORMAT(/,' DISK FILE CONTAINING MATRIX A ',$)
      CALL ASSIGN(1,,-1,'RDO')
C     ASKS FOR FILE NAME FROM KEYBOARD
      TYPE 30
30    FORMAT(/,' DISK FILE CONTAINING MATRIX B ',$)
      CALL ASSIGN(2,,-1,'RDO')
      TYPE 40
40    FORMAT(/,' DISK FILE TO CONTAIN MATRIX C ',$)
      CALL ASSIGN(3,,-1,'NEW')
C     NOW READ IN B
      DO 50 J=1,N
50    READ(2)(B(J,I),I=1,N)
C     ARRAYS ARE STORED COLUMNWISE IN FORTRAN
      DO 100 J=1,N
      READ(1)(A(I),I=1,N)
      DO 60 I=1,N
60    C(I)=RINNER(A,B(1,I))
      WRITE(3)(C(I),I=1,N)
100   CONTINUE
      STOP
      END
      FUNCTION RINNER(X,Y)
      COMMON /SIZE/N
      REAL X(2),Y(2)
      REAL*8 D
      D=0.0
      DO 10 I=1,N
10    D=D+DBLE(X(I))*DBLE(Y(I))
      RINNER=SNGL(D)
      RETURN
      END
```

```
C       UNIT CELL ANALYSIS
C       THIS PROGRAM FIRST SYMMETRISES FC,S MATRIX
C       THEN COMPUTES THE EIGENVALUES OF
C       G(1/2)*F*G(1/2).
C       LC, THE EIGENVECTORS OF G(1/2)*F*G(1/2), ARE
C       CONVERTED BACK TO L, THE EIGENVECTORS OF
C       G*F, BY L=G(1/2)*LC.
C
C       THE DIAGONAL GC,S MATRIX IS INPUT AS A ROW
C       MATRIX.
C
C       SUBROUTINE REQUIRED: EIGEN
C       CCCCCCCCCCCCCCCCCCCCCCCCCCCCCCCCCCCCCCCCCCCC
C
        REAL G(84),GF(84,84), UP8(36),UP13(91),EIGVAL(13)
        REAL BUFF(84),DUM8(8,8),DUM13(13,13)
        INTEGER BLKSIZ(8),BSIZE
        DATA BLKSIZ/ 13, 8, 13, 8, 8, 13, 8, 13 /
        TYPE 1
1       FORMAT(' ENTER FCS FILE NAME---',$)
        CALL ASSIGN(1,,-1,'RDO')
        TYPE 2
2       FORMAT(' ENTER GCS FILE NAME---',$)
        CALL ASSIGN(5,,-1,'RDO')
        DO 5 I=1,84
5       READ (5) (G(I))
        DO 6 I=1,84
        READ(1)BUFF
        SQRTGI=SQRT(G(I))
        DO 4 J=1,84
4       GF(J,I)=SQRTGI*BUFF(J)*SQRT(G(J))
6       CONTINUE
        TYPE 30
30      FORMAT(' ENTER LIST FILE NAME ---',$)
        CALL ASSIGN(2,,-1,'NEW')
        TYPE 40
40      FORMAT(' ENTER EIGENVECTOR MATRIX FILE NAME---',$)
        CALL ASSIGN(3,,-1,'NEW')
C
C
        ICNT=0
        DO 1000 IBLK=1,8
        BSIZE=BLKSIZ(IBLK)
        IF (BSIZE.NE.8) GO TO 300
C
        DO 110 I=1,8
        DO 110 J=1,8
110     DUM8(I,J)=GF(I+ICNT,J+ICNT)
        K=1
        DO 120 I=1,8
        DO 120 J=1,I
        UP8(K)=DUM8(I,J)
120     K=K+1
        CALL EIGEN(UP8,DUM8,8,0)
        K=0
        DO 130 I=1,8
        K=K+I
        EIGVAL(I)=UP8(K)
130     CONTINUE
```

Continued

```
      DO 180 I=1,8
      SQRTGI=SQRT(G(I+ICNT))
      DO 180 J=1,8
      DUM8(I,J)=SQRTGI*DUM8(I,J)
180   CONTINUE
200   FORMAT(/,' ',8F10.7)
      DO 140 I=1,8
      WRITE(3,200) (DUM8(I,J),J=1,8)
140   CONTINUE
      GO TO 500
C
300   DO 310 I=1,13
      DO 310 J=1,13
310   DUM13(I,J)=GF(I+ICNT,J+ICNT)
      K=1
      DO 320 I=1,13
      DO 320 J=1,I
      UP13(K)=DUM13(I,J)
320   K=K+1
      CALL EIGEN(UP13,DUM13,13,0)
      K=0
      DO 330 I=1,13
      K=K+1
      EIGVAL(I)=UP13(K)
330   CONTINUE
      DO 390 I=1,13
      SQRTGI=SQRT(G(I+ICNT))
      DO 390 J=1,13
      DUM13(I,J)=SQRTGI*DUM13(I,J)
390   CONTINUE
400   FORMAT(/,' ',13F10.7)
      DO 340 I=1,13
      WRITE(3,400) (DUM13(I,J),J=1,13)
340   CONTINUE
C
C
500   WRITE(2,510)(I,I=1,BSIZE)
510   FORMAT(//,13I10)
      WRITE(2,525) (EIGVAL(I),I=1,BSIZE)
525   FORMAT(' ',13F10.7)
      DO 520 I=1,BSIZE
520   EIGVAL(I)=1302.8*SQRT(ABS(EIGVAL(I)))
      WRITE (2,530) (EIGVAL(I),I=1,BSIZE)
530   FORMAT(' ',13F10.4)
C
C
1000  ICNT=ICNT+BSIZE
      END
```

```
C                                                                      10001000
C     .................................................................10002000
C                                                                      10003000
C     SUBROUTINE EIGEN                                                 10004000
C                                                                      10005000
C        PURPOSE                                                       10006000
C           COMPUTE EIGENVALUES AND EIGENVECTORS OF A REAL SYMMETRIC   10007000
C           MATRIX                                                     10008000
C                                                                      10009000
C        USAGE                                                         10010000
C           CALL EIGEN(A,R,N,MV)                                       10011000
C                                                                      10012000
C        DESCRIPTION OF PARAMETERS                                     10013000
C           A - ORIGINAL MATRIX (SYMMETRIC), DESTROYED IN COMPUTATION. 10014000
C               RESULTANT EIGENVALUES ARE DEVELOPED IN DIAGONAL OF     10015000
C               MATRIX A IN DESCENDING ORDER.                          10016000
C           R - RESULTANT MATRIX OF EIGENVECTORS (STORED COLUMNWISE,    10017000
C               IN SAME SEQUENCE AS EIGENVALUES)                       10018000
C           N - ORDER OF MATRICES A AND R                              10019000
C           MV- INPUT CODE                                             10020000
C                 0  COMPUTE EIGENVALUES AND EIGENVECTORS              10021000
C                 1  COMPUTE EIGENVALUES ONLY (R NEED NOT BE          10022000
C                    DIMENSIONED BUT MUST STILL APPEAR IN CALLING      10023000
C                    SEQUENCE)                                         10024000
C                                                                      10025000
C        REMARKS                                                       10026000
C           ORIGINAL MATRIX A MUST BE REAL SYMMETRIC (STORAGE MODE=1)  10027000
C           MATRIX A CANNOT BE IN THE SAME LOCATION AS MATRIX R        10028000
C                                                                      10029000
C        SUBROUTINES AND FUNCTION SUBPROGRAMS REQUIRED                 10030000
C           NONE                                                       10031000
C                                                                      10032000
C        METHOD                                                        10033000
C           DIAGONALIZATION METHOD ORIGINATED BY JACOBI AND ADAPTED     10034000
C           BY VON NEUMANN FOR LARGE COMPUTERS AS FOUND IN 'MATHEMATICAL10035000
C           METHODS FOR DIGITAL COMPUTERS', EDITED BY A. RALSTON AND    10036000
C           H.S. WILF, JOHN WILEY AND SONS, NEW YORK, 1962, CHAPTER 7   10037000
C                                                                      10038000
C     .................................................................10039000
C                                                                      10040000
      SUBROUTINE EIGEN(A,R,N,MV)                                       10041000
      DIMENSION A(1),R(1)                                              10042000
C                                                                      10043000
C     .................................................................10044000
C                                                                      10045000
C        IF A DOUBLE PRECISION VERSION OF THIS ROUTINE IS DESIRED, THE  10046000
C        C IN COLUMN 1 SHOULD BE REMOVED FROM THE DOUBLE PRECISION      10047000
C        STATEMENT WHICH FOLLOWS.                                      10048000
C                                                                      10049000
C     DOUBLE PRECISION A,R,ANORM,ANRMX,THR,X,Y,SINX,SINX2,COSX,        10050000
C    1                 COSX2,SINCS,RANGE                               10051000
C                                                                      10052000
C        THE C MUST ALSO BE REMOVED FROM DOUBLE PRECISION STATEMENTS    10053000
C        APPEARING IN OTHER ROUTINES USED IN CONJUNCTION WITH THIS      10054000
C        ROUTINE.                                                      10055000
C                                                                      10056000
C        THE DOUBLE PRECISION VERSION OF THIS SUBROUTINE MUST ALSO      10057000
C        CONTAIN DOUBLE PRECISION FORTRAN FUNCTIONS.  SQRT IN STATEMENTS10058000
C        40, 68, 75, AND 78 MUST BE CHANGED TO DSQRT.  ABS IN STATEMENT 10059000
C        62 MUST BE CHANGED TO DABS. THE CONSTANT IN STATEMENT 5 SHOULD 10060000
C        BE CHANGED TO 1.0D-12.                                        10061000
C                                                                      10062000
C     .................................................................10063000
```

```
C
C         GENERATE IDENTITY MATRIX                                      10064000
C                                                                       10065000
C                                                                       10066000
    5 RANGE=1.0E-6                                                      10067000
      IF(MV-1) 10,25,10                                                 10068000
   10 IQ=-N                                                             10069000
      DO 20 J=1,N                                                       10070000
      IQ=IQ+N                                                           10071000
      DO 20 I=1,N                                                       10072000
      IJ=IQ+I                                                           10073000
      R(IJ)=0.0                                                         10074000
      IF(I-J) 20,15,20                                                  10075000
   15 R(IJ)=1.0                                                         10076000
   20 CONTINUE                                                          10077000
C                                                                       10078000
C         COMPUTE INITIAL AND FINAL NORMS (ANORM AND ANORMX)            10079000
C                                                                       10080000
   25 ANORM=0.0                                                         10081000
      DO 35 I=1,N                                                       10082000
      DO 35 J=I,N                                                       10083000
      IF(I-J) 30,35,30                                                  10084000
   30 IA=I+(J*J-J)/2                                                    10085000
      ANORM=ANORM+A(IA)*A(IA)                                           10086000
   35 CONTINUE                                                          10087000
      IF(ANORM) 165,165,40                                              10088000
   40 ANORM=1.414*SQRT(ANORM)                                           10089000
      ANRMX=ANORM*RANGE/FLOAT(N)                                        10090000
C                                                                       10091000
C         INITIALIZE INDICATORS AND COMPUTE THRESHOLD, THR              10092000
C                                                                       10093000
      IND=0                                                             10094000
      THR=ANORM                                                         10095000
   45 THR=THR/FLOAT(N)                                                  10096000
   50 L=1                                                               10097000
   55 M=L+1                                                             10098000
C                                                                       10099000
C         COMPUTE SIN AND COS                                           10100000
C                                                                       10101000
   60 MQ=(M*M-M)/2                                                      10102000
      LQ=(L*L-L)/2                                                      10103000
      LM=L+MQ                                                           10104000
   62 IF( ABS(A(LM))-THR) 130,65,65                                     10105000
   65 IND=1                                                             10106000
      LL=L+LQ                                                           10107000
      MM=M+MQ                                                           10108000
      X=0.5*(A(LL)-A(MM))                                               10109000
   68 Y=-A(LM)/ SQRT(A(LM)*A(LM)+X*X)                                   10110000
      IF(X) 70,75,75                                                    10111000
   70 Y=-Y                                                              10112000
   75 SINX=Y/ SQRT(2.0*(1.0+( SQRT(1.0-Y*Y))))                          10113000
      SINX2=SINX*SINX                                                   10114000
   78 COSX= SQRT(1.0-SINX2)                                             10115000
      COSX2=COSX*COSX                                                   10116000
      SINCS =SINX*COSX                                                  10117000
C                                                                       10118000
C         ROTATE L AND M COLUMNS                                        10119000
C                                                                       10120000
      ILQ=N*(L-1)                                                       10121000
      IMQ=N*(M-1)                                                       10122000
      DO 125 I=1,N                                                      10123000
      IQ=(I*I-I)/2                                                      10124000
      IF(I-L) 80,115,80                                                 10125000
   80 IF(I-M) 85,115,90                                                 10126000
   85 IM=I+MQ                                                           10127000
      GO TO 95                                                          10128000
   90 IM=M+IQ                                                           10129000
   95 IF(I-L) 100,105,105                                               10130000
  100 IL=I+LQ                                                           10131000
      GO TO 110                                                         10132000
  105 IL=L+IQ                                                           10133000
  110 X=A(IL)*COSX-A(IM)*SINX                                           10134000
      A(IM)=A(IL)*SINX+A(IM)*COSX                                       10135000
      A(IL)=X                                                           10136000
```

```
  115 IF(MV-1) 120,125,120                                          10137000
  120 ILR=ILQ+I                                                     10138000
      IMR=IMQ+I                                                     10139000
      X=R(ILR)*COSX-R(IMR)*SINX                                     10140000
      R(IMR)=R(ILR)*SINX+R(IMR)*COSX                                10141000
      R(ILR)=X                                                      10142000
  125 CONTINUE                                                      10143000
      X=2.0*A(LM)*SINCS                                             10144000
      Y=A(LL)*COSX2+A(MM)*SINX2-X                                   10145000
      X=A(LL)*SINX2+A(MM)*COSX2+X                                   10146000
      A(LM)=(A(LL)-A(MM))*SINCS+A(LM)*(COSX2-SINX2)                 10147000
      A(LL)=Y                                                       10148000
      A(MM)=X                                                       10149000
C                                                                   10150000
C     TESTS FOR COMPLETION                                          10151000
C                                                                   10152000
C     TEST FOR M = LAST COLUMN                                      10153000
C                                                                   10154000
  130 IF(M-N) 135,140,135                                           10155000
  135 M=M+1                                                         10156000
      GO TO 60                                                      10157000
C                                                                   10158000
C     TEST FOR L = SECOND FROM LAST COLUMN                          10159000
C                                                                   10160000
  140 IF(L-(N-1)) 145,150,145                                       10161000
  145 L=L+1                                                         10162000
      GO TO 55                                                      10163000
  150 IF(IND-1) 160,155,160                                         10164000
  155 IND=0                                                         10165000
      GO TO 50                                                      10166000
C                                                                   10167000
C     COMPARE THRESHOLD WITH FINAL NORM                             10168000
C                                                                   10169000
  160 IF(THR-ANRMX) 165,165,45                                      10170000
C                                                                   10171000
C     SORT EIGENVALUES AND EIGENVECTORS                             10172000
C                                                                   10173000
  165 IQ=-N                                                         10174000
      DO 185 I=1,N                                                  10175000
      IQ=IQ+N                                                       10176000
      LL=I+(I*I-I)/2                                                10177000
      JQ=N*(I-2)                                                    10178000
      DO 185 J=I,N                                                  10179000
      JQ=JQ+N                                                       10180000
      MM=J+(J*J-J)/2                                                10181000
      IF(A(LL)-A(MM)) 170,185,185                                   10182000
  170 X=A(LL)                                                       10183000
      A(LL)=A(MM)                                                   10184000
      A(MM)=X                                                       10185000
      IF(MV-1) 175,185,175                                          10186000
  175 DO 180 K=1,N                                                  10187000
      ILR=IQ+K                                                      10188000
      IMR=JQ+K                                                      10189000
      X=R(ILR)                                                      10190000
      R(ILR)=R(IMR)                                                 10191000
  180 R(IMR)=X                                                      10192000
  185 CONTINUE                                                      10193000
      RETURN                                                        10194000
      END                                                           10195000
```

Ready

APPENDIX V $\underset{\sim}{S}$ MATRIX ELEMENTS

Referring to figure 4.2.1, each atom in the unit cell is assigned a set of three displacement vectors, $A_n(x)$, $A_n(y)$, $A_n(z)$, parallel to the unit cell edges; n is the numbering of atom A in the figure. The symmetry elements for space group $Pnma$-D_{2h}^{16} are obtained from reference 140 (see figure below).

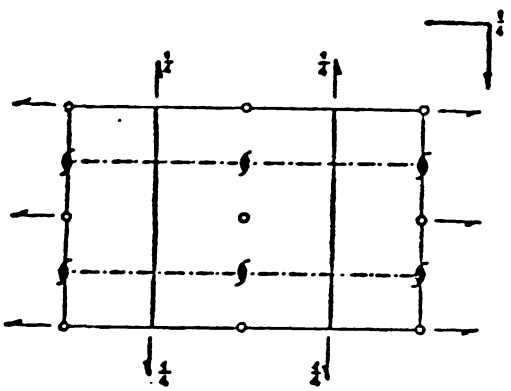

By successive application of the symmetry operations of the factor group, the transformation of the Cartesian vectors into themselves or other equivalent vectors in the unit cell can be followed. The normalised symmetry coordinates are obtained by the usual group theoretical method. These are given below, classified into different symmetry species of D_{2h} point group which is isomorphic

with the factor group. The 84 symmetry coordinates thus constitute the elements of $\underset{\sim}{S}$ column matrix.

A_g

$$\varepsilon_1 = 2^{-1}(Cu_1(x) + Cu_2(x) - Cu_3(x) - Cu_4(x))$$

$$\varepsilon_2 = 2^{-1}(Cu_1(z) - Cu_2(z) + Cu_3(z) - Cu_4(z))$$

$$\varepsilon_3 = 2^{-1}(Cs_1(x) + Cs_4(x) - Cs_6(x) - Cs_7(x))$$

$$\varepsilon_4 = 2^{-1}(Cs_1(z) - Cs_4(z) + Cs_6(z) - Cs_7(z))$$

$$\varepsilon_5 = 2^{-1}(Cs_2(x) + Cs_3(x) - Cs_5(x) - Cs_8(x))$$

$$\varepsilon_6 = 2^{-1}(Cs_2(z) - Cs_3(z) + Cs_5(z) - Cs_8(z))$$

$$\varepsilon_7 = 2^{-1}(C\ell_1(x) + C\ell_6(x) - C\ell_{10}(x) - C\ell_{13}(x))$$

$$\varepsilon_8 = 2^{-1}(C\ell_1(z) - C\ell_6(z) + C\ell_{10}(z) - C\ell_{13}(z))$$

$$\varepsilon_9 = 2^{-1}(C\ell_2(x) + C\ell_5(x) - C\ell_9(x) - C\ell_{14}(x))$$

$$\varepsilon_{10} = 2^{-1}(C\ell_2(z) - C\ell_5(z) + C\ell_9(z) - C\ell_{14}(z))$$

$$\varepsilon_{11} = 8^{-\frac{1}{2}}(C\ell_3(x) + C\ell_4(x) + C\ell_7(x) + C\ell_8(x) - C\ell_{11}(x) - C\ell_{12}(x) - C\ell_{15}(x) - C\ell_{16}(x))$$

$$\varepsilon_{12} = 8^{-\frac{1}{2}}(C\ell_3(y) - C\ell_4(y) + C\ell_7(y) - C\ell_8(y) + C\ell_{11}(y) - C\ell_{12}(y) + C\ell_{15}(y) - C\ell_{16}(y))$$

$$\varepsilon_{13} = 8^{-\frac{1}{2}}(C\ell_3(z) + C\ell_4(z) - C\ell_7(z) - C\ell_8(z) + C\ell_{11}(z) + C\ell_{12}(z) - C\ell_{15}(z) - C\ell_{16}(z))$$

B_{1g}

$$\varepsilon_{14} = 2^{-1}(Cu_1(y) + Cu_2(y) - Cu_3(y) - Cu_4(y))$$

$$\varepsilon_{15} = 2^{-1}(Cs_1(y) + Cs_4(y) - Cs_6(y) - Cs_7(y))$$

$$\varepsilon_{16} = 2^{-1}(Cs_2(y) + Cs_3(y) - Cs_5(y) - Cs_8(y))$$

$$\varepsilon_{17} = 2^{-1}(Cl_1(y) + Cl_6(y) - Cl_{10}(y) - Cl_{13}(y))$$

$$\varepsilon_{18} = 2^{-1}(Cl_2(y) + Cl_5(y) - Cl_9(y) - Cl_{14}(y))$$

$$\varepsilon_{19} = 8^{-\frac{1}{2}}(Cl_3(x) - Cl_4(x) + Cl_7(x) - Cl_8(x) + Cl_{11}(x) - Cl_{12}(x) + Cl_{15}(x) - Cl_{16}(x))$$

$$\varepsilon_{20} = 8^{-\frac{1}{2}}(Cl_3(y) + Cl_4(y) + Cl_7(y) + Cl_8(y) - Cl_{11}(y) - Cl_{12}(y) - Cl_{15}(y) - Cl_{16}(y))$$

$$\varepsilon_{21} = 8^{-\frac{1}{2}}(Cl_3(z) - Cl_4(z) - Cl_7(z) + Cl_8(z) - Cl_{11}(z) + Cl_{12}(z) + Cl_{15}(z) - Cl_{16}(z))$$

B_{2g}

$$\varepsilon_{22} = 2^{-1}(Cu_1(x) - Cu_2(x) + Cu_3(x) - Cu_4(x))$$

$$\varepsilon_{23} = 2^{-1}(Cu_1(z) + Cu_2(z) - Cu_3(z) - Cu_4(z))$$

$$\varepsilon_{24} = 2^{-1}(Cs_1(x) - Cs_4(x) + Cs_6(x) - Cs_7(x))$$

$$\varepsilon_{25} = 2^{-1}(Cs_1(z) + Cs_4(z) - Cs_6(z) - Cs_7(z))$$

$$\varepsilon_{26} = 2^{-1}(Cs_2(x) - Cs_3(x) + Cs_5(x) - Cs_8(x))$$

$$s_{27} = 2^{-1}(Cs_2(z) + Cs_3(z) - Cs_5(z) - Cs_8(z))$$

$$s_{28} = 2^{-1}(Cl_1(x) - Cl_6(x) + Cl_{10}(x) - Cl_{13}(x))$$

$$s_{29} = 2^{-1}(Cl_1(z) + Cl_6(z) - Cl_{10}(z) - Cl_{13}(z))$$

$$s_{30} = 2^{-1}(Cl_2(x) - Cl_5(x) + Cl_9(x) - Cl_{14}(x))$$

$$s_{31} = 2^{-1}(Cl_2(z) + Cl_5(z) - Cl_9(z) - Cl_{14}(z))$$

$$s_{32} = 8^{-\frac{1}{2}}(Cl_3(x) + Cl_4(x) - Cl_7(x) - Cl_8(x) + Cl_{11}(x) + Cl_{12}(x) - Cl_{15}(x) - Cl_{16}(x))$$

$$s_{33} = 8^{-\frac{1}{2}}(Cl_3(y) - Cl_4(y) - Cl_7(y) + Cl_8(y) - Cl_{11}(y) + Cl_{12}(y) + Cl_{15}(y) - Cl_{16}(y))$$

$$s_{34} = 8^{-\frac{1}{2}}(Cl_3(z) + Cl_4(z) + Cl_7(z) + Cl_8(z) - Cl_{11}(z) - Cl_{12}(z) - Cl_{15}(z) - Cl_{16}(z))$$

B_{3g}

$$s_{35} = 2^{-1}(Cu_1(y) - Cu_2(y) + Cu_3(y) - Cu_4(y))$$

$$s_{36} = 2^{-1}(Cs_1(y) - Cs_4(y) + Cs_6(y) - Cs_7(y))$$

$$s_{37} = 2^{-1}(Cs_2(y) - Cs_3(y) + Cs_5(y) - Cs_8(y))$$

$$s_{38} = 2^{-1}(Cl_1(y) - Cl_6(y) + Cl_{10}(y) - Cl_{13}(y))$$

$$s_{39} = 2^{-1}(Cl_2(y) - Cl_5(y) + Cl_9(y) - Cl_{14}(y))$$

$$\varepsilon_{40} = 8^{-\frac{1}{2}}(Cl_3(x) - Cl_4(x) - Cl_7(x) + Cl_8(x) - Cl_{11}(x)$$
$$+ Cl_{12}(x) + Cl_{15}(x) - Cl_{16}(x))$$

$$\varepsilon_{41} = 8^{-\frac{1}{2}}(Cl_3(y) + Cl_4(y) - Cl_7(y) - Cl_8(y) + Cl_{11}(y)$$
$$+ Cl_{12}(y) - Cl_{15}(y) - Cl_{16}(y))$$

$$\varepsilon_{42} = 8^{-\frac{1}{2}}(Cl_3(z) - Cl_4(z) + Cl_7(z) - Cl_8(z) + Cl_{11}(z)$$
$$- Cl_{12}(z) + Cl_{15}(z) - Cl_{16}(z))$$

A_u

$$\varepsilon_{43} = 2^{-1}(Cu_1(y) - Cu_2(y) - Cu_3(y) + Cu_4(y))$$

$$\varepsilon_{44} = 2^{-1}(Cs_1(y) - Cs_4(y) - Cs_6(y) + Cs_7(y))$$

$$\varepsilon_{45} = 2^{-1}(Cs_2(y) - Cs_3(y) - Cs_5(y) + Cs_8(y))$$

$$\varepsilon_{46} = 2^{-1}(Cl_1(y) - Cl_6(y) - Cl_{10}(y) + Cl_{13}(y))$$

$$\varepsilon_{47} = 2^{-1}(Cl_2(y) - Cl_5(y) - Cl_9(y) + Cl_{14}(y))$$

$$\varepsilon_{48} = 8^{-\frac{1}{2}}(Cl_3(x) - Cl_4(x) - Cl_7(x) + Cl_8(x) + Cl_{11}(x)$$
$$- Cl_{12}(x) - Cl_{15}(x) + Cl_{16}(x))$$

$$\varepsilon_{49} = 8^{-\frac{1}{2}}(Cl_3(y) + Cl_4(y) - Cl_7(y) - Cl_8(y) - Cl_{11}(y)$$
$$- Cl_{12}(y) + Cl_{15}(y) + Cl_{16}(y))$$

$$\varepsilon_{50} = 8^{-\frac{1}{2}}(Cl_3(z) - Cl_4(z) + Cl_7(z) - Cl_8(z) - Cl_{11}(z)$$
$$+ Cl_{12}(z) - Cl_{15}(z) + Cl_{16}(z))$$

B_{1u}

$$s_{51} = 2^{-1}(Cu_1(x) - Cu_2(x) - Cu_3(x) + Cu_4(x))$$

$$s_{52} = 2^{-1}(Cu_1(z) + Cu_2(z) + Cu_3(z) + Cu_4(z))$$

$$s_{53} = 2^{-1}(Cs_1(x) - Cs_4(x) - Cs_6(x) + Cs_7(x))$$

$$s_{54} = 2^{-1}(Cs_1(z) + Cs_4(z) + Cs_6(z) + Cs_7(z)).$$

$$s_{55} = 2^{-1}(Cs_2(x) - Cs_3(x) - Cs_5(x) + Cs_8(x))$$

$$s_{56} = 2^{-1}(Cs_2(z) + Cs_3(z) + Cs_5(z) + Cs_8(z))$$

$$s_{57} = 2^{-1}(C\ell_1(x) - C\ell_6(x) - C\ell_{10}(x) + C\ell_{13}(x))$$

$$s_{58} = 2^{-1}(C\ell_1(z) + C\ell_6(z) + C\ell_{10}(z) + C\ell_{13}(z))$$

$$s_{59} = 2^{-1}(C\ell_2(x) - C\ell_5(x) - C\ell_9(x) + C\ell_{14}(x))$$

$$s_{60} = 2^{-1}(C\ell_2(z) + C\ell_5(z) + C\ell_9(z) + C\ell_{14}(z))$$

$$s_{61} = 8^{-\frac{1}{2}}(C\ell_3(x) + C\ell_4(x) - C\ell_7(x) - C\ell_8(x) - C\ell_{11}(x)$$
$$- C\ell_{12}(x) + C\ell_{15}(x) + C\ell_{16}(x))$$

$$s_{62} = 8^{-\frac{1}{2}}(C\ell_3(y) - C\ell_4(y) - C\ell_7(y) + C\ell_8(y) + C\ell_{11}(y)$$
$$- C\ell_{12}(y) - C\ell_{15}(y) + C\ell_{16}(y))$$

$$s_{63} = 8^{-\frac{1}{2}}(C\ell_3(z) + C\ell_4(z) + C\ell_7(z) + C\ell_8(z) + C\ell_{11}(z)$$
$$+ C\ell_{12}(z) + C\ell_{15}(z) + C\ell_{16}(z))$$

B_{2u}

$$\varepsilon_{64} = 2^{-1}(Cu_1(y) + Cu_2(y) + Cu_3(y) + Cu_4(y)$$

$$\varepsilon_{65} = 2^{-1}(Cs_1(y) + Cs_4(y) + Cs_6(y) + Cs_7(y))$$

$$\varepsilon_{66} = 2^{-1}(Cs_2(y) + Cs_3(y) + Cs_5(y) + Cs_8(y))$$

$$\varepsilon_{67} = 2^{-1}(C\ell_1(y) + C\ell_6(y) + C\ell_{10}(y) + C\ell_{13}(y))$$

$$\varepsilon_{68} = 2^{-1}(C\ell_2(y) + C\ell_5(y) + C\ell_9(y) + C\ell_{14}(y))$$

$$\varepsilon_{69} = 8^{-\frac{1}{2}}(C\ell_3(x) - C\ell_4(x) + C\ell_7(x) - C\ell_8(x) - C\ell_{11}(x)$$
$$+ C\ell_{12}(x) - C\ell_{15}(x) + C\ell_{16}(x))$$

$$\varepsilon_{70} = 8^{-\frac{1}{2}}(C\ell_3(y) + C\ell_4(y) + C\ell_7(y) + C\ell_8(y) + C\ell_{11}(y)$$
$$+ C\ell_{12}(y) + C\ell_{15}(y) + C\ell_{16}(y))$$

$$\varepsilon_{71} = 8^{-\frac{1}{2}}(C\ell_3(z) - C\ell_4(z) - C\ell_7(z) + C\ell_8(z) + C\ell_{11}(z)$$
$$- C\ell_{12}(z) - C\ell_{15}(z) + C\ell_{16}(z))$$

B_{3u}

$$\varepsilon_{72} = 2^{-1}(Cu_1(x) + Cu_2(x) + Cu_3(x) + Cu_4(x))$$

$$\varepsilon_{73} = 2^{-1}(Cu_1(z) - Cu_2(z) - Cu_3(z) + Cu_4(z))$$

$$\varepsilon_{74} = 2^{-1}(Cs_1(x) + Cs_4(x) + Cs_6(x) + Cs_7(x))$$

$$\varepsilon_{75} = 2^{-1}(Cs_1(z) - Cs_4(z) - Cs_6(z) + Cs_7(z))$$

$$\varepsilon_{76} = 2^{-1}(Cs_2(x) + Cs_3(x) + Cs_5(x) + Cs_8(x))$$

$$\varepsilon_{77} = 2^{-1}(Cs_2(z) - Cs_3(z) - Cs_5(z) + Cs_8(z))$$

$$\varepsilon_{78} = 2^{-1}(C\ell_1(x) + C\ell_6(x) + C\ell_{10}(x) + C\ell_{13}(x))$$

$$\varepsilon_{79} = 2^{-1}(C\ell_1(z) - C\ell_6(z) - C\ell_{10}(z) + C\ell_{13}(z))$$

$$\varepsilon_{80} = 2^{-1}(C\ell_2(x) + C\ell_5(x) + C\ell_9(x) + C\ell_{14}(x))$$

$$\varepsilon_{81} = 2^{-1}(C\ell_2(z) - C\ell_5(z) - C\ell_9(z) + C\ell_{14}(z))$$

$$\varepsilon_{82} = 8^{-\frac{1}{2}}(C\ell_3(x) + C\ell_4(x) + C\ell_7(x) + C\ell_8(x) + C\ell_{11}(x) + C\ell_{12}(x) + C\ell_{15}(x) + C\ell_{16}(x))$$

$$\varepsilon_{83} = 8^{-\frac{1}{2}}(C\ell_3(y) - C\ell_4(y) + C\ell_7(y) - C\ell_8(y) - C\ell_{11}(y) + C\ell_{12}(y) - C\ell_{15}(y) + C\ell_{16}(y))$$

$$\varepsilon_{84} = 8^{-\frac{1}{2}}(C\ell_3(z) + C\ell_4(z) - C\ell_7(z) - C\ell_8(z) - C\ell_{11}(z) - C\ell_{12}(z) + C\ell_{15}(z) + C\ell_{16}(z))$$

APPENDIX VI — $\underset{\sim}{X}$ MATRIX ELEMENTS

Let $A_n(x)$, $A_n(y)$ and $A_n(z)$ be the Cartesian displacement vectors of the nth atom in the unit cell (figure 4.2.1). The elements x_i of the column matrix $\underset{\sim}{X}$ are given below for $i = 1, 2, \ldots, 84$:

$Cu_1(x)$; $Cu_2(x)$; $Cu_3(x)$; $Cu_4(x)$; $Cu_1(z)$; $Cu_2(z)$; $Cu_3(z)$; $Cu_4(z)$;

$Cs_1(x)$; $Cu_4(x)$; $Cu_6(x)$; $Cs_7(x)$; $Cs_1(z)$; $Cs_4(z)$; $Cs_6(z)$; $Cs_7(z)$;

$Cs_2(x)$; $Cs_3(x)$; $Cs_5(x)$; $Cs_8(x)$; $Cs_2(z)$; $Cs_3(z)$; $Cs_5(z)$; $Cs_8(z)$;

$Cl_1(x)$; $Cl_6(x)$; $Cl_{10}(x)$; $Cl_{13}(x)$; $Cl_1(z)$; $Cl_6(z)$; $Cl_{10}(z)$; $Cl_{13}(z)$;

$Cl_2(x)$; $Cl_5(x)$; $Cl_9(x)$; $Cl_{14}(x)$; $Cl_2(z)$; $Cl_5(z)$; $Cl_9(z)$; $Cl_{14}(z)$;

$Cl_3(x)$; $Cl_4(x)$; $Cl_7(x)$; $Cl_8(x)$; $Cl_{11}(x)$; $Cl_{12}(x)$; $Cl_{15}(x)$; $Cl_{16}(x)$;

$Cl_3(y)$; $Cl_4(y)$; $Cl_7(y)$; $Cl_8(y)$; $Cl_{11}(y)$; $Cl_{12}(y)$; $Cl_{15}(y)$; $Cl_{16}(y)$;

$Cl_3(z)$; $Cl_4(z)$; $Cl_7(z)$; $Cl_8(z)$; $Cl_{11}(z)$; $Cl_{12}(z)$; $Cl_{15}(z)$; $Cl_{16}(z)$;

$Cu_1(y)$; $Cu_2(y)$; $Cu_3(y)$; $Cu_4(y)$; $Cs_1(y)$; $Cs_4(y)$; $Cs_6(y)$; $Cs_7(y)$;

$Cs_2(y)$; $Cs_3(y)$; $Cs_5(y)$; $Cs_8(y)$; $Cl_1(y)$; $Cl_6(y)$; $Cl_{10}(y)$; $Cl_{13}(y)$;

$Cl_2(y)$; $Cl_5(y)$; $Cl_9(y)$; $Cl_{14}(y)$;

APPENDIX VII $\underset{\sim}{R}$ MATRIX ELEMENTS

Eighty internal coordinates have been chosen for the unit cell force field defined in section 4.3.1. The internal coordinates associated with the Cs ... Cℓ central force constants and Cℓ ... Cℓ central force constants have been described in tables 4.3.1 and 4.3.3 respectively; these constitute the 41st to the 80th elements of the $\underset{\sim}{R}$ matrix.

The first 40 elements of $\underset{\sim}{R}$ matrix are associated with the general valence force constants of the $CuCl_4^{2-}$ ions. Only the 10 elements of the first $CuCl_4^{2-}$ ion (refer figure 4.2.1) are given here as the next 30 are merely the corresponding equivalent coordinates of the other three $CuCl_4^{2-}$ ions.

r_i	i
$\Delta r(Cu_1\text{-}Cl_1)$	1
$\Delta r(Cu_1\text{-}Cl_2)$	2
$\Delta r(Cu_1\text{-}Cl_3)$	3
$\Delta r(Cu_1\text{-}Cl_4)$	4
$\Delta\phi(Cl_1\text{-}Cu\text{-}Cl_2)$	5
$\Delta\phi(Cl_3\text{-}Cu_1\text{-}Cl_4)$	6
$\Delta\phi(Cl_1\text{-}Cu_1\text{-}Cl_3)$	7

$\Delta\phi(C\ell_1\text{-}Cu_1\text{-}C\ell_4)$ 8

$\Delta\phi(C\ell_2\text{-}Cu_1\text{-}C\ell_3)$ 9

$\Delta\phi(C\ell_2\text{-}Cu_1\text{-}C\ell_4)$ 10

APPENDIX VIII DETERMINATION OF $\underset{\sim}{B}$ MATRIX ELEMENTS

For simplicity, the method for determining $\underset{\sim}{B}$ matrix elements is demonstrated using an AB_2 molecule as an example.

(A) Elements between a Cartesian coordinate, say $B_1(z)$, and a bond stretching coordinate:

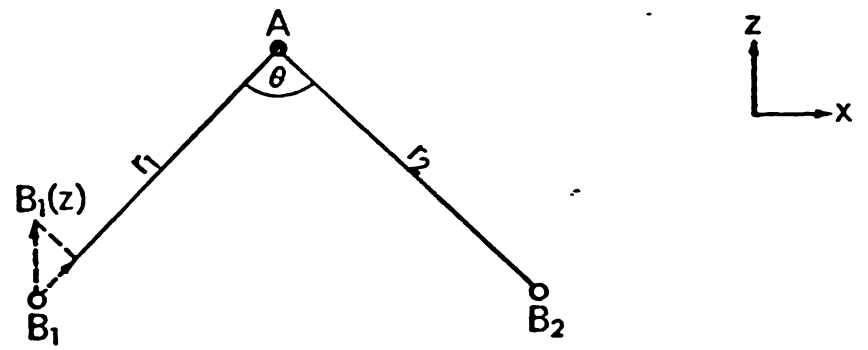

The Cartesian vector $B_1(z)$ must be resolved along the bond axis. The magnitude of this component is $B_1(z)\cos(\theta/2)$. So, for a unit Cartesian displacement of B_1 along the z-direction, the change in r_1 will be $-\cos(\theta/2)$, i.e. the bond shortens. This will be the appropriate $\underset{\sim}{B}$ matrix element. Note that the corresponding element between $B_1(z)$ and r_2 is zero - moving B_1 does not affect r_2 - but the element between $B_2(z)$ and r_2 will be $-\cos(\theta/2)$.

(B) Elements between a Cartesian coordinate, say $B_1(z)$, and an angle-bending coordinate (where the atom concerned in the Cartesian displacement is not at the apex of the angle):

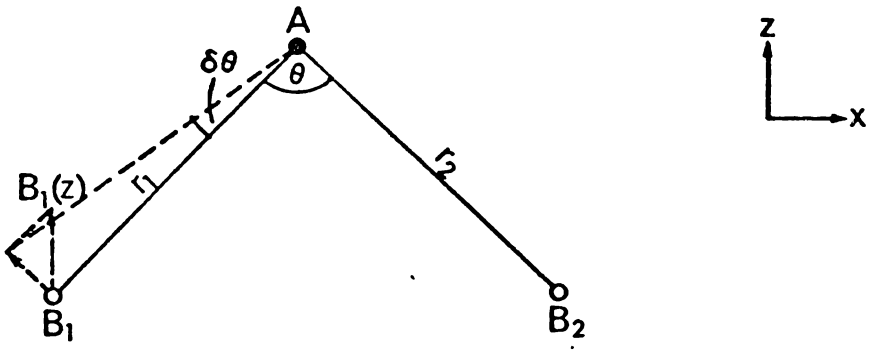

The component of $B_1(z)$ in a direction perpendicular to r_1 and in the xz-plane will be most effective in altering θ. The magnitude of this component is $B_1(z)\sin(\theta/2)$. Now $\tan\delta\theta = B_1(z)\sin(\theta/2)/r_1$, which is very nearly equal to $\delta\theta$ (in radians) for small displacements. So, the matrix element is $\left((1/r_1)\sin(\theta/2)\right)$.

(C) Elements between a Cartesian coordinate, say $B_1(z)$, and an angle-bending coordinate (where the atom concerned in the Cartesian displacement is at the apex of the angle):

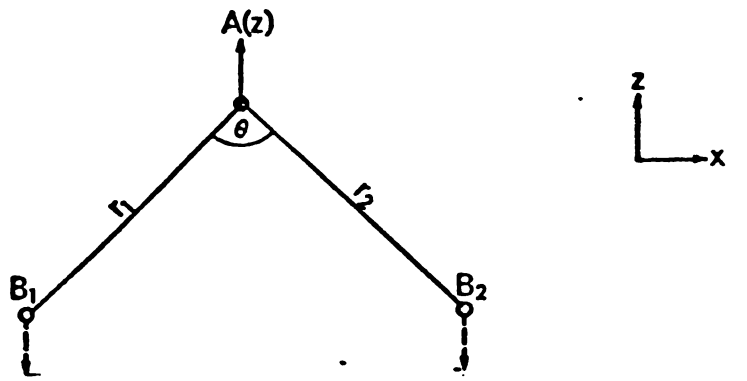

It will be seen that the effect of a unit displacement of A along z has the same effect on θ as simultaneously performing unit displacements of B_1 and B_2 in the negative z-direction. So the matrix element is $-(1/r_1 + 1/r_2)\sin(\theta/2)$. Displacements $A(y)$ and $A(x)$, if small, do not affect θ. In the general case, a Cartesian vector must be resolved into

its component along a direction which bisects the angle and lies in the plane defined by the angle.

Based on the method outlined above, the $\underset{\sim}{B}$ matrix elements for the unit cell of Cs_2CuCl_4 were calculated with the aid of simple Basic programs. Since 80 internal coordinates were chosen, the final $\underset{\sim}{B}$ matrix assumed a dimension of 80 × 84.

The format of the $\underset{\sim}{B}$ matrix is as shown below:

Cartesian vectors x_j, j = 1, 2, ..., 84

(order of vectors as in $\underset{\sim}{X}$ matrix, appendix VI)

Internal Coordinates r_i, i = 1, 2, ..., 80 (order of coordinates as in $\underset{\sim}{R}$ matrix, appendix VII)

$$\begin{matrix} b_{1,1}, & b_{1,2}, & \cdots\cdots & b_{1,84} \\ b_{2,1}, & & & \\ \vdots & & \ddots & \\ b_{80,1}, & & & b_{80,84} \end{matrix}$$

Owing to its massive size, the entire $\underset{\sim}{B}$ matrix could not feasibly be included in this thesis.

APPENDIX IX $\underset{\sim}{G}^{c}$ MATRIX ELEMENTS

Let $\mu_A = (M_A)^{-1}$ where M is the atomic mass of atom A. The order in which a $\underset{\sim}{G}^{c}$ matrix element associated with atom A appears corresponds directly to that of the $\underset{\sim}{X}$ matrix (appendix VI) element associated with the same atom. Thus, the non-zero diagonal elements of $\underset{\sim}{G}^{c}$ matrix (84, 84) are:

$(g^c)_{ii} = \mu_{Cu}$ for i = 1 to 8;

$(g^c)_{ii} = \mu_{Cs}$ for i = 9 to 24;

$(g^c)_{ii} = \mu_{Cl}$ for i = 25 to 64;

$(g^c)_{ii} = \mu_{Cu}$ for i = 65 to 68;

$(g^c)_{ii} = \mu_{Cs}$ for i = 69 to 76;

$(g^c)_{ii} = \mu_{Cl}$ for i = 77 to 84.